CHALMERS
UNIVERSITY OF TECHNOLOGY

Analysis of Potential in Asymmetric Braking for Autonomous Applications

Master's thesis

PATRICK VOLZ

Department of Applied Mechanics
CHALMERS UNIVERSITY OF TECHNOLOGY
Gothenburg, Sweden 2018

MASTER'S THESIS

Analysis of Potential in Asymmetric Braking for Autonomous Applications

PATRICK VOLZ

Department of Applied Mechanics
Division of Vehicle Engineering and Autonomous Systems
Vehicle Dynamics group
CHALMERS UNIVERSITY OF TECHNOLOGY
Gothenburg, Sweden 2018

Analysis of Potential in Asymmetric Braking for Autonomous Applications
PATRICK VOLZ

Master's Thesis 2017:87
ISSN 1652-8557
Department of Applied Mechanics
Division of Vehicle Engineering and Autonomous Systems
Vehicle Dynamics group
Chalmers University of Technology
SE-412 96 Gothenburg
Sweden
Telephone: + 46 (0)31-772 1000

Examiner: Bengt J H Jacobson, Department of Applied Mechanics, Chalmers University of Technology, Gothenburg, Sweden
Supervisor: Kristoffer Tagesson, Volvo Group Trucks Technology, Gothenburg, Sweden

Cover:
Visualized operation of the asymmetric braking system in a Volvo FH 6x2;
Photographer: Magnus Pajnert, © Volvo Truck Corporation

Department of Applied Mechanics
Gothenburg, Sweden 2018

Analysis of Potential in Asymmetric Braking for Autonomous Applications
Master's thesis
PATRICK VOLZ
Department of Applied Mechanics
Division of Vehicle Engineering and Autonomous Systems
Vehicle Dynamics group
Chalmers University of Technology

Abstract

Striving for automated commercial vehicles, the execution of steering commands has to be highly reliable in order to guarantee the manoeuvrability in any driving situation: In the event of the primary steering actuator's failure, highly and fully automated vehicles have to provide their own fall-back performance since the human driver is relieved of any driving responsibility. Consequently, an additional, independent fall-back level for this steering actuator is essential, which undertakes the steering task and guarantees the driving safety. Although it is possible to establish the required levels of redundancy by implementing similar, additional steering actuators, this design would significantly increase the cost and the box volume of the system. On that account, this thesis project investigates the manoeuvrability of over-actuated commercial vehicles using the mounted wheel brakes in detail. This approach uses the existing actuators of the respective vehicle configuration, limiting the system costs and the development effort.

The first part of the project aims at the development of a reconfigurable motion control system which generates the desired vehicle motion to perform a defined driving manoeuvre while ensuring driving safety. Accordingly, this system covers all the steps from the computation of directional and velocity related commands, the control of the involved vehicle motions, to the coordination and control of the accessible brake actuators. This results in an asymmetric brake torque distribution. In order to structure the system functionalities and to enable the reusability of the controller for various vehicle configurations, the architecture of the control design needs to be modular.

For the verification of the control unit's development, the project scope comprises the analysis of the system performance in predefined driving manoeuvres. Therefore, several demanding manoeuvres are carried out on the test track and in the simulation environment. Based on the simulation and vehicle testing results, the vehicle's steerability as well as the driving precision and stability are evaluated. Finally, the system's performance is compared to the primary steering actuator intended for the driving task, since it sets the benchmark for the manoeuvrability. In direct comparison of the steering characteristics, the asymmetric braking technology is able to keep up with the intended steering actuator. Despite the lower steering dynamics, the motion control system ensures a stable motion in all the manoeuvres. In conclusion, the asymmetric braking has the potential of providing the required fall-back level and ensure the execution of the steering commands.

Key words: Motion control system, asymmetric braking, steer by braking, fall-back level, active safety, commercial vehicles, control allocation

Contents

Preface

This Master's thesis project was carried out at Volvo Group Truck Technology (GTT) in Gothenburg in the field of vehicle analysis and motion control within a processing period of 6 months. The examination of this industrial concluding degree project is the responsibility of the Chalmers University of Technology in Gothenburg in exchange with the University of Stuttgart. Comprehensively, the thesis project concludes the Master's studies in Technology Management with an emphasis on Vehicle Mechatronics in Stuttgart.

In the first place, I would like to thank my supervisor at Volvo, Kristoffer Tagesson for his support and guidance. You really pushed and encouraged me to work self-reliant and to look at all the details to achieve a great overall result. With your large network, you helped me a lot to find the right person for every topic. Besides the project aspects, your good mood and positive attitude was very enriching and motivating for me. Many thanks to my colleagues and coinventors Björn Källstrand, Leon Henderson and Leo Laine for the intense as well as fruitful meetings which made this project a success and concluded in an invention disclosure of our ideas. Despite your overbooked timetables, you always found a few minutes for me. Furthermore, I would like to thank my workmate Sachin Janardhanan for supporting me with the simulation environment and the vehicle models.

Moreover, I would like to extend my sincere gratitude to my examining Professor Bengt Jacobson at Chalmers for making this thesis project and the exchange programme with Stuttgart possible. Your dedication, along with your critical questioning of my results and the valuable literature recommendations, ensured that I conceived new approaches and that the project made excellent progress. In addition, many thanks to Dan Keilhoff from the University of Stuttgart for his supervision and assistance.

Finally, thanks to all my other colleagues, fellow students and friends at both Volvo and Chalmers for your interest and collaboration. You made my stay in Gothenburg as well as Sweden rewarding and memorable.

Gothenburg January 2018-01-01

PATRICK VOLZ

Notations

Parameters

In this thesis work, the notation and technical terms follow the International Standard 8855 for road vehicle dynamics (ISO, 2011). The standard applies to passenger cars, commercial vehicles as well as vehicle combinations.

Property	Unit	Description
a_X	$\mathrm{m/s^2}$	Longitudinal acceleration
a_Y	$\mathrm{m/s^2}$	Lateral acceleration
A_{Cyl}	$\mathrm{m^2}$	Effective membrane area of the brake cylinder
B		Effectiveness matrix in control allocation problem
C_α	$\mathrm{N/rad}$	Cornering stiffness of the tyre, function of the tyre normal load
C_λ	$\mathrm{N/rad}$	Longitudinal slip stiffness of the tyre, function of the tyre normal load
F_X	N	Longitudinal virtual force acting on the vehicle reference frame
F_Y	N	Lateral virtual force acting on the vehicle reference frame
F_Z	N	Normal
F_{XC}	N	Longitudinal coupling force
F_{YC}	N	Lateral coupling force
F_{XT}	N	Longitudinal tyre force
F_{YT}	N	Lateral tyre force
F_{ZT}	N	Tyre normal load
$F_{T,res}$	N	Combined tyre force
g	$\mathrm{m/s^2}$	Constant of gravity
i	1	Index for tyres, wheels or brake actuators
i_{Cyl}	1	Lever ratio of the brake actuator
I_{Steer}	$\mathrm{kgm^2}$	Moment of inertia of the steering system, relative to the tyre steering rotation
I_{ZV}	$\mathrm{kgm^2}$	Moment of inertia of the vehicle about the vertical axis
j	1	Index for axles
K_B	$\mathrm{Nm/bar}$	Relational brake parameter
K_I		Proportional control gain
K_P		Integral control gain
l_j	m	Wheelbase
l_{ah}	m	Look-ahead distance of the pure pursuit path tracker
l_{eq}	m	Equivalent wheelbase of a multi-axle vehicle
m_L	kg	Load mass of the vehicle

m_V	kg	Total mass of the vehicle
M_{Fr}	Nm	Steering friction moment
M_{Steer}	Nm	Steering moment from the longitudinal tyre forces acting on the steering system
M_X	Nm	Virtual actuation moment about x-axis
M_Y	Nm	Virtual actuation moment about y-axis
M_Z	Nm	Virtual actuation moment about z-axis
M_{XT}	Nm	Steering moment from tyre longitudinal forces
M_{YT}	Nm	Steering moment from tyre lateral forces
M_{ZT}	Nm	Steering moment from tyre normal forces
N	1	Number of wheels or brake actuators on vehicle unit. Every wheel is connected to the associated brake actuator
N_A	1	Number of axles on the truck unit
N_R	1	Number of non-steered rear axles on the truck unit
P_B	Pa	Absolut braking pressure
P_{eff}	Pa	Effective braking pressure
P_T	Pa	Pressure threshold
r_{dyn}	m	Dynamic rolling radius, derived from the travelled distance during one rotation of the wheel
r_k	m	Steering-axis offset at ground / kingpin offset at ground
r_{stat}	m	Static, laden tyre radius
r_0	m	Unladen tyre radius
R_B	m	Mean radius of brake pad to brake disc centre
R_P	m	Path or road radius
t	s	Time
T_B	Nm	Brake torque
t_m	m	Mechanical trail length
t_p	m	Pneumatic trail length
v	m/s	Vehicle velocity acting on the reference frame
v_X	m/s	Longitudinal vehicle velocity acting on the reference frame
v_{XT}	m/s	Longitudinal tyre velocity
w_j	m	Track width
W_u		Diagonal weighting matrix: Minimize the use of the actuators
W_v		Diagonal weighting matrix: Prioritise the elements in $\mathbf{v}$ to emphasise their importance to the allocation problem
α	rad	Tyre slip angle
β	rad	Vehicle sideslip angle
γ	1	Scalar weighting parameter for allocation problem

δ	rad	Actual steer angle of the vehicle
δ_{PF}	rad	Requested steer angle from the path following function
δ_{SS}	rad	Self-steering angle
ε	rad	Wheel inclination angle
η_B	1	Efficiency factor of the brake actuator
κ	m^{-1}	Path curvature; inverse of path radius
λ	1	Longitudinal tyre slip
λ_{res}	1	Combined tyre slip
μ	1	Force or friction coefficient
μ_B	1	Kinetic friction coefficient of brake pad/disc
σ	rad	Kingpin inclination angle
τ	rad	Kingpin caster angle
φ	rad	Angular deviation between vehicle reference frame and driving path
ψ	rad	Yaw angle of the vehicle
$\Delta\psi_C$	rad	Yaw articulation angle between the reference frames of tractor and first trailing unit
ω_W	rad/s	Wheel-spin velocity about the rotation axis of the wheel
ω_X	rad/s	Roll rate of the vehicle, vehicle rotation about x-axis
ω_Y	rad/s	Pitch rate of the vehicle, vehicle rotation about y-axis
ω_Z	rad/s	Yaw rate of the vehicle, vehicle rotation about z-axis

Acronyms

ABS	Anti-lock Braking System
COG	Centre Of Gravity
CVC	Complete Vehicle Control
EBS	Electronic Braking System
EPS	Electronic Power Steering
ESF	Exponential-Spring-Friction element
ESC	Electronic Stability Control
FF	Feed-Forward (controller)
GPS	Global Positioning System
GTT	(Volvo) Group Trucks Technology
ICR	Instantaneous Centre of Rotation
ISO	International Organization for Standardization
NHTSA	National Highway Traffic Safety Administration
PCV	Pressure Control Valve
PI	Proportional-Integral (controller)
PM	Pressure Modulator
SBB	Steer By Braking
VDS	Volvo Dynamic Steering
VTM	Volvo Transport Models

1 Introduction

1.1 Background

The present decade shapes the automobile's history and simultaneously sets the course for the vehicle's future by an unprecedented number of innovations. According to (Dannenberg & Burgard, 2015) the main innovation objectives, triggered by megatrends, are safety and security, comfort, performance and dynamics as well as infotainment and connectivity. Consequently, not only the way of propulsion but also the driver's role and the mobility concept are redefined: The vehicles are turned into individualized, autonomously moving multimedia zones. Aiming for these highly integrated innovative systems, the importance of electrics, electronics and software inside the vehicles will increase further. In short, the automotive sector is facing a complete upheaval and the vehicles are about to be reinvented.

Focusing on the progressive automation in terms of vehicle motion, the development of related systems is guided by three axioms (Reuss, 2015): With automated driving systems, automotive locomotion will become more comfortable and particularly, it will become safer. In addition, the application of these automation systems will lead to an improvement in traffic flow, which will contribute to a reduction in fuel consumption and emissions.

Automated driving systems are classified into six levels from “no automation” (level 0) to “full automation” (level 5) by the SAE standard J3016, listed in Table 1.1 (SAE, 2014). This standard identifies the assisting performance of the combined system and ranks it accordingly. The more comprehensive the capability of handling the automobile even in complex driving situations is, the higher is its level of automation. At present, car manufacturers, suppliers and research institutes are concerned with the further development of driving assistance systems towards highly automated driving (Reuss, 2015). The overall target is to feature the level of “full automation” so the driving system performs under all road and environmental conditions and no human driver needs to intervene (SAE, 2014).

Table 1.1: SAE standard J3016 – levels of automated driving (SAE, 2014)

SAE level	Name	Execution of steering and acceleration	Monitoring of driving environment	Fall-back performance
0	No automation	Driver	Driver	Driver
1	Driver assistance	Driver	Driver	Driver
2	Partial automation	***System*** + Driver	Driver	Driver
3	Conditional auto.	***System***	***System***	Driver
4	High automation	***System***	***System***	***System***
5	Full automation	***System***	***System***	***System***

To enable a higher level of automation, more vehicle functions need to be integrated. The major proportion of these new features is based on electronics and on software (Waldron, 2014). Due to the rising integration density, the E/E complexity is increasing, along with the amount of electronic components and the number of networked control units (Hettich, 2016). Concurrently, also the quantity of software code is growing rapidly (Waldron, 2014). Before the introduction of the AUTomotive Open System ARchitecture (AUTOSAR) in 2003, (Reuss, 2016) ascertained a linear correlation between the number of electronic features and the overall failure rate. AUTOSAR's modular approach in technological development ensures improvements in terms of quality, reusability of software modules and engineering costs (Svensson, 2010). In spite of the standard's implementation, the complexity of the system structure for automated driving will increase (Pischinger & Seiffert, 2016), which leads to unavoidable errors in the development process and during operation (Băjenescu & Bâzu, 1999).

Pursuant to the ISO standard 26262, systems related to automated driving need to comply with the highest level of functional safety as they are controlling the transversal and lateral vehicle dynamics. Consequently, these functions are subject to strict requirements regarding reliability, availability and safety (Temple & Vilela, 2014). Therefore, the safety-critical applications' fault tolerance must ensure redundancies, so the system will operate despite malfunction (Reuss, 2016).

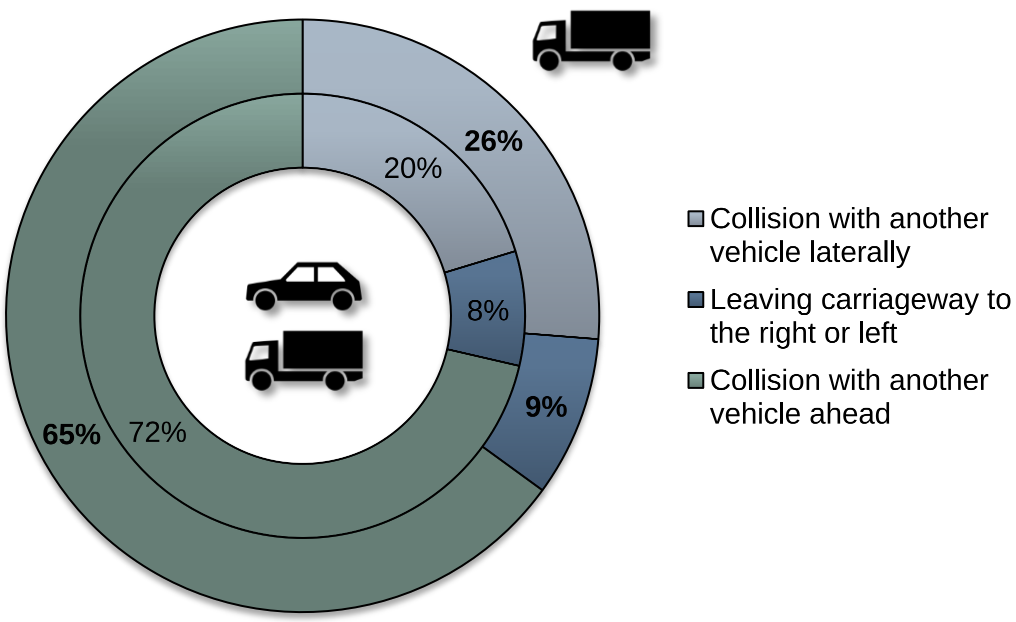

Figure 1.1: Kinds of road accidents in 2015 (Statistisches Bundesamt, 2015). The accident kinds of all road vehicles are represented as a percentage in the inner ring. The outer ring involves the accident kinds of heavy vehicles.

Systems affecting the vehicle’s steering and braking behaviour are considered to be exceedingly safety-critical. The total failure of such a system is hardly controllable and entails high extent of damage (Reuss, 2016) (ISO, 2011). According to the annual report of the Federal Statistical Office of Germany, 28 % of all road accidents in 2015 where caused by a motion error in lateral direction, illustrated in Figure 1.1. The mentioned accident number comprises lateral collisions with other vehicles as well as accidents in consequence of a departure from the carriageway. Considering only heavy vehicles, more than one third of the accidents are caused by an incorrect steering of the truck.

With regard to the future of automated driving systems, it is absolutely essential to guarantee the vehicle’s steerability in any case. A loss of the steerability would have a similar and highly disastrous outcome like aquaplaning, emergency braking without ABS-system or a locked steering column. The last scenario is still very present when referring to the ignition switch issue, which General Motors faced recently: About 30 million cars were equipped with a defective ignition lock which possibly blocks the steering when moving. The attorney Bob Hilliard associates around 5000 killed people with the faulty component (Rocco, 2014).

1.2 Motivation

In 2013, Volvo Trucks Technology launched its innovative Volvo Dynamic Steering (VDS). This steering system extends the conventional steering group with its hydraulic steering gear by an electric motor, mounted on the steering shaft. The additional drive assists the driver with supplementary steering force or rather torque in low speed ranges. Reversely, the control system compensates irregularities caused by the road surface or side winds at higher velocities to increase the driving safety and comfort (Volvo, 2013). Going one step further, an extended version of the VDS will be capable to control the vehicle’s lateral dynamics, commanded by a superordinate automated driving system.

The VDS system acts as an electronic power steering unit and consists of an electric drive and a control unit. If either the electronic actuator or the control unit fails, the human driver is going to steer the truck conventionally, being exposed to a reduced steering assistance. This means conversely, that the driver forms the ultimate fall-back level. Establishing the level of high or full automation, the driving system is obliged to manage the entire fall-back performance itself (SAE, 2014). Consequently the implementation of only one steering actuator will be insufficient to ensure a comprehensive fall-back performance and to preserve the system’s operational functionality.

1.3 Envisioned Solution

Striving for highly as well as fully automated commercial vehicles, another level of redundancy for executing steering commands has to be implemented. Referring to the previous chapter of motivation, an additional control system, ideally based on a different operating principle, is fundamental to guarantee the required fail-operational fault tolerance.

In order to succeed on the vehicle market, an innovation has to convince users with its beneficial functionalities and in particular with the system's pricing or rather the total cost of ownership (Dannenberg & Burgard, 2015). Both criteria can often be put into practice by an intelligent combination of existing components and modules. As a result, users can be offered an innovative functionality at a competitive value for money without increasing the system's weight by additional components. In conclusion, the fall-back level for the EPS should preferably be implemented by using the existing components of a truck.

In compliance with the functional safety standard for road vehicles, the detection of a malfunctioning steering actuator requires either the vehicle's transition to a safe state or the activation of a fault tolerance mechanism (ISO, 2011). If the steerability of the vehicle is no longer ensured, the only safe state is a stop by initiating an emergency braking. In good road conditions, the breaking distance of a passenger with an initial speed of 80 km/h is approximately 23 meters. Under the same conditions, it takes 36 meters to stop a commercial vehicle at best (ADAC, 2015).

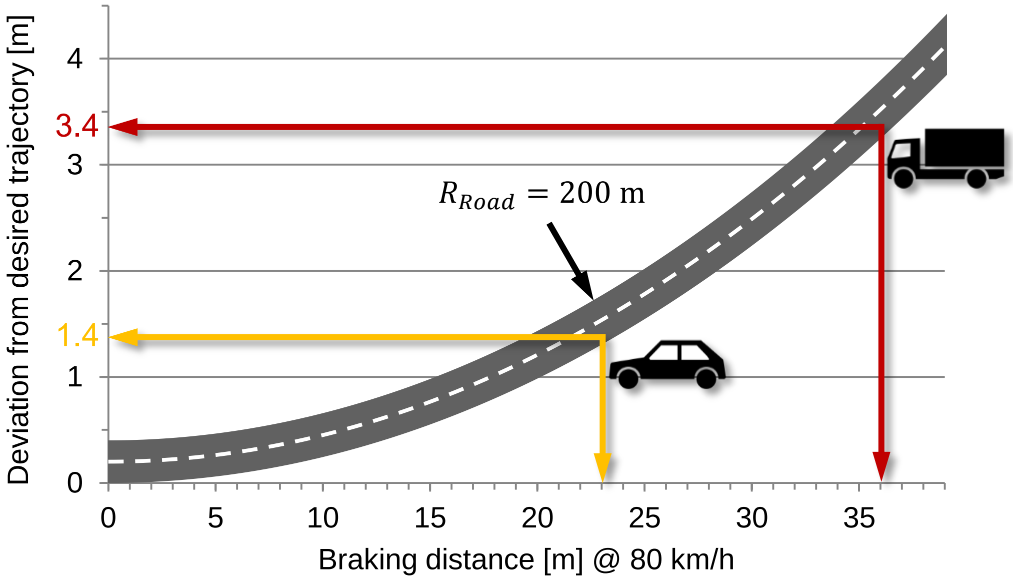

Figure 1.2: Deviation of the vehicle position from lane in case of a malfunction of the steering actuator and the execution of an emergency braking

In case of a faulty steering, the vehicle's motion trajectory is going to deviate from the desired driving path. Consequently, especially curves or lane changes constitute a high safety risk. The minimum road radius for international roads with a permissible speed limit of 80 km/h is 200 meters (Brilon & Krammes, 1997). Figure 1.2 illustrates the scenario in which the steering actuator fails before or throughout a cornering manoeuvre at 80 km/h. As proposed in the previous paragraph, an emergency braking is initiated to transition the vehicle to a safe state. For the reason of simplification, the alignment of the front wheels together with the heading direction is straight and the braking conditions are perfect.

At standstill the passenger car's position has departed 1.4 meters from a road with a radius of 200 m whereas the commercial vehicle is even 3.4 meters off. But also a road with a smaller curvature causes an inadmissible deviation from the desired path of more than 0.5 meters. In consequence, emergency braking after the detection of a faulty steering actuator will transition the vehicle to the safe state but it misses the safety goal of preventing a lateral collision with another vehicle or leaving the carriageway.

As a result, the steerability of the vehicle has to be guaranteed also in case of a malfunction of the primary steering actuators. The vehicle's lateral dynamic and thus its cornering behaviour depend on the applied yaw torque, which is affected by both the steer angle and the brake torque. The manipulation of the yaw torque is already used in the ESC for stabilizing the vehicle by controlling the individual brake torques (Pischinger & Seiffert, 2016). Therefore, it is possible not only to stabilize a vehicle but also to control its cornering, applying asymmetric brake torques. Consequently, differential braking shapes a promising approach to constitute the aspired redundancy level. The envisioned solution uses the conventional braking system for regulating the yaw torque with an additional control unit or a software module, appended to a consisting control device.

1.4 Objective

The objective of this thesis is to analyse the steerability of over-actuated commercial vehicles in case of failure of the primary steering system, applying asymmetric brake torques with an innovative and reconfigurable motion control system. This analysis comprises the feasibility and effectiveness of controlling the vehicle's motion by implementing this device as well as the influencing parameters and their specific impact on the controlled vehicle.

1.5 Deliverables

The deliverables, being covered by this thesis project, are listed subsequently and are going to be detailed within the present report:

- Modelling and simulation of a motion coordination prioritising the vehicle's stability, including the yaw, roll and articulation angle stability.
- Integration as well as coordination of available braking actuators to achieve a defined vehicle motion, minimizing the deviation from longitudinal and lateral control demanded by a path controller
- Design of a robust and adaptable system, to cope with sudden changes of the brake actuator characteristics during vehicle motion. Such changes can be caused by the environment, saturation or even failure among the controlled actuators
- Design of a reusable control system for several trucks or rather vehicle configurations. This enables a wider range of application as well as a facilitated transfer of the steering by braking technology.
- Design of a controller, that covers diverse driving situations like normal driving, but also driving near vehicle's handling limits
- Simulation and real vehicle testing of the designed controller. Subsequent validation of the simulation results with the vehicle data.

1.6 Limitation

The subsequent list outlines the limitations of this thesis project, thus covered neither in the report nor in the system development:

- This thesis considers a driverless, automated system, where the motion controller is only fed with longitudinal and lateral motion demands by the path controller. Consequently, the human machine interface is not considered any further and the driver is assumed to not interfere with the pedals or steering wheel.
- The vehicle motion coordination only allows the wheel brakes as actuators to control the dynamics. Neither electronic or hydraulic retarders, nor the front or back wheel steering are considered by the motion controller. Furthermore, all rear wheels are expected to be mounted on a rigid axle.
- This thesis only regards heavy vehicles as well as truck combinations with gross combination weight above 3.5 tonnes.
- This thesis considers an opened clutch that decouples motor and drive shaft. Therefore, the engine does not have any propulsion or braking effects on the power train. Consequently, the latter is represented in the simulation only by its inertia.
- This thesis covers neither the design, nor the implementation of sensors. The sensors' properties and output signals are taken from the data sheet.
- This thesis includes neither a friction estimation module nor a vehicle velocity estimation module. Consequently, the tyre-road friction as well as the vehicle speed is considered to be prescribed.
- This thesis only covers parts that are currently used in trucks.

2 Modelling

Pursuant to the Objective of section 1.4, this thesis work aims to design a system that is able to control the vehicle's steering. In this context, steering refers primarily to the ground vehicle motion and not to the change in the directional angle of the steerable wheels. Accordingly, the motion control system's task is to control the vehicle dynamics in longitudinal and lateral direction, which is based on the global forces and moments. Therefore, the control system has to be model-based which implies the derivation of a vehicle model. Furthermore, the vehicle model is used for the validation of the simulation results.

This chapter deals with the modelling of components and subsystems which are assigned to the objective of controlling the vehicle dynamics only with the wheel brakes. Consequently, it is important to model the elements which link the braking to the global forces and moments, illustrated in the subsequent Figure 2.1.

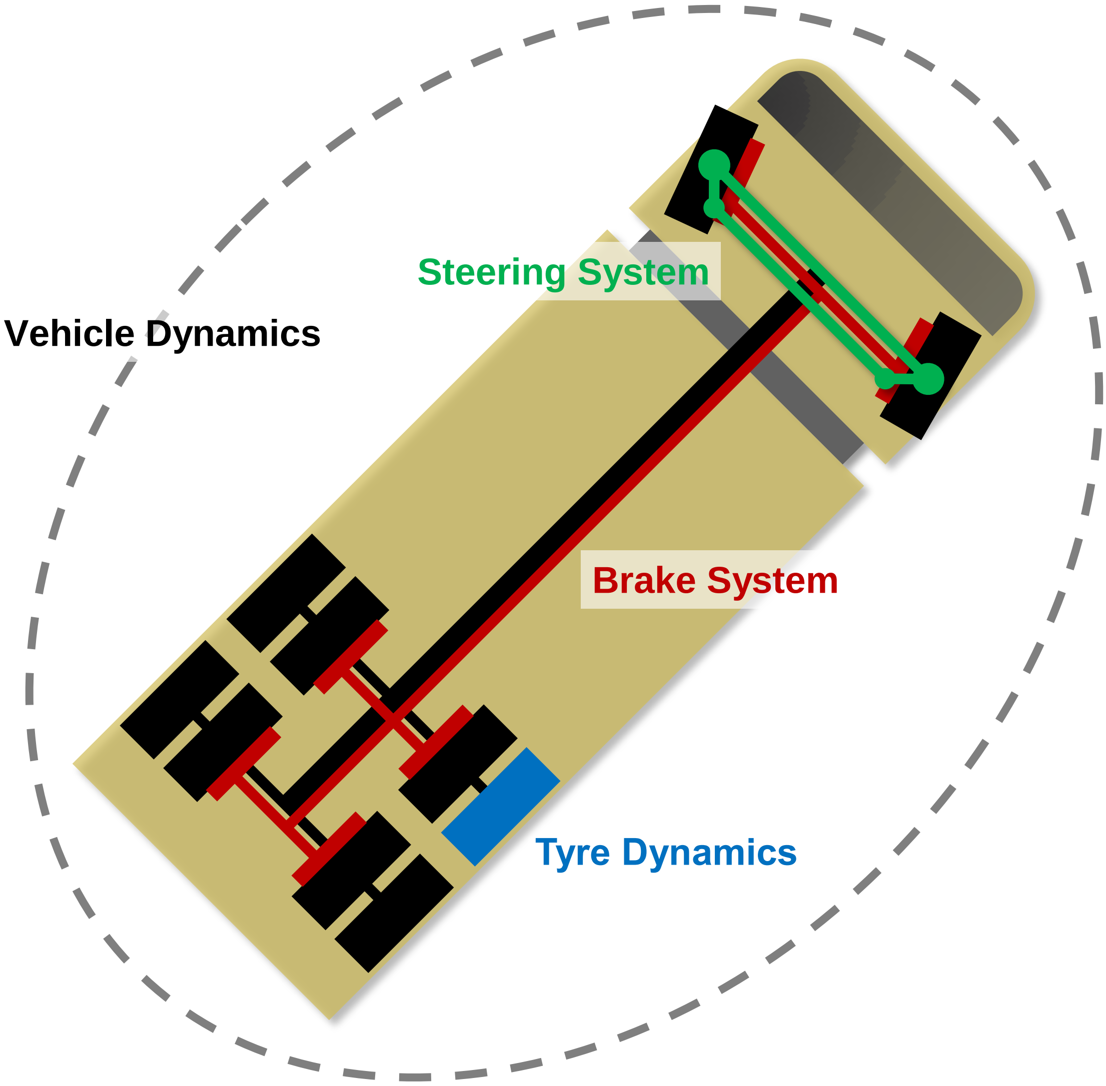

Figure 2.1: Overview of the modelled components and subsystems for the motion control system

All the highlighted items from Figure 2.1 are discussed in detail in the following subchapters. For the purpose of simplification, the modelling only covers a single-unit, rigid 6x4-truck which is equipped with a steerable front axle and two non-steerable rear axles. As stated in the project Limitations, the rear axles are not driven by decoupling them from the engine. Therefore, the engine has no braking or propelling effect on the rear wheels.

2.1 Vehicle Dynamics

The description of the vehicle's dynamics follows the ISO 8855 standard (ISO, 2011), defining the principal terms for road vehicles. According to the standard, the vehicle dynamics are expressed by the forces and moments acting on the vehicle reference point. The latter is fixed to the vehicle sprung mass and forms the origin of the vehicle axis system. In this thesis work the location of the reference point with the axis system is located in the centre of gravity (COG).

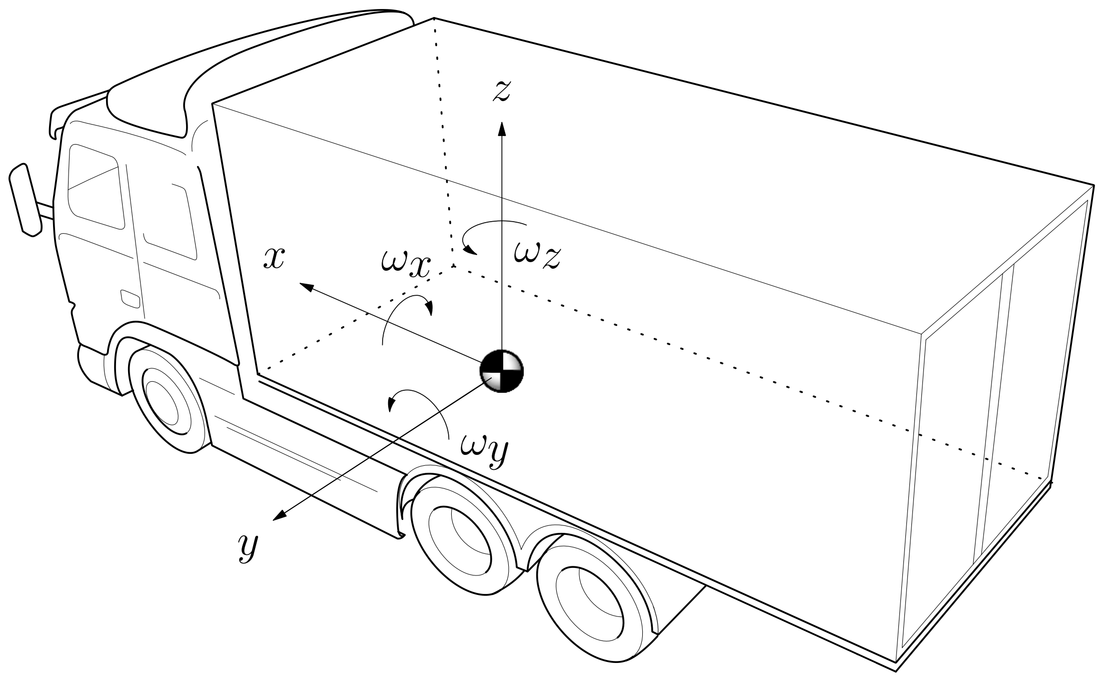

Figure 2.2: Vehicle axis system of the rigid 6x4 vehicle system (Källstrand, 2016)

The xy-plane of the vehicle axis system is connected to the body frame which is considered to be rigid. In accordance with the definition, the x-axis is pointing along the vehicle longitudinal axis in forward direction, while the y-axis points to the left side. The z-axis is perpendicular to this plane and points upwards. Whereas the standard uses the designation $X_V Y_V Z_V$, the vehicle coordinates are referred to as XYZ in this thesis work.

The Newton-Euler dynamics describe the transversal motion $\mathbf{v}$ as well as the rotational motion $\boldsymbol{\omega}$, which are defined in the vehicle axis system (Jazar, 2017), (Wiedemann, 2016) [1]:

$$\mathbf{v} = \begin{bmatrix} v_X \\ v_Y \\ v_Z \end{bmatrix} \quad (2.1)$$

$$\boldsymbol{\omega} = \begin{bmatrix} \omega_X \\ \omega_Y \\ \omega_Z \end{bmatrix} \quad (2.2)$$

Referring to the Deliverables in section 1.5, this thesis project aims to develop a system for controlling the manoeuvring dynamics of the vehicle. The manoeuvring primarily covers the transversal motions v_X and v_Y as well as the yaw rotation ω_Z. In comparison with these motion capabilities, the variations of the vertical velocity v_Z as well as the roll rotation ω_X and the pitch rotation ω_Y are low. As a consequence, their impact on the vehicle ground motion is minor and therefore negligible:

$$\dot{v}_Z = \dot{\omega}_X = \dot{\omega}_Y = 0 \quad (2.3)$$

Accordingly, the related forces and moments are assumed to be at equilibrium:

$$F_Z = M_X = M_Y = 0 \quad (2.4)$$

With these assumptions, the manoeuvring of the vehicle can be transitioned to a planar motion, which offers three degrees of freedom in the xy-plane of the inertial frame: longitudinal, lateral and yaw motion. As a result, the xy-planes of the vehicle frame and the inertial system are always parallel. The related planar dynamics of a rigid vehicle are described by the following Newton-Euler equations (Jazar, 2017):

$$\sum_i F_{Xi} = m(\dot{v}_X - v_Y \omega_Z) - F_{XR} = 0 \quad (2.5)$$

$$\sum_i F_{Yi} = m(\dot{v}_Y + v_X \omega_Z) - F_{YR} = 0 \quad (2.6)$$

$$\sum_i M_{Zi} + \sum_i x_i F_{Yi} - \sum_i y_i F_{Xi} = I_Z \dot{\omega}_Z - M_{ZR} = 0 \quad (2.7)$$

According to the Newton-Euler equations, the sums of the individual forces and moments induce a specific change in the vehicle motion, which is related to the chassis reference point, illustrated in the vehicle system of Figure 2.3. Conversely, the same change in motion can be assigned to representative forces and moments which act solely on the COG and are referred to as virtual actuation variables. Consequently, the virtual variables substitute the respective sums of forces or moments of the Newton-Euler equations:

---

[1] Note: In this report, all vectors are written in bold letters.

$$F_X = \sum_i F_{Xi} \tag{2.8}$$

$$F_Y = \sum_i F_{Yi} \tag{2.9}$$

$$M_Z = \sum_i M_{Zi} + \sum_i x_i F_{Yi} - \sum_i y_i F_{Xi} \tag{2.10}$$

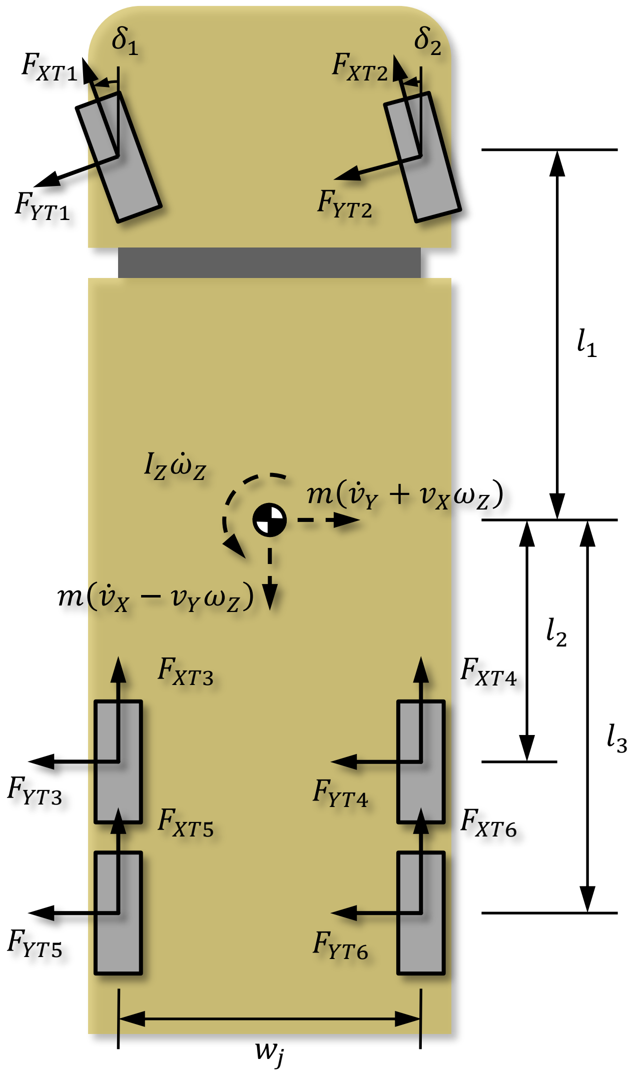

Figure 2.3: Vehicle system model of a rigid 6x4 truck, showing the vehicle actuation in the reference frame as well as the individual tyre forces in their respective axis system[2]

[2] Note: The illustration shows a simplified vehicle model with single tyres. The actual number of tyres per axle and side is then considered in the characteristics of the representative single tyre, for instance, twice the value of the cornering stiffness when dual tyres are mounted.

The index i denotes the tyre number, starting with the front left wheel. Besides, the numbering of tyres on the left vehicle side is odd.
The index j denotes the axle number, starting with the front axle.

The applied individual forces and moments in the Newton-Euler equations can be traced back to the bearing reactions between the wheel suspensions and the tyres. Hereby, the feasible bearing reaction depends on the respective type of bearing: Non-steerable wheels only have one degree of freedom (rolling, constant steer angle $\delta_i = 0$), whereas steerable wheels have two degrees of freedom (rolling, variable steer angle $\delta_i \in [\delta_{i,min}, \delta_{i,max}]$). Nevertheless, the origin of the forces and moments acting on the wheel suspension points is in the tyre-road contact zone of Figure 2.4.

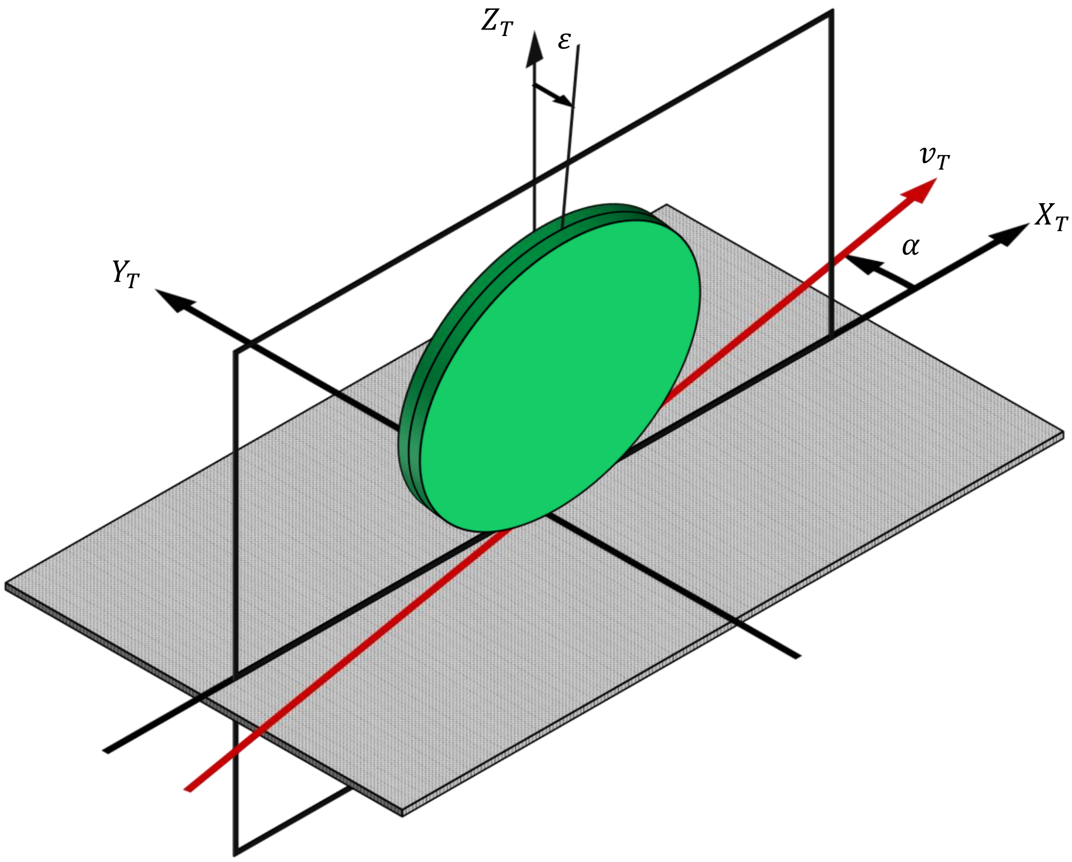

Figure 2.4: Tyre axis system according to the ISO standard (ISO, 2011). Grey: tyre-road contact plane, green: wheel plane

Each tyre uses an independent axis system, which is denoted as $X_T Y_T Z_T$ (ISO, 2011) and illustrated in Figure 2.4. Following the ISO standard, X_T and Y_T are placed in the tyre-road contact plane, having their origin fixed at the contact centre. In addition, X_T lies in the wheel plane, which is central to the rim flanges, and points forward, whereas Y_T is perpendicular to X_T. Note: Y_T is only perpendicular to the wheel plane if the wheel is not inclined ($\varepsilon = 0$). For reasons of simplification it is assumed that the road surface is level. This, together with the planar vehicle motion, results in the parallelism of the xy-planes of the vehicle frame and the individual tyre axis systems. Due to the displaceability of the tyre forces in z-direction, they are moved into the plane of the virtual variables. The individual tyre axis systems, and thus the tyre forces, are rotated by the steer angle δ_i of the respective wheel to the vehicle reference system. Consequently the tyre forces as well as the moment in z-direction can be transformed into the suspension point variables (Jazar, 2017):

$$F_{Xi} = F_{XTi} \cos(\delta_i) - F_{YTi} \sin(\delta_i) \tag{2.11}$$

$$F_{Yi} = F_{XTi} \sin(\delta_i) + F_{YTi} \cos(\delta_i) \tag{2.12}$$

$$M_{Zi} = M_{ZTi} \tag{2.13}$$

The aligning moment M_{Zi} results from the dynamic and geometric displacement of the tyre contact centre to the intersection point of the wheel suspension axis or the steering axis with the road plane. As this displacement is small in relation to the vehicle geometry, the aligning moment is neglected:

$$M_{Zi} \approx 0 \tag{2.14}$$

In the next step, the sums of the wheel suspension forces of the virtual actuation variables in the definitions (2.8), (2.9) and (2.10) are substituted by the particular tyre force formulations (2.11), (2.12) and (2.13). The vehicle geometry for the xy-positions in the yaw moment calculation is taken into consideration by inserting the longitudinal and lateral suspension positions in reference to the COG. Furthermore, the rear wheels of the considered vehicle are not steerable which is why their steer angles can be set to zero ($\delta_3 = \delta_4 = \delta_5 = \delta_6 = 0$). The application of the tyre force formulations together with the vehicle configuration results in the subsequent equations for the virtual actuation variables:

$$F_X = \sum_{i=1}^{2} (F_{XTi} \cos(\delta_i) - F_{YT1} \sin(\delta_i)) + \sum_{i=3}^{6} F_{XTi} \tag{2.15}$$

$$F_Y = \sum_{i=1}^{2} (F_{XTi} \sin(\delta_i) + F_{YT1} \cos(\delta_i)) + \sum_{i=3}^{6} F_{YTi} \tag{2.16}$$

$$\begin{aligned} M_Z = \sum_{i=1}^{2} \big(& l_1 \cdot (F_{XTi} \sin(\delta_i) + F_{YT1} \cos(\delta_i)) \big) \\ & + (-1)^i \frac{w_1}{2} (F_{XTi} \cos(\delta_i) - F_{YT1} \sin(\delta_i)) \\ & + \sum_{i=3}^{4} \left(-l_2 \cdot F_{YTi} + (-1)^i \cdot \frac{w_2}{2} \cdot F_{XTi} \right) \\ & + \sum_{i=5}^{6} \left(-l_3 \cdot F_{YTi} + (-1)^i \cdot \frac{w_3}{2} \cdot F_{XTi} \right) \end{aligned} \tag{2.17}$$

Due to a small deviation between the left and right front wheel angle, a combined steer angle is permissible ($\delta_1 = \delta_2 = \delta$). Furthermore, the trigonometric functions are replaced by the assumption of small steer angles ($\sin(\delta) = \delta$, $\cos(\delta) = 1$). This results in simplifications in the equations (2.15), (2.16) and (2.17):

$$F_X = \sum_{i=1}^{2}(F_{XTi} - F_{YT1}\delta) + \sum_{i=3}^{6} F_{XTi} \tag{2.18}$$

$$F_Y = \sum_{i=1}^{2}(F_{XTi}\delta + F_{YT1}) + \sum_{i=3}^{6} F_{YTi} \tag{2.19}$$

$$\begin{aligned} M_Z = &\sum_{i=1}^{2}\big(l_1 \cdot (F_{XTi} \cdot \delta + F_{YT1})\big) + (-1)^i \cdot \frac{w_1}{2} \cdot (F_{XTi} - F_{YT1} \cdot \delta) \\ &+ \sum_{i=3}^{4}\left(-l_2 \cdot F_{YTi} + (-1)^i \cdot \frac{w_2}{2} \cdot F_{XTi}\right) \\ &+ \sum_{i=5}^{6}\left(-l_3 \cdot F_{YTi} + (-1)^i \cdot \frac{w_3}{2} \cdot F_{XTi}\right) \end{aligned} \tag{2.20}$$

The equations (2.18), (2.19) and (2.20) represent the virtual actuation variables of the planar vehicle dynamics and are going to be used for the motion control in this thesis project. Due to the general approach, based on the number of axles and their relative position to the centre of gravity, the formulas can be easily adapted to various vehicle configurations.

2.2 Tyre Dynamics

The tyres form the frictional connection between vehicle and road surface. Due to the tyre deflection around the contact centre, this connection zone is a two-dimensional contact patch (light grey area in Figure 2.5). During the motion of the vehicle, forces are built up in the tyre-road contact zones. As outlined in the equations (2.18), (2.19) and (2.20) of the previous section about Vehicle Dynamics, the tyre forces result in a change of the planar vehicle motion. Conversely, this means that the virtual actuation variables can be actively influenced by controlling the tyre forces. In the previous Vehicle Dynamics chapter, tyres are regarded a rigid element on which the forces apply centrally. In contrast, this section on Tyre Dynamics describes the tyres as elastic components. For further consideration, the tyres as three-dimensional objects are reduced to their contact zones, since the forces originate there.

2.2.1 Tyre Contact Patch

According to the ISO standard 8855, the contact patch of every tyre is described in an independent axis system $X_T Y_T Z_T$ and the tyre contact plane is held by the vectors X_T and Y_T (ISO, 2011). Furthermore, X_T lies in the wheel plane and thus in the middle of the undeformed contact patch, whereas Y_T is perpendicular to the forward-pointing X_T-axis (see Figure 2.5).

During the vehicle motion, each tread element which is part of the current contact patch at the time t transmits an elementary force in both the longitudinal and lateral direction. The sum of all the elementary forces in X_T and Y_T results in a representative tyre force F_{XT} or F_{YT}, respectively (green force vectors in Figure 2.5). As soon as wheel torque is applied to brake or accelerate the vehicle, a certain longitudinal tyre force F_{XT} arises. On the contrary, a change in the heading direction of the vehicle due to steering commands, builds up lateral tyre forces F_{YT}. In course of this, the transmitted forces are the product of the longitudinal or lateral slip ratio and the respective tyre stiffness value C_{λ} or C_{α} (Pacejka, 2012). For simplification, the contact patch in Figure 2.5 is shown undeformed despite the applied forces F_{XT} and F_{YT}, which is why the point of force application is at the coordinate origin of the axis system (blue dot). In reality, however, the applied forces deform the contact zone, so that the point of force application is moved out of the stationary coordinate centre. The dynamics in the longitudinal and lateral are described in detail in the two following subchapters.

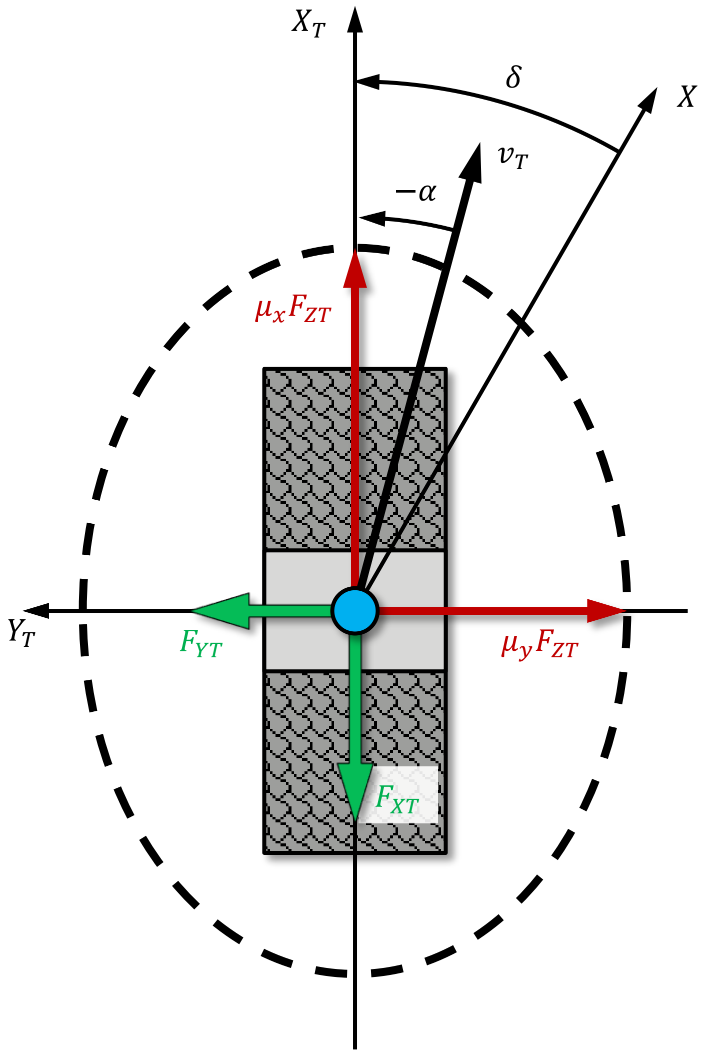

Figure 2.5: Tyre contact patch in the tyre coordinate system, illustrating the forces in longitudinal and lateral direction as well as the maximum forces which define the friction ellipse

Tyre membranes are composed of several layers in order to target specific characteristics such as flexibility or carrying capacity. The outer tread layer is made of rubber and defines the properties of the adhesive tyre-road contact zone (Thorvald, et al., 2011). Like every rubber friction connection the tyre-road contact zone is considered to be both nonlinear and complex as it is subject to various influencing parameters. The latter are considered in the tyre stiffness values describing the tyre properties with respect to their force generation capability in X_T- or Y_T-direction. It is important to note that longitudinal and lateral characteristics and thus the stiffness values differ from each other. As mentioned above, the stiffness values are dependent on several input parameters:

- Friction coefficient μ_{XT} and μ_{YT}
- Surface pressure in the contact patch due to the tyre normal load F_{ZT}
- Inclination of the wheel
- Temperature of road and tyre

The maximum available force is described in equations (2.21) and (2.22) as simplified, linear function of the tyre-road friction coefficient and the normal load (Pacejka, 2012).

$$F_{XT,max} = \mu_{XT} F_{ZT} \tag{2.21}$$

$$F_{YT,max} = \mu_{YT} F_{ZT} \tag{2.22}$$

In addition to the tyre normal forces, the calculation of the maximum forces requires the precise friction coefficients, which vary depending on the road surface. However, it is expensive to determine these friction values, which is why it is excluded from this thesis project (see Limitations). Instead, a friction estimator informs the control system about the road-tyre slip level. This estimator can either be an external function which determines the friction value online or it can be constant values that have been defined offline. Furthermore, it is assumed that the difference of the friction coefficients in longitudinal and lateral direction is negligible. Therefore, the common friction value μ is used in this project work.

$$\mu_{XT} = \mu_{YT} = \mu \tag{2.23}$$

Nevertheless, the friction coefficient may vary depending on the tyre position to give the control system the ability of handling split friction manoeuvres.

In reality, the relationship between maximum force and normal load is characterized in a nonlinear regression function. The reason for this disproportion is the increasing flattening of the tyre and the associated greater flexing, which reduces the stiffness. Consequently, any load transfer due to rolling and pitching will reduce the maximum acceleration or cornering ability of the vehicle, since the force transmission capability increases non-linearly with the tyre load. Due to this phenomenon, it is important for the manoeuvrability and driving safety to reduce oscillating normal loads that occur with any chassis motion, since the peak value of the normal load determines the maximum transmission performance (Wiedemann, 2016).

2.2.2 Longitudinal Tyre Dynamics

A longitudinal or circumferential tyre force F_{XT} is built up, when torque is applied to the respective wheel. With respect to vehicle dynamics, a positive wheel torque is applied to overcome the driving resistances and to accelerate the vehicle, while a negative wheel torque reduces the driving velocity.

If no wheel torque is applied, the wheel is considered to be free-rolling as it is free of longitudinal forces. The ratio of longitudinal speed v_{XT} at the wheel suspension point to angular speed ω_W of the free-rolling wheel is referred to as dynamic or effective rolling radius r_{dyn} (Pacejka, 2012).

$$r_{dyn} = \frac{v_{XT}}{\omega_W} \tag{2.24}$$

If distances are used instead of speeds, the driving distance of one tyre rotation corresponds to the circumference of a rigid, non-deformable wheel with the radius of r_{dyn}. Furthermore, the dynamic tyre radius is greater than the static, laden radius r_{stat} of a deflected tyre at standstill, but it is smaller than the radius r_0 of the unladen and undeformed tyre.

$$r_{stat} < r_{dyn} < r_0 \tag{2.25}$$

This definition is illustrated in Figure 2.6.

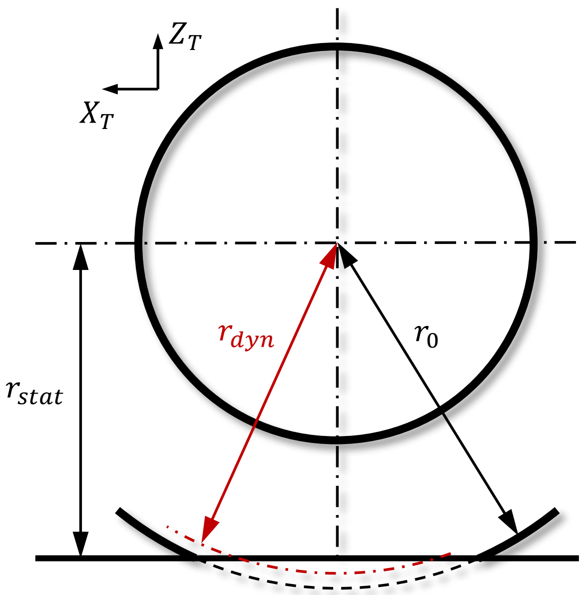

Figure 2.6: Tyre cross-section, outlining the dynamic radius r_{dyn}, the static radius r_{stat} and the unladen radius r_0

As soon as wheel torque is applied, the circumferential speed of the tyre changes and differs from the driving speed of a free rolling wheel v_{XT}. This difference in speed in relation to the driving speed v_{XT} is referred to as longitudinal slip λ, which arises in the contact zone (Pacejka, 2012).

$$\lambda = \frac{r_{dyn}\omega_W - v_{XT}}{v_{XT}} \tag{2.26}$$

If no torque is applied, the wheel is free rolling, because the speed difference in the numerator is zero ($\lambda_{free} = \lambda = 0$). In contrast, a positive wheel torque accelerates the wheel and increases its angular speed. Therefore, the wheel speed is higher than the speed of free rolling wheel, which results in positive slip value ($\lambda_{acc} = \lambda > 0$). Conversely, a brake torque reduces the wheel speed and causes a negative slip ($-1 < \lambda_{brake} < 0$). When the generated brake force exceeds the maximum longitudinal force allowed by the tyre-road friction (Equation (2.21)), the wheel locks ($\omega_W = 0$) and the slip decreases to its minimum of $\lambda_{lock} = \lambda = -1$.

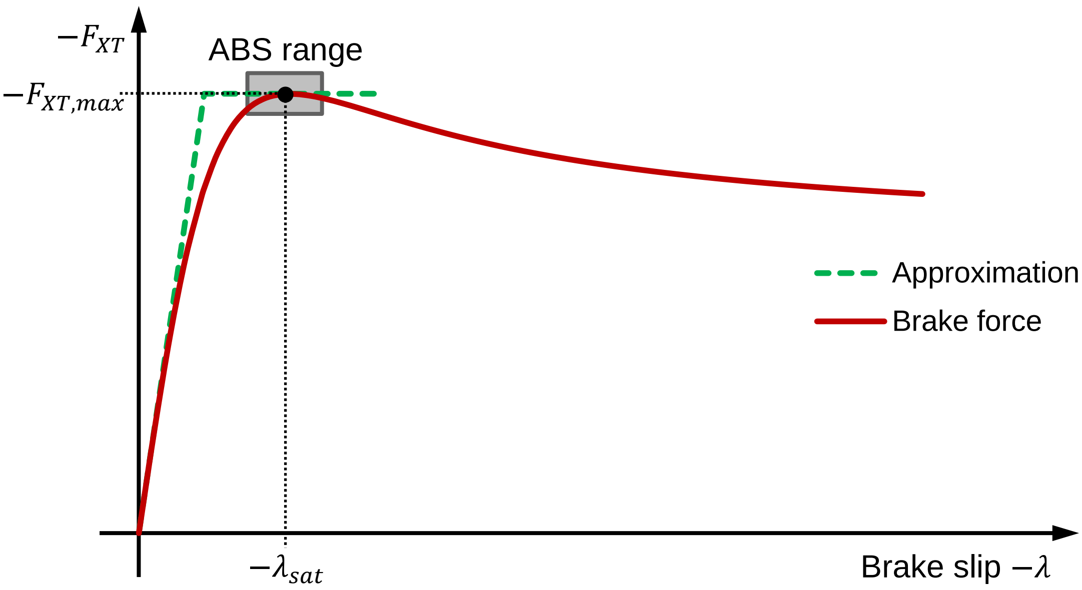

Figure 2.7: Longitudinal force as function of the braking slip (Pacejka, 2012)

The slip or the difference in the wheel speeds is compensated in the tread layer, by shearing of the elastic rubber elements. This shear deformation generates the circumferential tyre forces F_{XT} and simultaneously determines the force alignment. Due to the elastic rubber characteristic, a linear dependency between tyre force and deformation or slip can be assumed, which is shown as linear approximation from the coordinate origin of Figure 2.7. The longitudinal slip stiffness C_λ is the gradient of this linear relation and depends on various parameters such as normal load or friction (Section Tyre Contact Patch for more information). Once the tyre force reaches its maximum, the deformation of the elastic tread is considered to be saturated. The linear approximation is described in equation (2.27) and illustrated as straight line in Figure 2.7:

$$F_{XT} = \begin{cases} C_\lambda(F_{ZT})\lambda, \text{for } |\lambda| < \lambda_{sat} \\ \mu_x F_{ZT}, \text{for } |\lambda| \geq \lambda_{sat} \end{cases} \tag{2.27}$$

If the slip increases further, the tyre becomes instable as the maximum tyre force decreases and the tread elements begin to slide (Thorvald, et al., 2011).

Moreover, a sliding tyre is unable to build up cornering forces, which is why the vehicle's driving stability is impaired. For safety and stability reasons, the maximum slip is limited by the anti-lock braking system (ABS) to a value, which does not exceed the saturation slip λ_{sat}. A standard ABS limits the maximum slip in a range around $\lambda_{ABS} = 10\%$ to ensure enough cornering forces to steer the vehicle (grey area in Figure 2.7) (Breuer & Bill, 2012). In reality the force curve progression as well as the maximum force for traction and braking are different because of the tyre structure.

As mentioned in the Objective, the wheel brakes are the only available actuators for the system to control the vehicle dynamics. Consequently, only the longitudinal forces of the tyres can be directly controlled via the wheel brakes. Accordingly only negative tyre forces and slip values can occur.

2.2.3 Lateral Tyre Dynamics

The lateral or cornering tyre forces F_{YT} are required to alter the heading direction of the vehicle and to stabilize the vehicle in its motion. As in the longitudinal dynamics, the rubber elements in the tread layer of the tyre have to be sheared in order to build up lateral tyre forces. The mentioned shear deformation arises, when the wheel plane is rotated by the slip angle α against the vehicle velocity v_T in the wheel suspension point (see Figure 2.5, which is based on a dynamic vehicle model to allow slip angles at the tyre plane). This directional deviation is compensated by the shear of the tread layer, resulting in a cornering tyre force F_{YT} (Thorvald, et al., 2011). In the definition, α is the angle between the velocity vectors which have been mapped on the X_T-axis in tyre frame:

$$\alpha_i = \operatorname{atan}\left(-\frac{v_{YTi}}{v_{XTi}}\right) \tag{2.28}$$

Using the assumption of small angles, the slip angle can be expressed by the global dynamic values in the vehicle reference frame (sideslip angle β, vehicle velocity v and yaw rate ω_Z) together with geometric data (steer angle δ_i and the wheel base l_i) (Wiedemann, 2016):

$$\alpha_i = \delta_i - \beta + \frac{l_i}{|v|} \cdot \omega_Z \tag{2.29}$$

The cornering force F_{YT} as function of the slip angle α is point symmetric to the coordinate origin (Figure 2.8). In addition, the tyre force F_{YT} is always opposing the lateral velocity v_{YT} and thus the slip angle α. Furthermore, the force characteristic can be divided into three different sections:

- Elastic: For small slip angles, a linear relation between lateral force and slip angle is assumed because of the elastic characteristic of the rubber tread layer. The lateral or cornering stiffness C_α is the gradient of this linear function.
- Transitional: The lateral force increases up to the maximum cornering force $F_{YT,max}$ in a nonlinear regression function of the slip angle.
- Frictional: The increase of the slip angle results in a decreasing lateral force, since the tyre starts to slide and becomes instable.

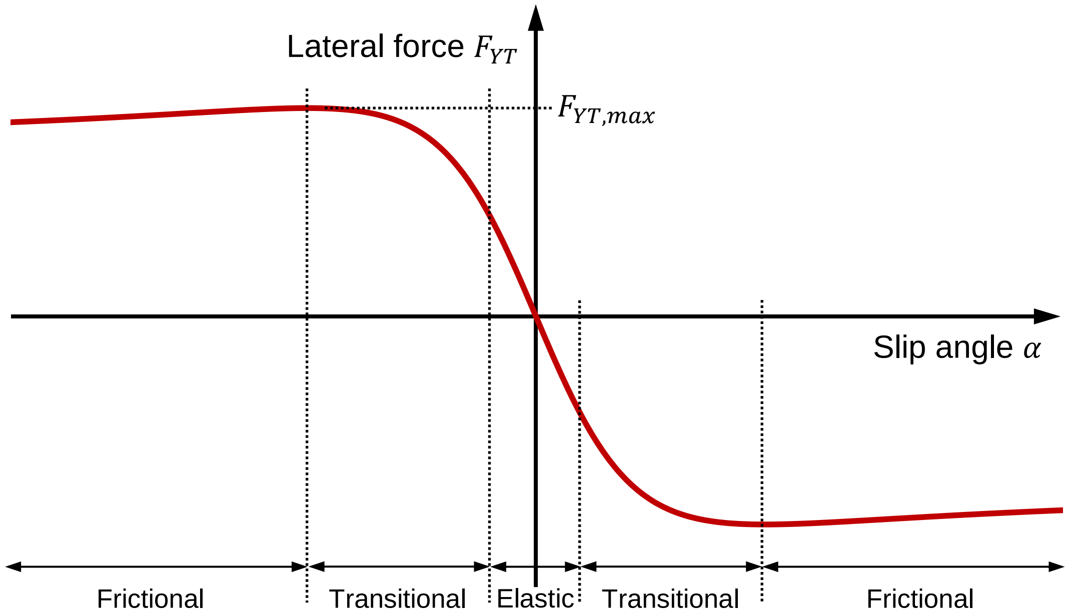

Figure 2.8: Lateral tyre force in dependence of the tyre slip angle α in normalised axis system. Presentation of the different tyre property sections (Thorvald, et al., 2011)

The cornering stiffness describes the tyre characteristics in the elastic region and is defined in the coordinate origin of the tyre force function (Thorvald, et al., 2011):

$$C_\alpha = -\left(\frac{\partial F_{YT}}{\partial \alpha}\right)_{\alpha=0} \tag{2.30}$$

For the description of the lateral tyre dynamics there exist models with different levels of complexity. Among these models, the physical brush model as well as the empirical model of Pacejka are widely used. The latter describes the tyre dynamics with a mathematical formula, which is the so called "magic formula" (Equation (2.31) and illustrated in Figure 2.9). This formula is based on force curves from measurements and requires characteristic tyre values such as the peak force $F_{YT,max}$ or the specific Pacejka stiffness factor B (Equation (2.32)) as input parameters. In addition, the shape factors C and E allow the adaption of the magic formula to the measurement data (Pacejka, 2012).

$$F_{YT}(\alpha) = F_{YT,max} \cdot \sin[C \arctan\{B\alpha - E(B\alpha - \arctan(B\alpha))\}] \tag{2.31}$$

$$B = \frac{C_\alpha(F_{ZT})}{C \cdot F_{YT,max}} \tag{2.32}$$

The Pacejka model defines the cornering stiffness as a trigonometric function of the tyre normal load together with the shape constants c_1 and c_2 (Pacejka, 2012)

$$C_\alpha(F_{ZT}) = c_1 \sin\left\{2 \arctan\left(\frac{F_{ZT}}{c_2}\right)\right\} \tag{2.33}$$

In this thesis work, the magic formula is approximated with a linear saturated function of the lateral tyre force (Equation (2.34)). This approximation describes a linear relation between cornering force and slip angle within the saturation limits $\alpha \in [-\alpha_{sat}, \alpha_{sat}]$. Once the slip angle exceeds the saturation slip angle α_{sat}, the lateral force is constant at the level of the maximum force $F_{YT,max}$ (Stoerkle, 2013).

$$F_{YT}(\alpha) = \begin{cases} -C_\alpha(F_{ZT})\alpha, \text{ for } |\alpha| < \alpha_{sat} \\ \mu_y F_{ZT}, \text{for } |\alpha| \geq \alpha_{sat} \end{cases} \tag{2.34}$$

For truck tyres without longitudinal slip, the saturation slip angle is about $\alpha_{sat} = 10°$ (Pacejka, 2012). The magic formula and the linear saturated approximation are compared in Figure 2.9.

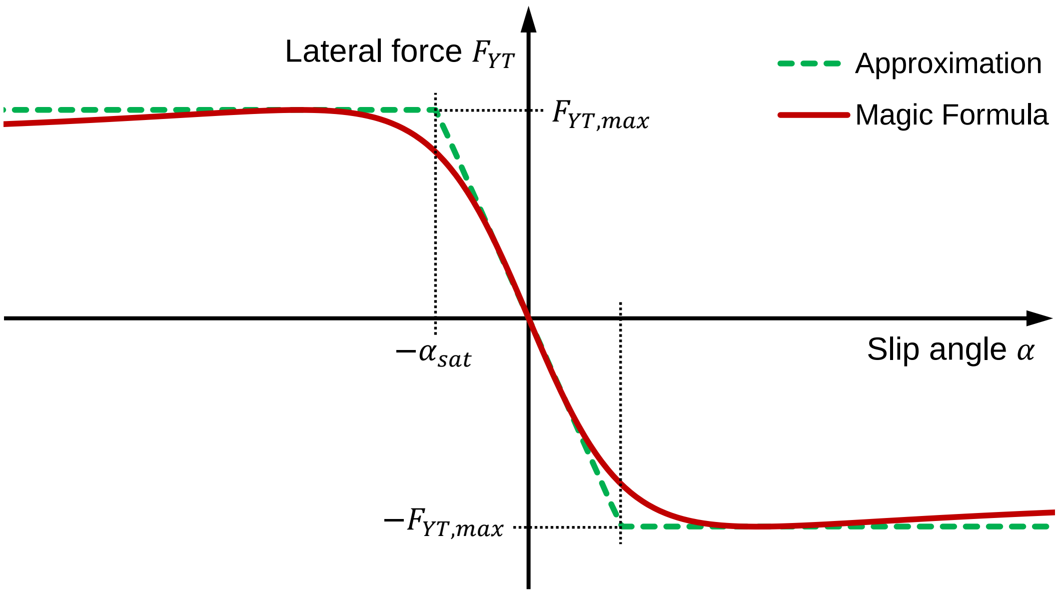

Figure 2.9: Lateral tyre force in dependence of the tyre slip angle α in normalised axis system. Comparison of the linearized approximation and Pacejka's tyre model (magic formula) (Pacejka, 2012)

In reality, the cornering tyre force F_{YT} causes an asymmetric deformation of the contact patch, which results in a longitudinal displacement of the point of force application towards the rear. This displacement is known as pneumatic trail t_p and is assumed to be constant in the elastic range of the force characteristic. Consequently, any lateral force in combination with the pneumatic trail results in an aligning moment, which tries to reduce the slip angle. (Thorvald, et al., 2011)

The previously considered models and functions represent the lateral force only in steady state. However, the step response of tyre force corresponds to a first-order system due to relaxation in the different layers (Wiedemann, 2016). Due to the complexity of measuring the step response of a truck tyre, the lateral dynamic characteristic is considered to be proportional.

2.2.4 Combined Tyre Dynamics

The Objective of this thesis is to control vehicles motion and in particular the yaw motion exclusively with the wheel brake actuators. Therefore, both circumferential and cornering tyre forces occur in all driving situations and apply together at the same rubber elements of the contact patch. Through this, the tread of the tyre is sheared in X_T- and Y_T-direction simultaneously, resulting in a combined force $F_{T,res}$ and a combined tyre slip λ_{res}. As a consequence, the tyre dynamics in longitudinal and lateral direction cannot be considered independently like in the previous subchapters 2.2.2 and 2.2.3. Instead, the combined tyre force $F_{T,res}$ is the sum of the applied force vectors in the directions X_T and Y_T (Breuer & Bill, 2012):

$$\left|F_{T,res}\right| = \sqrt{F_{XT}^2 + F_{YT}^2} \tag{2.35}$$

According to equation (2.35), the elements of the tread layer are sheared with the force $F_{T,res}$, which is always higher than one of the single forces. Consequently, the saturation limit of the tyre is defined by the combined force $F_{T,res}$. For reasons of vehicle stability, it is important to prevent the saturation of the tyre as the rubber elements of the contact zone begin to slide, reducing the transmittable tyre force in longitudinal and lateral direction.

The friction ellipse provides a straightforward, geometric approach to determine the tyre capacities for combined forces (dashed ellipse in Figure 2.5): Whereas the ellipse itself describes the friction and saturation limitation of the tyre, the bounded area indicates the adhesion range of the tyre contact patch. The friction ellipse is defined by the maximum permissible tyre forces $F_{XT,max}$ and $F_{YT,max}$, which are based on the tyre-road friction (Equations (2.21) and (2.22)) and represented by the semi-axis. Due to tyre properties, slightly higher long forces can be generated in longitudinal direction, which is why the semi-major axis points along the X_T-axis (Breuer & Bill, 2012). The adhesion area of the ellipse is described in equation (2.36) (Jazar, 2017).

$$\left(\frac{F_{XT}}{\mu_x F_{ZT}}\right)^2 + \left(\frac{F_{YT}}{\mu_y F_{ZT}}\right)^2 \leq 1 \tag{2.36}$$

With the simplification of (2.23), the maximum force in all directions and hence the semi-major and the semi-minor axis of the ellipse are equal, resulting in a friction circle. The radius of this friction circle is determined by the maximum tyre force μF_{ZT}.

In accordance with the Objective of this thesis, the control system can only utilize the wheel brakes to control the vehicle dynamics. Consequently, the controller requires information about the brake and tyre capabilities. Due to the fact that the controller is only able to directly control the longitudinal tyre force via the wheel brakes, the lateral force occupancy of the tyre is an input to the system and determines the maximum permissible circumferential force:

$$F_{XT} \leq \mu_x F_{ZT} \cdot \sqrt{1 - \left(\frac{F_{YT}}{\mu_y F_{ZT}}\right)^2} \tag{2.37}$$

The information about the permissible braking force is then processed by the actuator limitation function, which calculates the allowable brake torque for each wheel. The knowledge of the permissible brake torque is important for two reasons: Firstly, the saturation of the tyres has to be avoided in order to ensure the driving stability. Secondly, the system requires information about the capabilities of the actuators and thus their contribution to the global goal of controlling the vehicle dynamics. The disregard of the actuator limitations would lead to an intervention of the ABS, so that the requested brake torque would be restricted, resulting in deviation from the expected and calculated vehicle motion.

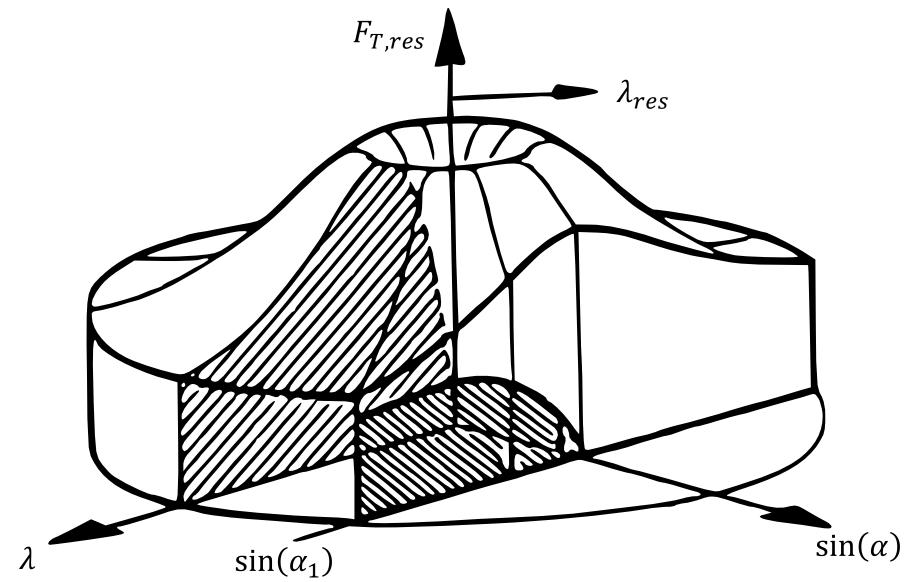

Figure 2.10: Spatial representation of the combined tyre forces in a friction cake chart (Weber, 1981)

The combined tyre characteristics can be represented spatially in a friction cake chart, wherein the combined force $F_{T,res}$ is a function of the longitudinal slip λ and the lateral slip $\sin(\alpha)$ (see Figure 2.10). The function and thus the diagram are defined by the pure longitudinal tyre dynamics along the λ-axis and the pure lateral tyre dynamics along the $\sin(\alpha)$-axis. Consequently, this allows the specification of the combined tyre dynamics in every operating status (λ, $\sin(\alpha)$) (Weber, 1981).

Moreover, the application combined forces entails a change of the tyre force characteristics in longitudinal and lateral direction: When the slip angle α increases from 0 to α_1, the longitudinal dynamics in Figure 2.10 changes from the shaded characteristic along the λ-axis (pure longitudinal tyre dynamics) to the shaded characteristic, which has been shifted parallel by $\sin(\alpha_1)$. Therefore, an increasing slip angle reduces not only the maximum permissible brake force but also the gradient C_λ of the characteristic curve. Consequently, the same brake force F_{XT} will cause a higher longitudinal tyre slip. Conversely, the cornering stiffness C_α is reduced, when a brake force F_{XT} is applied. As a result, the same lateral force F_{YT} will cause a wider slip angle which impairs the yaw stability. To conclude, the vehicle stability and the tyre stiffness values are influenced by combined tyre forces. Nevertheless, the tyre stiffnesses are assumed to be constant in this thesis project.

2.3 Steering System

The principal task of the steering system is to determine the heading direction of the vehicle by adjusting the steer angle of the wheels. According to the equations (2.29) and (2.34) a particular slip angle occurs as function of the steer angle and the vehicle state, resulting in a lateral force on the steered tyre. Consequently, the steering system enables the direct control of the yawing motion of the vehicle, which is why it is considered to be safety-critical. The components of the steering system can be assigned in two groups:

- Steering actuators: The actuators exert a force/torque on the steering mechanics, in order to control the steer angle of the wheels. As stated in Objective, the aim of this thesis project is to develop a fall-back level for the existing steering actuators, which is based on the wheel brake actuators.
- Steering mechanism: The mechanism allows the wheels to turn and transmits the force/torque from the actuators. In this thesis project, it is assumed that the mechanical parts always work correctly.

2.3.1 Electronic Steering Actuator

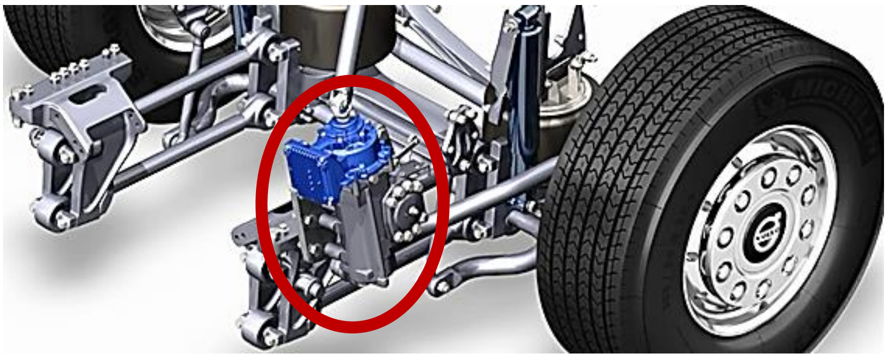

Figure 2.11: Steered rigid front axle of a Volvo truck which is equipped with the VDS module (red circle), connecting the vertical steering shaft with the horizontal steering rod. (AB Volvo, 2017)

Volvo introduced the Volvo Dynamic Steering (VDS) to improve the manoeuvrability, the driving comfort as well as the driving safety of heavy vehicles. The technical basis for the innovative VDS is the steerable front axle, which is either rigid or with independent wheel suspension. Depending on the embodiment, the steering mechanism is an Ackermann steering with a steering gear or a rack-and-pinion steering. In the steering mechanism, the

VDS is connected to the steering shaft, as shown in Figure 2.11 (Volvo Group Trucks Technology, 2016).

The VDS system itself extends the existing hydraulic power steering module by an electric power steering actuator and its associated control unit (Figure 2.12). Both actuators, the electric and the hydraulic, cooperate to generate a steering torque that turns the wheels. During the actuation, the output torque of the electric motor is electronically controlled by the computing unit and recalculated two thousand times per second. In normal driving situations, the electric motor adds a torque at low speeds to assist the driver in steering. At higher speeds, the VDS compensates for steering disturbances due to road unevenness or side winds (Volvo Group Trucks Technology, 2016).

Figure 2.12: The VDS system combines a hydraulic power steering (grey component) with an electric power steering actuator that receives commands from the flange-mounted control unit (blue component). (AB Volvo, 2017)

The output torque is calculated by the control unit, which considers the driver's steering request as well as steering disturbances. With regard to the future of automated driving, the VDS is suitable as steering actuator for heavy vehicles due to its electronic controllability, its dynamics as well as its maximum torque of $25\ \mathrm{Nm}$. The use of this existing steering actuator would save Volvo costs and time in the development and production of automated vehicles.

However, the current VDS design provides no redundancy, since the electric motor of is only equipped with a single coil. Therefore, mechanical stress, wear or external influences such as large magnetic fields can cause the motor to fail or to reduce its maximum output power. Considering the automation levels, the steering actuator is extremely safety critical and requires multiple levels of redundancy, which compensate either for a reduced performance or the overall failure of the primary steering actuator. Therefore, another independent system is required to guarantee the full fall-back performance for the automated driving.

In the case of failure, the VDS system either generates no output torque or only a small torque, which is opposed to the steering motion and can therefore be regarded as friction torque. Both cases result in a free-floating steering system with a constant additional friction torque. In contrast, blocking of the steering system can be excluded.

2.3.2 Steering Kinematics

In order to control the vehicle dynamics with the wheel brake actuators, the knowledge of the vehicle kinematics is essential. The equations (2.18), (2.19) and (2.20) describe the planar dynamics from a tyre based view, in which the tyre forces are coupled to the virtual forces and moment via geometric quantities. Due to the focus on a 6x4 truck model, solely the wheels of the front axle are steerable ($\delta_i \in [\delta_{i,min}, \delta_{i,max}]$), whereas the wheels of the two drive axles are rigidly pointing in longitudinal direction ($\delta_i = 0$). Besides the wheelbase and the track width of the individual axles, the steer angle of the wheels is the only geometric quantity which affects the virtual variables of the planar motion. Consequently, the motion capabilities of the steerable wheels and the connection between the wheels have to be defined by the steering kinematics (ISO, 2011).

Assuming a fully functional steering actuator, the steer angle of the front wheels can be adjusted by controlling the output torque of the actuator. In contrast to this, the malfunction of the steering actuator results in a limited or interrupted direct controllability of the steer angle. In case of an overall failure of the primary steering actuator, the steering system becomes free-floating with an opposing friction torque. Consequently, the steer angle has to be considered as geometric input or state variable for the control system.

Due to the free-floating characteristic of the steering system in the case of failure, there is no counteracting torque which compensates for the forces in the pivoted wheel suspensions to keep the steer angle constant. Therefore, the steer angle of the wheels becomes a function of the forces that are applied at the wheel suspension. The Objective of this project is to control the vehicle motion by using the brake actuators individually, resulting in an asymmetric distribution of the brake and tyre forces on all the axles. This creates a coupling between the braking forces of the front wheels, the steer angle and the virtual control variables. For this reason, the dependency between the wheel forces and the steer angle has to be integrated as a model in the control unit.

2.3.2.1 Front Axle Geometry

Figure 2.13: Steered rigid front axle for Mercedes-Benz trucks (Mercedes-Benz, 2014)

The model for the steer angle as function of the suspension forces can be derived from the kinematics of the steering system, which is described by the pivot joint to the steering knuckle with the wheel hub, the wheel suspension and the front axle itself. Modern heavy vehicles are mainly equipped with one of the following front axle and wheel suspension combinations (MAN Truck & Bus AG, 2016):

- Steered axle with a rigid wheel suspension and a sprung axle suspension on the vehicle chassis(Figure 2.13)
- Steered axle with an individual wheel suspension and a rigid axle suspension on the vehicle chassis (Figure 2.14)

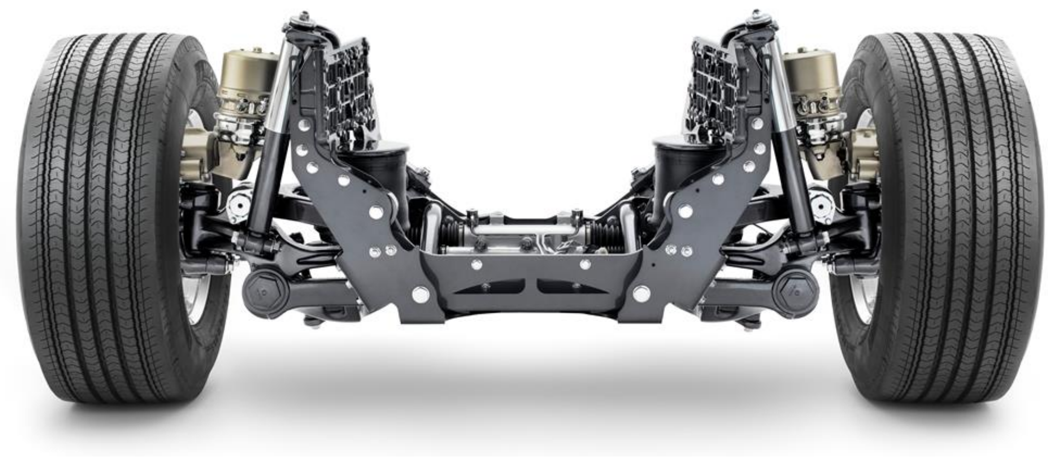

Figure 2.14: Steered axle with individual front suspension for Volvo trucks (AB Volvo, 2017)

In the direct comparison of the two axle types, the complexity in the assembly of the axle with independent suspension is significantly higher. Apart from that, the main difference is the kinematic for the vertical movement of the wheels. As the designation shows, the independent wheel suspension makes an independent movement of each wheel possible. Conversely, the wheels of the steered axle with a rigid wheel suspension are connected in a stiff way. Therefore, any vertical movement of one wheel is transferred to the other wheel, so that the wheels influence each other. Furthermore, the unsprung weight of an axle with individual suspension is lower, since only the wheel moves independently and the axle is rigidly connected to the body frame. As a result, the independent suspension reduces the vertical motion of the chassis while increasing the road holding. Consequently, the driving performance as well as the driving safety is enhanced (MAN Truck & Bus AG, 2016). In addition, the vertical movement of the front wheels changes the steer angle due to the suspension kinematics (ISO, 2011).

Since the vehicle motion is considered to be planar, the vertical movement of the wheels and the associated change in the steer angle are not considered any further. Moreover, the different steering mechanisms (Ackermann steering or rack-and-pinion steering) can be neglected, as they mainly affect the input from a steering actuator or the driver. Both mechanisms can be reduced to the steering link between the wheels, which is assumed to be stiff. Consequently, the axle type is of minor interest for this thesis work.

2.3.2.2 Kingpin Geometry

Irrespective of the differences between the axles and the wheel suspensions, the design of the pivot joint to the steering knuckle, which is referred to as kingpin, is always similar. This special joint is illustrated in the example of an axle with independent suspension in Figure 2.15. The same kingpin geometry is shown in a more detailed view as a technical drawing in Figure 2.16. It should be noted, that the wheels are pointing straight ahead (steer angle $\delta = 0$), which is why the tyre coordinate system and the vehicle frame are parallel.

Figure 2.15: Kingpin geometry of a steerable front axle. The red pointed line shows the axis of rotation which is determined by the kingpin mounting. The blue line marks the lateral centre line of the contact patch whereas the wheel plane points out the longitudinal centre line (AB Volvo, 2017)

The kingpin joint is tilted and consists of an upper and lower pivot point. Towards the wheel, these two hinges are rigidly attached to the steering knuckle, while their connection with the wheel suspension and thus the chassis is rotatable by the kingpin bolt (Kkandiyil, 2016). This design allows the wheel and hub assembly to rotate relative to the vehicle frame (ISO, 2011). The inclination and position of steering axis is determined by the two pivot points of the kingpin joint (Kkandiyil, 2016). Since the steering axis is defined in the vehicle coordinate system, its tilt can be divided into the caster angle τ in X-direction as well as the inclination angle σ in Y-direction (ISO, 2011).

As shown in Figure 2.15 and Figure 2.16, the intersection point of the steering axis with the tyre contact plane does not coincide with the application point of tyre forces (blue point in Figure 2.16). Furthermore, the wheel rotates about the kingpin axis. As a result, the distance between the point of force application and the intersection point constitutes a lever for the tyre forces, which is defined in the tyre coordinate system (ISO, 2011). Consequently, this lever arm can be decomposed in a lever along the X_T-axis for the lateral forces, which is the sum of the mechanical trail t_m and the pneumatic trail t_p.

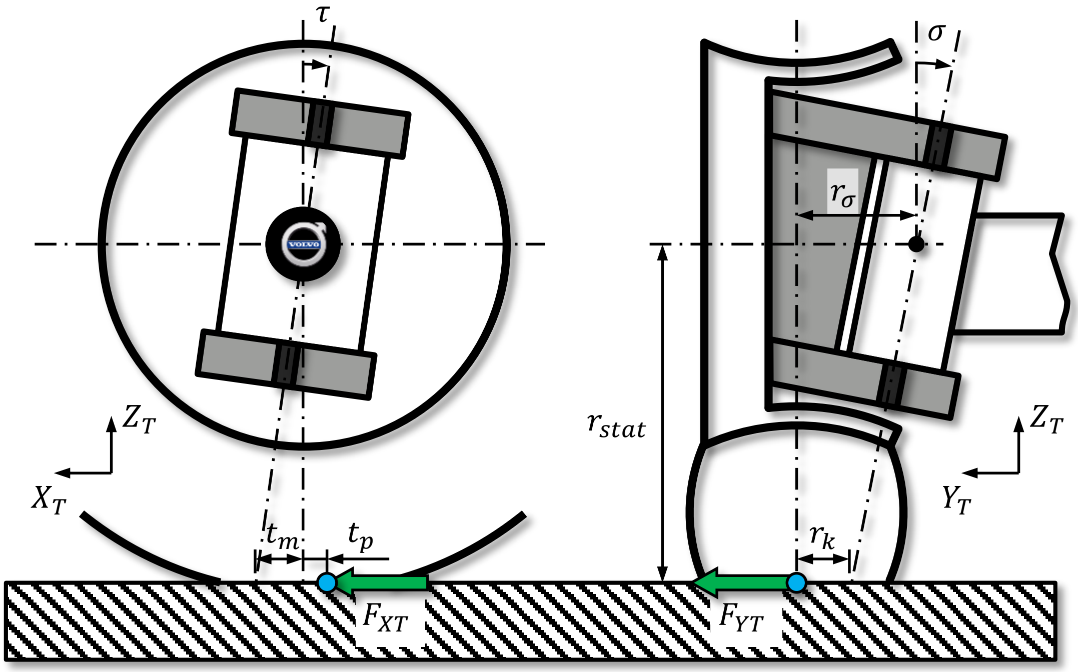

Figure 2.16: Kingpin geometry of the left front tyre at a steer angle of $\delta = 0$. The tilt of steering axis can be segmented into caster angle τ and inclination angle σ. Kingpin-axis offset over ground in X_T and Y_T, since tyre centre and steering axis do not coincide in the ground plane. Steering knuckle in grey, pivot points in black

As described in section about the Lateral Tyre Dynamics, the lateral tyre forces deform the contact patch asymmetrically, so that the point of force application is moved to the rear by the length of the pneumatic trail. In contrast, the mechanical trail is a kinematic value, which can be derived from the caster angle and the static tyre radius.

$$t_m = r_{stat} \cdot \tan(\tau) \tag{2.38}$$

The lever for the longitudinal forces in Y_T-direction is called steering-axis offset at ground r_k. The latter is often mistakenly referred to as scrub radius which is the distance from the tyre contact centre to the intersection point of the steering axis (ISO, 2011). The size and the sign of the steering-axis offset r_k are dependent not only on the inclination angle but also on the static tyre radius as well as the offset at the wheel centre r_σ. This offset corresponds to the distance from the wheel hub to the kingpin axis and is referred to as kingpin offset at wheel centre.

For reasons of driving stability, the caster angle is positive for all vehicle types, which is why the steering axis always intersects the tyre plane in front of the contact centre. With an increasing caster angle, the driving stability improves while the steering effort intensifies. The front axles installed in Volvo trucks have a caster angle of $\tau = 3°$.

Like the caster angle, the inclination angle σ is always positive, which means that the top of the steering axis is inclined inward (ISO, 2011). The kingpin axis of Volvo trucks is inclined by approximately $\sigma \approx 6°$. In contrast to the mechanical trail, the steering-axis offset at ground also depends on the distance between wheel hub and kingpin axis. In dependence of r_σ, the offset at ground can be positive or negative. Whereas a positive steering-axis offset reduces the steering effort and improves the returnability, a negative offset results in a stabilization of the vehicle handling (Kkandiyil, 2016). Due to the robust wheel hub and brake assembly in commercial vehicles, the distance between hub and kingpin axis is relatively large, which is why the offset at ground is always positive for truck steering axles. For this thesis project, it is assumed that r_k and t_m are constant and positive. In addition, camber and toe-in angle affect the steering system as well, but can be neglected due to their small impact.

2.3.3 Steering Dynamics

Due to the described Steering Kinematics, the tyre forces interact with the steering system (Gillespie, 1992). The dynamic steering response follows the applied moment in the system and turns the steerable wheels. This moment results from the applied forces in the tyre contact patch, which is why it can be described as functions of the tyre forces.

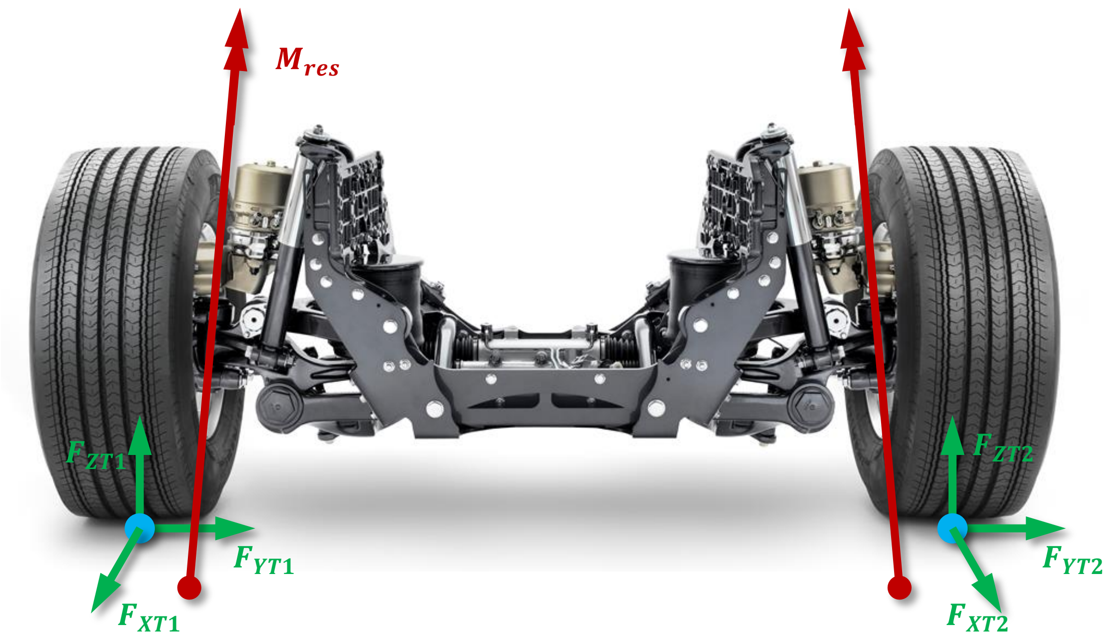

Figure 2.17: Interaction of the tyre forces with the steering system resulting in a moment M_{res}. The red line shows the inclined kingpin axis with the intersection point at ground. The blue dot defines the application point of the tyre forces and thus the origin of the tyre axis system. (AB Volvo, 2017)

Figure 2.17 illustrates the kinematic relation between the inclined steering axis and the application point of the tyre forces. As the steering intersection point does not coincide with the force application point, the tyre forces together with the offset result in a moment M_{res}, which turns the steerable wheels.

$$M_{res} = I_{Steer} \cdot \ddot{\delta} \tag{2.39}$$

In reality, the steer angles of the front wheels differ, since their turning radii around the centre of rotation vary in size. For the reason of simplification, this small difference can be neglected and the steer angles are assumed to be equal ($\delta_1 = \delta_2 = \delta$). Consequently, the tyre coordinate systems are always parallel. Furthermore, the approximation for small angles is valid for the steer angle as well as for the caster and kingpin inclination angle (Tagesson, 2017). Whereas the tyre forces are represented in their associated tyre axis system, the angles and moments are described in the global vehicle coordinate system.

In the following subchapters, the tyre forces and their influence on the steering moment are examined separately. The individual steering moment proportions are denoted according to the direction of the force. Furthermore, the steering kinematics combines the forces and moments of the two wheels.

2.3.3.1 Moment from the tyre longitudinal forces

The longitudinal tyre forces F_{XT} generate a steering moment M_{XT} which is linear to the steering-axis offset at ground r_k. As the moment at the left and right wheel is opposed, the moment M_{XT} is the difference of the forces.

$$M_{XT} = -(F_{XT1} - F_{XT2}) \cdot r_k \tag{2.40}$$

The effect of differential longitudinal forces is known from specific driving situations such as braking on split friction surfaces or getting up a kerbstone. Equally, the propelling forces of front wheel drive vehicles influence the steering.

According to equation (2.20) of the Vehicle Dynamics, differential longitudinal forces produce a yaw moment about the COG. At the same time, a negative r_k-value causes a steering motion which counteracts this yaw moment. Consequently, a negative steering offset at ground reduces the yaw motion by different longitudinal forces and stabilizes the vehicle motion in braking manoeuvres. Conversely, a positive offset at r_k generates a steering motion which amplifies the yaw moment: The braking of the left front wheel produces a yaw moment for a left turn and simultaneously turns the wheels to the left.

Pursuant to the Kingpin Geometry, the kingpin offset for heavy vehicles is assumed to be positive and constant. Hence, the differential brake moment at the front wheels generates a steering moment, which boosts the yaw motion. Inversely, the control of the differential brake moment gives the possibility of generating a steering moment and thus a steering motion. The steering moment by the longitudinal forces will be referred to as M_{Steer} in the further course of this work.

$$M_{Steer} = -M_{XT} = (F_{XT1} - F_{XT2}) \cdot r_k \tag{2.41}$$

2.3.3.2 Moment from tyre lateral forces

In most driving situations, lateral tyre forces occur when the wheels are steered and the vehicle is cornering. The lateral forces generate a moment M_{YT} which is linear to the longitudinal offset of the intersection point of the steering axis from the force application point (sum of mechanical trail t_m and pneumatic trail t_p). As this moment counteracts the steer angle, it is denoted as aligning moment.

$$M_{YT} = (F_{YT1} + F_{YT2}) \cdot \left(t_m + t_p\right) \tag{2.42}$$

2.3.3.3 Moment from the tyre normal forces

The normal load distribution on the steerable tyres causes a steering moment M_{ZT}. In the first term of the moment equation (2.44), the total vertical tyre load produces a returning moment, whereas the difference in the load distribution results a steering pull, which is expressed in the second term (Tagesson, 2017).

$$\begin{aligned} M_{ZT} = -(F_{ZT1} + F_{ZT2}) \cdot r_k \sin\sigma \sin\delta + (F_{ZT1} - F_{ZT2}) \\ \cdot r_k \sin\tau \cos\delta \end{aligned} \tag{2.43}$$

The approximation of small angles simplifies the previous equation (2.44):

$$M_{ZT} = -(F_{ZT1} + F_{ZT2}) \cdot r_k \cdot \sigma \cdot \delta + (F_{ZT1} - F_{ZT2}) \cdot r_k \cdot \tau \tag{2.44}$$

2.3.3.4 Friction moment

The various components of the steering mechanism cause friction, which can be combined in a steering friction moment M_{Fr}, which counteracts the steering motion. The main share of this friction moment can traced back to the steering gear or the rack-and-pinion gear, respective (Pfeffer, et al., 2008). In general, the steering friction is a function of the steer angle and its derivatives:

$$M_{Fr} = f\left(\ddot{\delta}, \dot{\delta}, \delta\right) \tag{2.45}$$

(Pfeffer, et al., 2008) developed the exponential-spring-friction elements (EFS) to the steering system, based on empirical research. This exponential friction model is a function of the steer angle and its first derivative. When the rotation reverses, the friction model switches between the branches for an increasing and decreasing steer angle. As shown in Figure 2.18, the two different branches produce a hysteresis in the friction characteristic. In the branch of a rising steer angle, the friction moment increases up to a maximum moment M_{lim} and remains constant. When the rotational direction reverses, the friction moment decreases and reaches a minimum moment $-M_{lim}$. It is assumed that the increase and decrease of the friction moment after a reversal point is linear. The linear coefficient k_{ESF} is determined by the stiffness of the system's mechanical components. Furthermore, a scaling factor allows the adaption of M_{lim}-value, which depends on the hydraulic pressure as well as the rotational speed (Pfeffer, et al., 2008).

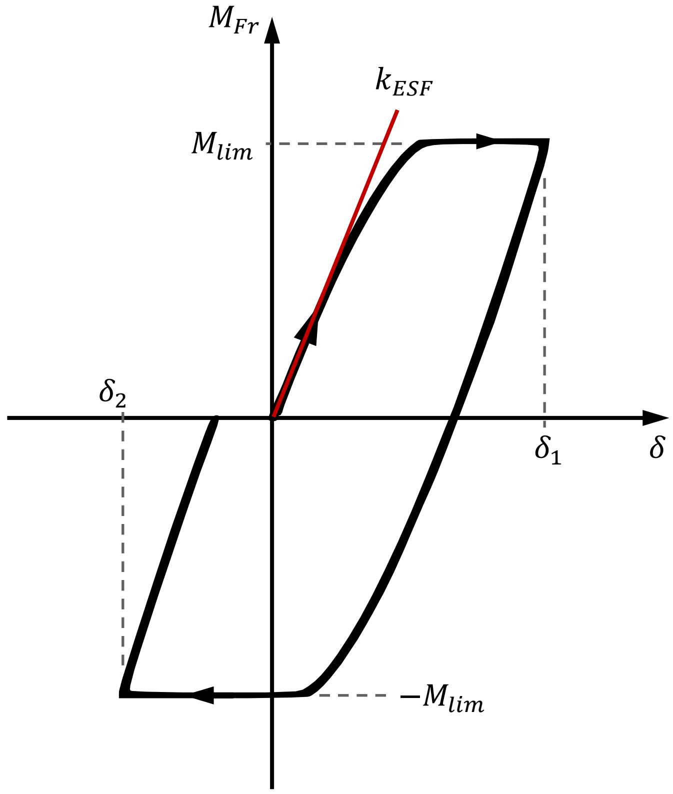

Figure 2.18: Exponential-spring-friction of the steering system. Maximum friction moment of $\pm M_{lim}$. Stiffness k_{ESF} expressing the linear characteristic after the reversal point (Pfeffer & Harrer, 2013)

The friction moment has a great influence on the characteristics and the controllability of the steering system. On the one hand, the friction reduces noise and damps oscillations, but on the other hand, it prevents the steering from going back to the central position. Whereas the hysteresis enables a human driver to drive a consistent corner, it impairs the controllability for a computing unit (Pfeffer & Harrer, 2013).

Regardless of the theoretical model, it is very difficult to measure the actual friction moment since it is a differential equation and has discontinuities. Furthermore, the friction moment changes with the wear of the components and the viscosities in the gears and bearings. Moreover, the friction moment of the faulty VDS is undefined and may be different from 0. Consequently, the controller has to be robust in order to compensate for these uncertainties.

2.3.3.5 Resulting moment in steer system

The resulting moment M_{res} is the difference of the steering moment M_{Steer} from the longitudinal forces and the counteracting moments from the lateral, normal and friction forces. The steering moment is controlled by the differential longitudinal tyre forces on the steerable wheel. In contrast the counteracting moments occur due to the vehicle or steering motion.

$$M_{res} = M_{Steer} - (M_{YT} + M_{ZT} + M_{Fr}) \tag{2.46}$$

The intended goal of this section is to maintain the controllability of the steering and thus the steer angle, although the VDS as primary steering actuator fails, by controlling the longitudinal forces with the wheel brakes.

In the term of the counteracting moments in equation (2.46), the aligning moment dominates over the moment from the normal forces and the friction moment. Therefore M_{ZT} as well as M_{Fr} are negligible.

$$M_{res} = M_{Steer} - M_{YT} \tag{2.47}$$

Whenever the moment difference is unequal zero ($M_{res} \neq 0$), the steering system shows a dynamic response. Conversely, the steering system is in steady state, when the steering and aligning moments cancel each other out. At the moment equilibrium, the steer angle of the system is stationary.

$$M_{Steer} = M_{YT} \tag{2.48}$$

The application of the aligning moment definition (2.42) in equation (2.48) yields:

$$M_{Steer} = (F_{YT1} + F_{YT2}) \cdot t \tag{2.49}$$

Assuming a non-saturated tyre, the lateral forces in equation (2.49) can replaced by the tyre dynamics definition (2.34) and the slip definition (2.29):

$$M_{Steer} = -(C_{\alpha 1} + C_{\alpha 2}) \cdot \left(\delta - \beta - l_1 \cdot \frac{\omega_Z}{v}\right) \cdot t \tag{2.50}$$

Subsequently, the difference of the longitudinal tyre forces is defined as differential tyre force ΔF_{XT}:

$$\Delta F_{XT} = F_{XT1} - F_{XT2} \tag{2.51}$$

In the next step, the steer moment as control variable in equation (2.50) is replaced by the definition of the differential tyre force (2.51) and the equation for moments from longitudinal tyre forces (2.41):

$$\Delta F_{XT} = -\frac{t_m + t_p}{r_k} \cdot (C_{\alpha 1} + C_{\alpha 2}) \cdot \left(\delta - \beta - l_1 \cdot \frac{\omega_Z}{v}\right) \tag{2.52}$$

The equation (2.52) demonstrates that the differential tyre force is a function of the actual steer angle in the steady state. Besides the steer angle, the differential force is dependent on various vehicle parameters:

- Vehicle state variables: sideslip angle, yaw motion and vehicle speed
- Vehicle geometry: wheel base
- Tyre dynamics: tyre stiffness and pneumatic trail
- Steering kinematics: mechanical trail, kingpin offset at ground (and steer angle)

In conclusion, the steer angle can be controlled by generating defined longitudinal tyre forces with the wheel brake actuators.

In contrast to the steady state solution of the steering system for a defined differential force, the dynamic response of the system is more complex and will not be modelled in this thesis project. Therefore, the system dynamics are determined and analysed with empirical methods.

In practice, the tyre forces are generated by the wheel brake actuators and can not be requested directly. Hence, the steering response is a combination of tyre, brake and steering dynamics. Consequently, the steering response can not be measured in isolation. Therefore, the simulation model of the truck is used to assess the dynamic characteristics of the steering system.

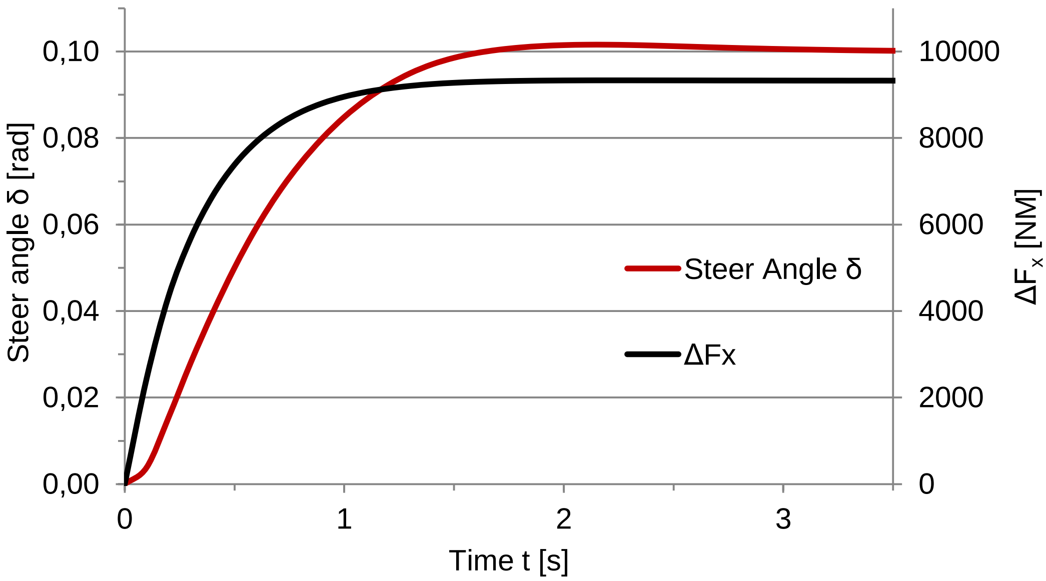

Figure 2.19: Simulation results of the dynamic response of the steering system when a differential longitudinal force ΔF_x is applied.

Due to the relaxation of the tyre tread layer, it is not possible to generate a step function of longitudinal tyre forces in the simulation model. Nevertheless, the simulation results in Figure 2.19 show that the steering system can be approximated and modelled as a stable second-order system.

2.4 Brake System

The main task of the brake system in terms of the global dynamics is the reduction and the control of the vehicle speed. Moreover, driving safety functionalities such as the electronic stability control system (ESC) actively engages the wheel brakes in order to stabilize the vehicle motion.

According to the Longitudinal Tyre Dynamics, the brake torque causes a negative tyre slip, as it reduces the wheel speed in relation to the vehicle speed. Due to the brake slip, a longitudinal force is produced in the tyre contact patch. On the one hand, the tyre forces are directly integrated in the virtual forces and yaw moment of the vehicle dynamics (Equations (2.18), (2.19), (2.20)) and on the other hand they interact with the steering system, as stated in equation (2.52) of the steering dynamics. Hence, the brake system is very powerful, since it enables the control of the vehicle dynamics and the steering. For this reason, the brake system is relevant for the vehicle's driving safety and has to meet stringent safety requirements in order to be highly reliable.

In this thesis project, the wheel brake actuators are used to control the vehicle dynamics as soon as the primary steering actuator fails. Since the controller is model-based, all components which affect the brake actuation have to be modelled. Therefore, the brake system technology as well as the important components are examined, before the dynamic characteristics are analysed.

2.4.1 Brake System Technology

Vehicles with a total mass exceeding 7.5 tonnes as well as truck combinations are equipped with a pneumatic power brake system, which is able to generate the required braking forces. In a pneumatic brake system, compressed air as working medium transmits the braking power and operates the wheel brake actuators. In comparison to the pneumatic systems, the braking performance of hydraulic systems with a brake booster is not powerful enough, which is why it is only installed in passenger cars or vans (MAN Truck & Bus AG, 2016).

Especially in long vehicles and alterable tractor-trailer combinations, pneumatic systems have several advantages over hydraulic systems, apart from the higher braking power. Firstly, the pressurised air as working medium is harmless to the environment. This is important because the truck's braking system consists of many components and also has separable connectors. Furthermore, the system is opened when a trailer is attached or removed. Hence, it is not possible to completely prevent small leakages and thus the escape of the working medium. In addition, the difference between the system pressure and the ambient pressure is relatively low, which is why the volume flow losses of leakages are minor and the hermetical sealing is simple. Secondly, the braking performance is still guaranteed for small leaks (Tagesson, 2017). Nevertheless, pneumatic systems have several disadvantages due to the working medium: Compressed air has to be constantly generated with energy, since it is consumed during braking and at the leaks. Furthermore, the compressibility of the medium together with the long air ducts causes delays in the brake dynamics (Day, 2014).

The pneumatic system is structured in several subsystems which have different tasks and scopes of application in order to guarantee a high reliability of the overall system through a multiple redundancy. During the vehicle movement, the service brake system provides the maximum braking power regardless of vehicle load, speed or road gradient. For safety reasons, the service brake system is designed as a dual circuit system in order to have the other brake circuit as a fall-back level when one circuit fails. The respective fall-back circuit is then referred to as secondary brake system, since it has a reduced braking performance in comparison to the dual circuit design. Nevertheless, the secondary system has to provide sufficient braking power to decelerate and halt the vehicle.

Whereas the service and secondary brake system act during the vehicle's motion, the parking brake system ensures the safe stationary halt at any road gradient. In contrast to the other two systems, the parking brake halts the vehicle purely mechanically. For all the systems, the driver has to be able to control them from the driving seat (United Nations Economic Commission for Europe, 2011). Apart from these systems, there are permanent brake systems, which do not use the wheel brake actuators. Instead, they brake the powertrain of the vehicle with an engine brake or a retarder (Day, 2014), (MAN Truck & Bus AG, 2016). The powertrain and thus the permanent brake systems are excluded from this thesis project.

The brake dynamics and delays of the pneumatic system can be enhanced by implementing an electronic control unit. This electro-pneumatic system is referred to as electronic brake system (EBS), since it activates the braking components electronically. Whereas the pneumatic system provides the braking power, the ECU individually controls the brake pressure and thus the brake power at the wheel brake actuators. Due to the electronic control and activation, the pressure response and build-up times are improved, resulting in an enhanced driving safety and comfort. In the EBS, the driver's brake pedal is decoupled from the brake system by establishing an electronic interface to transmit the command variable in form of a brake torque request to the brake ECU. This electronic layout enables other authorized high-layer functions to request a particular brake torque at each brake actuator. Moreover, it creates the opportunity to request an optimized, asymmetric brake torque distribution (MAN Truck & Bus AG, 2016). Optimisations can be made for various factors, such as different axle loads, individual brake wear or failure (Tagesson, 2017). Following the Objective of this thesis project, the individual brake torque distribution is optimized to control the vehicle and steering dynamics.

2.4.2 Brake System Components

The components of the electronic brake system in Figure 2.20 are divided into three groups according to their function for the braking operation:

- The ECU (green in Figure 2.20) of the electronic braking system is the central computing unit, which coordinates and controls the pneumatic components. On the input side, the control unit receives information about the pressure distribution in the pneumatic system as well as brake torque commands from the foot pedal module or other high-layer functions. Based on this information the controller calculates the pneumatic manipulated variables in order to fulfil the torque requests. Subsequently, these control variables are transmitted to the pneumatic components. To send and receive variables, the ECU is electronically connected to command and control modules via a CAN network.
- The pneumatic components (blue in Figure 2.20) are connected to each other via pipes and together they form the pneumatic brake system. The task of the pneumatic system is to generate, provide, transport and regulate the braking power. Via CAN bus, the components inform the control unit about the system status and, conversely, receive the brake pressure requests.
- The wheel brake actuators (red in Figure 2.20) transform the pneumatic energy into mechanical energy and generate the actual brake torque at the wheel hub.

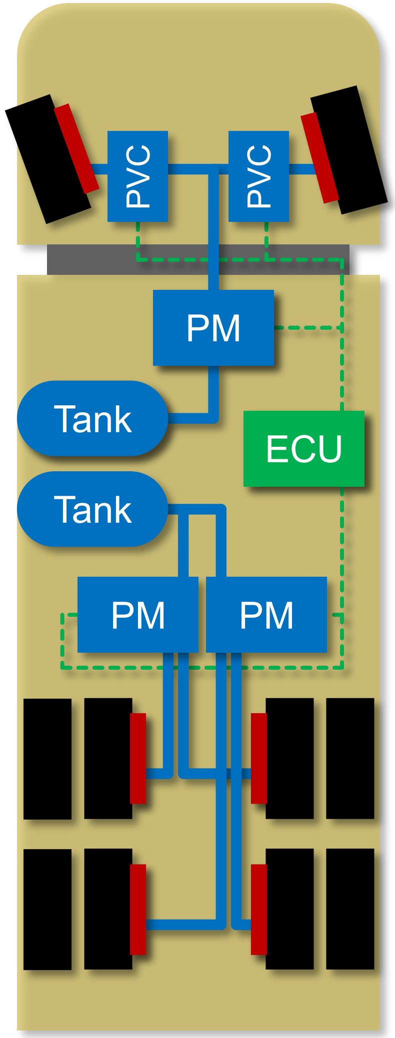

Figure 2.20: Main components of the electronic brake system in a commercial vehicle. Central EBS control unit (ECU); two pressure supply tanks for the dual circuit system; pressure modulators (PM) and pressure control valves (PVC), attached to the axles; wheel brake actuators which are attached to the wheels. The solid blue lines illustrate the pneumatic pipes for the brake power transmission whereas dashed green lines represent electric wires for the pressure signals

2.4.2.1 Pneumatic System

In the first step, the energy required for braking has to be produced in the form of pneumatic energy by pressurising the surrounding air with an air compressor, which is driven by the combustion engine. Since the braking power exceeds the compressing power, the pressurised air is stored in the supply tanks which are able to provide the pneumatic energy for several braking operations. The pneumatic layout is a dual circuit system, which is why each of the brake circuits is supplied by a separate tank. The supply pressure from the tanks is about 10 bars, which corresponds to the maximum braking pressure.

In the next step, the pressure modulators (PM) set the pressure to the wheel brake actuators. The modulators reduce the supply pressure to the brake pressures requested by the control unit. The rear axles are equipped with two-channel modulators, which are able to set the wheel-specific brake pressure directly through their two pneumatic outputs. In contrast, a one-channel modulator is attached to the front axle, which only outputs the higher of the two pressures to both wheel brakes. Consequently, the two downstream pressure control valves (PCV) are required to independently adjust the pressure to the respective wheel brake (Tagesson, 2017) (MAN Truck & Bus AG, 2016).

2.4.2.2 Wheel Brake Actuators

As mentioned in the introduction of the Brake System Components section, the brake actuators generate the actual brake torque. In commercial vehicles either drum brakes or disc brakes are used as brake actuators. The two types of wheel brakes differ in terms of construction, braking characteristics and performance.

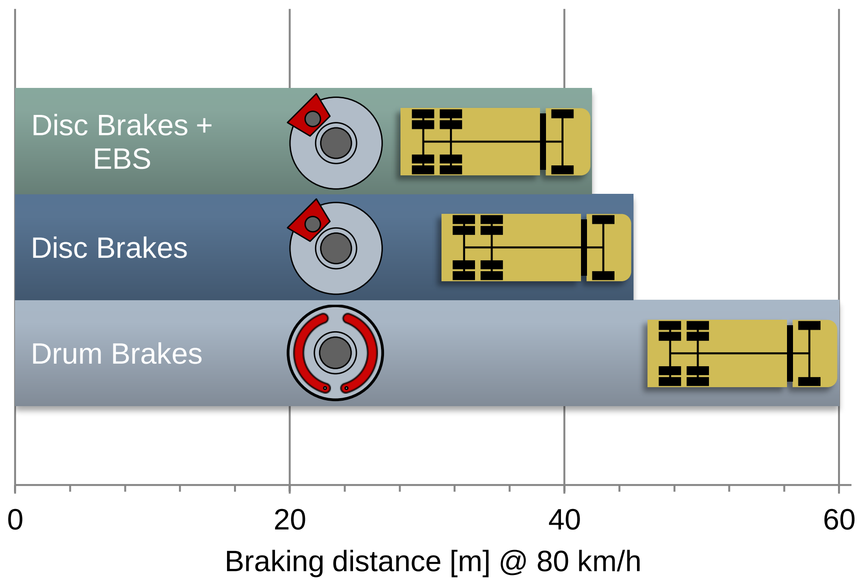

Figure 2.21: Braking distance from 80 km/h in dependence of the brake system technology (MAN Truck & Bus AG, 2016)

Due to the increasing requirements, more and more disc brakes are installed in modern commercial vehicles. The superiority of the disc brake actuators over the drum brakes in terms of braking performance and thus driving safety is illustrated in Figure 2.21. Apart from the shorter braking distances, the fading behaviour of the disc brake technology is reduced, so that the braking characteristics remain stable for an increasing system temperature. In addition to the wider operation temperature range, the internal ventilation of the disc improves the brake cooling. The thermal advantages results in constant braking distances even with multiple brake actuations. In comparison to the drum brakes, the wear of the brake pads increases, but due to the mechanical design, they can be replaced more easily. Furthermore, the amplification of brake pressure to brake torque is lower, which requires higher braking pressures, but reduces the influence of a changing friction coefficient. In summary, the braking characteristics of disc brakes are more stable (Breuer & Bill, 2012).

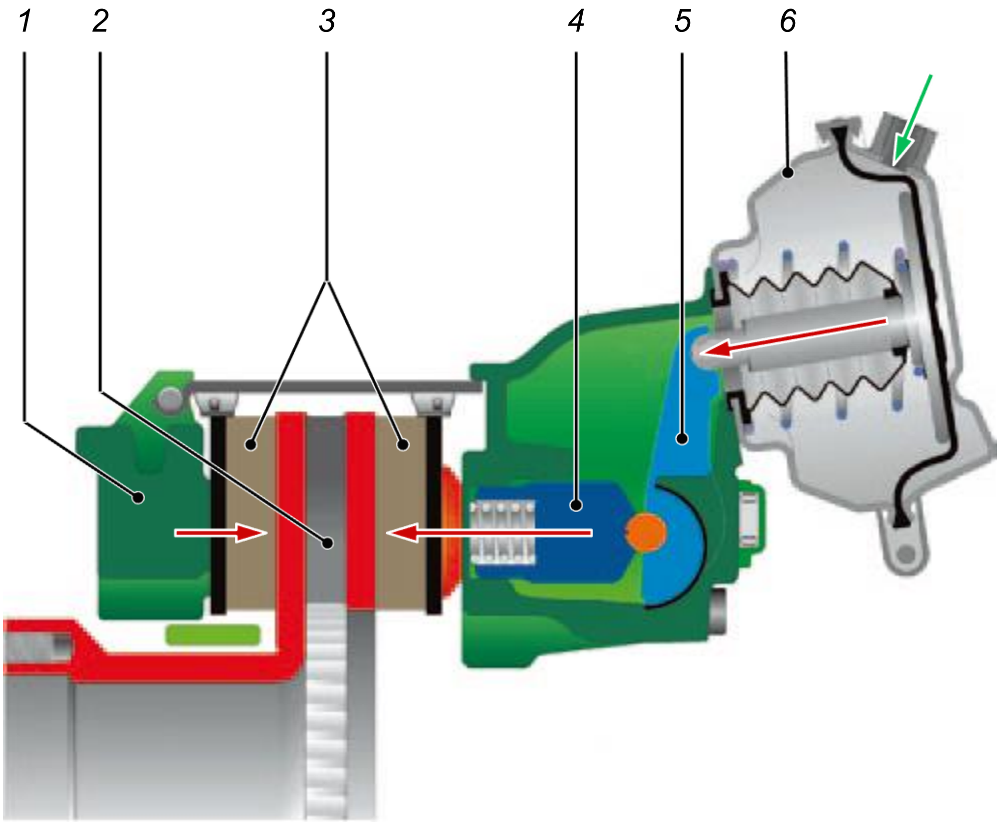

Figure 2.22: Structure of the service disc brake unit. Brake calliper (1), brake disc (2), brake pads (3), brake stamp (4), lever arm (5) and membrane brake cylinder (6). The green arrow illustrates the pressure connection, whereas the red arrows show the force transmission to the disc brake (Breuer & Bill, 2012).

The cross section of the service brake actuator in Figure 2.22 represents the important components. While the brake disc (2) is firmly connected to the rotating wheel hub, the calliper (1) is statically attached to the wheel suspension. In order to actuate the brake, the membrane brake cylinder (6) is ventilated. Inside the cylinder, the effective membrane area converts the applied brake pressure into a force, which moves the piston and compresses the return spring. The lever arm (5) amplifies and transmits the piston force to the brake stamp (4). Subsequently, the stamp presses the pads (3) on the disc (2), whereby the brake torque is generated. By venting the brake cylinder (6), the brake pressure decreases and the spring pushes back the assembly (MAN Truck & Bus AG, 2016).

2.4.3 Brake System Dynamics

This section focuses on the dynamic characteristics of the brake system and analyses the conversion of brake pressure to brake torque in order to derive a model of the EBS.

The braking process is initiated by the specified pressure request of the control unit, which is sent via CAN bus to the pressure modulators and pressure control valves. Since the CAN bus uses a serial technology for the data transmission, the transfer together with the processing of the data is time-consuming (Reuss, 2016). As a result, the PMs and PVCs receive the pressure request signal delayed. The delayed request is then processed by the PMs and PVCs by adjusting the air volume flow in the pneumatic pipes to the brake actuators. This actuation results in a pressure increase or decrease which is modelled as a second-order system. The system's time constants are dependent on the air volume and thus on the diameter as well as the length of the pipes. Based on experimental data of the dynamic pressure response, the system parameters were identified. The system behaviour is displayed in the subsequent transfer function (Tagesson, 2013):

$$P_B(s) = \frac{1}{0.002s^2 + 0.089s + 1} \cdot e^{-0.0269s} \cdot P_{req}(s) \tag{2.53}$$

The pressure response is delayed by 26.9 ms due to the initial data transmission via CAN bus. Once the signal has been received by the PMs and PCVs, the pressure rises within 147.6 ms from 10% to 90% with respect to the input step level (Tagesson, 2013). The step response of the pneumatic system with the identified parameters is illustrated in Figure 2.23.

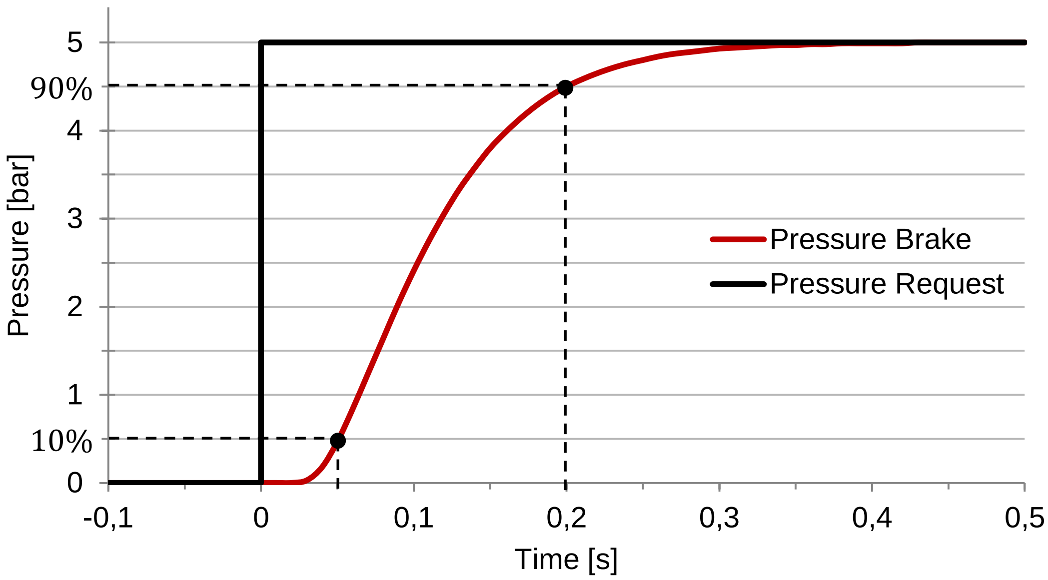

Figure 2.23: Dynamic braking response of the brake system for a step request of 5 bars.

The second dynamic element of the brake system is the wheel brake actuator which transforms the applied pressure into a brake torque. Due to the pretension of the return spring, the system behaviour of the actuator is nonlinear. In order to generate a brake actuation, the applied braking pressure P_B has to exceed the constant pressure threshold P_T, which is dependent on the spring's pretension (Tagesson, 2017). In order to use linear models, the offset is compensated by introducing the effective braking pressure P_{eff}:

$$P_{eff} = P_B - P_T \tag{2.54}$$

Using equation (2.54), the pressure-to-torque transformation is modelled in a first-order system. The associated transfer function of the service brake actuator is defined by the relational operator K_B and the time constant τ_B (Eklöv, 2013):

$$T_B(s) = \frac{-K_B}{1 + \tau_B s} \cdot P_{eff}(s) \tag{2.55}$$

Consequently, the steady state solution of equation (2.55) is a linear relation between brake torque T_B and an effective pressure P_{eff}. Since the membrane acts against the return spring, the time constant of the system changes in dependence of the sign of pressure gradient. In contrast, the relational parameter K_B is assumed to be constant, since it solely depends on the geometry as well as the materials of the service brake actuator (Breuer & Bill, 2012):

$$K_B = A_{Cyl} \cdot i_{Cyl} \cdot 2 \cdot \mu_B \cdot R_B \cdot \eta_B \tag{2.56}$$

Seen from the input side, the brake pressure is applied on the effective membrane area of the brake cylinder A_{Cyl}. The piston force is amplified by the lever ratio i_{Cyl}, resulting in the stamp force. Thereby, the brake pads are pressed on the brake disc by the stamp and generate a frictional force, which counteracts the disc rotation. This kinetic friction is a linear function of the friction coefficient μ_B, which depends on the pad/disc material pairing. The common friction value between pad and disc is $\mu_B = 0.38$ (MAN Truck & Bus AG, 2016). Consequently, the brake torque results from the friction force and the mean radius R_B of the brake pad to the axis of rotation. All losses are considered in the efficiency factor η_{mech} (Breuer & Bill, 2012).

In order to allow a free rotation of the wheel, the brake pads do not contact the disc. For a brake actuation, the pads must compensate for this offset once, causing a delay. Due to the relatively slow dynamics of the pneumatic system (2.53), both this offset delay as well as the time constant of the service brake actuator in equation (2.55) are negligible.

An ABS intervention reduces the operating pressure of the respective actuator and thus overruns the pressure request. In order to avoid any tyre saturation, the maximum permissible tyre force from equation (2.37) has to be considered in the calculation of the pressure request.

2.5 Wheel Dynamics

The wheel is rigidly attached to the wheel hub and thus to the brake disc. This connection enables the transmission of the brake torque to the tyre in order to generate a longitudinal tyre force. Since the wheel is subjected to a moment of inertia, the brake torque does not only affect the circumference force of the wheel but also the rotational motion (Pacejka, 2012):

$$I_{YW} \cdot \dot{\omega}_{YW} = T_B - r_{dyn} F_{XT} \tag{2.57}$$

Due to the force-slip characteristics of the tyre tread, the longitudinal force is a function of the slip and thus the rotational speed. The rewriting of equation (2.57) with the definitions for the longitudinal tyre dynamics (2.26) and (2.27) yields:

$$I_{YW} \cdot \dot{\omega}_{YW} = T_B - r_{dyn} \cdot C_\lambda(F_{ZT}) \cdot \left(\frac{r_{dyn}\omega_{YW}}{v_{XT}} - 1\right) \tag{2.58}$$

This results in the first-order differential equation (2.59) for the wheel dynamics:

$$I_{YW} \cdot \dot{\omega}_{YW} + r_{dyn} \cdot C_\lambda(F_{ZT}) \cdot \frac{r_{dyn}}{v_{XT}} \cdot \omega_{YW} = T_B + r_{dyn} \cdot C_\lambda(F_{ZT}) \tag{2.59}$$

For the reason of simplification, only the steady state solution for the wheel dynamics is used in this thesis project. This assumption linearizes the relation between brake torque and tyre force of equation (2.57):

$$F_{XT} = \frac{1}{r_{dyn}} \cdot T_B \tag{2.60}$$

2.6 Tractor-Trailer Combinations

The previous course of this thesis work focussed on single truck units without trailer. Nevertheless, truck combinations are widespread as their transport efficiency is higher in comparison with single units. Furthermore, due to the increase in road freight traffic, it is desirable to favour truck-combinations since they make better use of the road as mode of transport (Prokop & Stoller, 2012).

The trailers have a significant impact on the driving dynamics of the tractor and thus on the entire truck combination. Since the instability of the trailer impairs the combination's stability, critical driving situations such as snaking, jack-knifing or trailer swing-out have to be avoided (Tagesson, 2017). Conversely, it is possible to stabilize an instable tractor by braking the trailer. Regardless of critical and instable driving situations, the trailer also affects the tractor's motion in normal driving manoeuvres. Therefore, it is important to analyse the motion and the coupling between tractor and trailer.

According to (ISO, 2011), there are three different types of trailers: full trailers with turnable steering, semi-trailers and centre-axle trailers. Depending on the trailer type, either a fifth-wheel coupling or a bolt coupling is installed on the tractor. Both couplings transmit forces in X, Y and Z-direction and enable a free rotational motion about the Z_C-axis of the coupling point. The trailer forces apply at the coupling point and influence the vehicle dynamics due to the geometry of the reference frame, which is illustrated in the vehicle model of Figure 2.24. The axis system of the coupling point is linked to the reference frame of the first trailer. Consequently, the axis system of the coupling is rotated by the difference of the yaw angles with respect to the tractor system. This difference is referred to as yaw articulation angle $\Delta\psi_C$ (ISO, 2011).

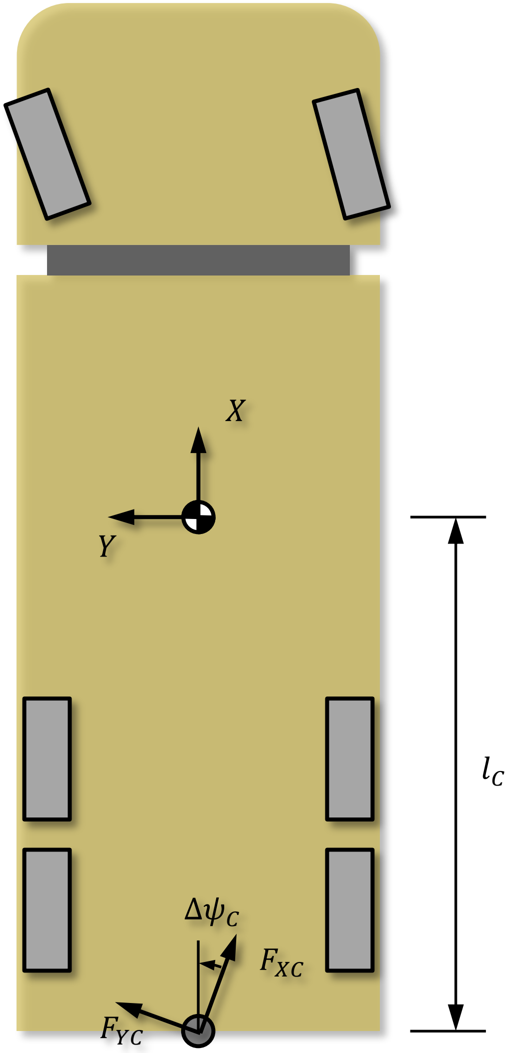

Figure 2.24: Vehicle system model of a rigid 6x4 truck, showing the coupling forces in their respective axis system, which is rotated by the yaw articulation angle

Rewriting the virtual actuation variables of the equations (2.18), (2.19) and (2.20) by adding the coupling forces and assuming small articulation angles $\Delta\psi_C$ yields the extended formulation of the planar dynamics in the following equations:

$$F_X = \sum_{i=1}^{2}(F_{XTi} - F_{YT1}\delta) + \sum_{i=3}^{6} F_{XTi} + (F_{XC} + \Delta\psi_C F_{YC}) \tag{2.61}$$

$$F_Y = \sum_{i=1}^{2}(F_{XTi}\delta + F_{YT1}) + \sum_{i=3}^{6} F_{YTi} + (-\Delta\psi_C F_{XC} + F_{YC}) \tag{2.62}$$

$$\begin{aligned} M_Z = \sum_{i=1}^{2}\big(l_1 \cdot (F_{XTi} \cdot \delta + F_{YT1})\big) + (-1)^i \cdot \frac{w_1}{2} \cdot (F_{XTi} - F_{YT1} \cdot \delta) \\ + \sum_{i=3}^{4}\left(-l_2 \cdot F_{YTi} + (-1)^i \cdot \frac{w_2}{2} \cdot F_{XTi}\right) \\ + \sum_{i=5}^{6}\left(-l_3 \cdot F_{YTi} + (-1)^i \cdot \frac{w_3}{2} \cdot F_{XTi}\right) \\ + l_C(-\Delta\psi_C F_{XC} + F_{YC}) \end{aligned} \tag{2.63}$$

The equations (2.61), (2.62) and (2.63) define the virtual variables for tractor-trailer combinations. Furthermore, the coupling forces can be expressed in wheel forces and steering angles of the trailer by setting up equations of motions for the trailer. Along with this, additional virtual actuation variables are defined for articulated vehicles. Typically used virtual variables are the yaw moment of the trailer as well as the yaw angular accelelration of the articulation angle (Nyman & Uhlén, 2014).

Due to the focus on the vehicle dynamics of single truck units, these extended formulations of the planar dynamics are not pursued any further. Instead, the development of the motion control system in this thesis project is based on the equations (2.18), (2.19) and (2.20) of the planar vehicle dynamics.

3 Control Design

In this chapter, the functional development of the individual modules of the motion controller is elaborated. In this development, the modular structure is based on the hierarchical system architecture, which is presented in the first subchapter 3.1.

The overall goal is to develop a motion control system which intervenes when the primary steering actuator fails. To generate the desired planar motion of the vehicle, the wheel brakes are the only accessible actuators for the control system. Since the system is designed as a fallback level for the steering actuator, the control functionality prioritises the vehicle's steerability in terms of the yaw motion. The function of applying asymmetric brake torque in order to steer the vehicle is referred to as Steer by Braking (SBB). The intervention of the SBB system ensures driving safety in the event of failure of the steering actuator, which contributes to the prevention of accidents. Consequently, the SBB functionality is categorised as active safety system. In comparison, passive safety systems increase the vehicle safety in the event of a collision (Reuss, 2015).

The SBB system is similar to the ESC, which influences the yaw motion by individual braking of the wheels. Because of asymmetric brake actuation, the ESC belongs to the active safety systems. Whereas the SBB functionality aims to ensure the steerability and thus a stable vehicle motion along a desired trajectory, the ESC engages the wheel brakes in order to stabilize an instable or skidding vehicle. Moreover, the type of intervention differs: As described above, the SBB system is designed as fallback solution for the primary steering actuator and intervenes as soon as a malfunction of this actuator is detected. The system subsequently controls the vehicle motion and remains active until the actuator problem is resolved. In contrast, the ESC observes the vehicle's sideslip angle β, which is a measure of driving stability. Whenever the sideslip angle exceeds a certain threshold, the ESC operates the wheel brakes to reduce the angle (Neubeck, 2016).

In the view of the control design, vehicles and especially trucks are over-actuated systems, since there are more actuators than control parameters. With a rising number of actuators which affect one parameter, the over-actuation increases. For the SBB system in trucks, the degree of over-actuation depends on the number of wheel brakes and thus on the axles. Along with the level of over-actuation, the complexity of control increases due to the variety of optimization possibilities (Laine, 2007).

The technical prerequisite for the SBB functionality is an EBS, since the control of the planar motion is based on the asymmetric brake torque distribution. In addition, the controller has to be embedded in the CAN network structure in order to communicate with the other ECUs, sensors and actuators. Via CAN, the SBB-ECU receives all sensor data and transmits the braking requests in return.

3.1 Motion Control Architecture

The overall control design is based on the complete vehicle control (CVC) architecture (Magnusson, et al., 2018), which is used at the automation department of Volvo Trucks Technology. This architecture is shown in Figure 3.1 and introduces a hierarchical control structure in which the individual function modules are implemented at a certain hierarchy level. Apart from the structural design, the hierarchy defines the importance as well as the cycle time of the modules. With the height of the level, the importance of executing a function increases, whereas the execution rate decreases. In contrast, the modules of the lower layers operate at a higher frequency, as they interact with the hardware such as sensors and actuators. As already indicated, the functionalities are not only arranged in hierarchy levels but also in modules. This modular structure enables the independent development, simulation and testing of the functions as well as the replacement of a module.

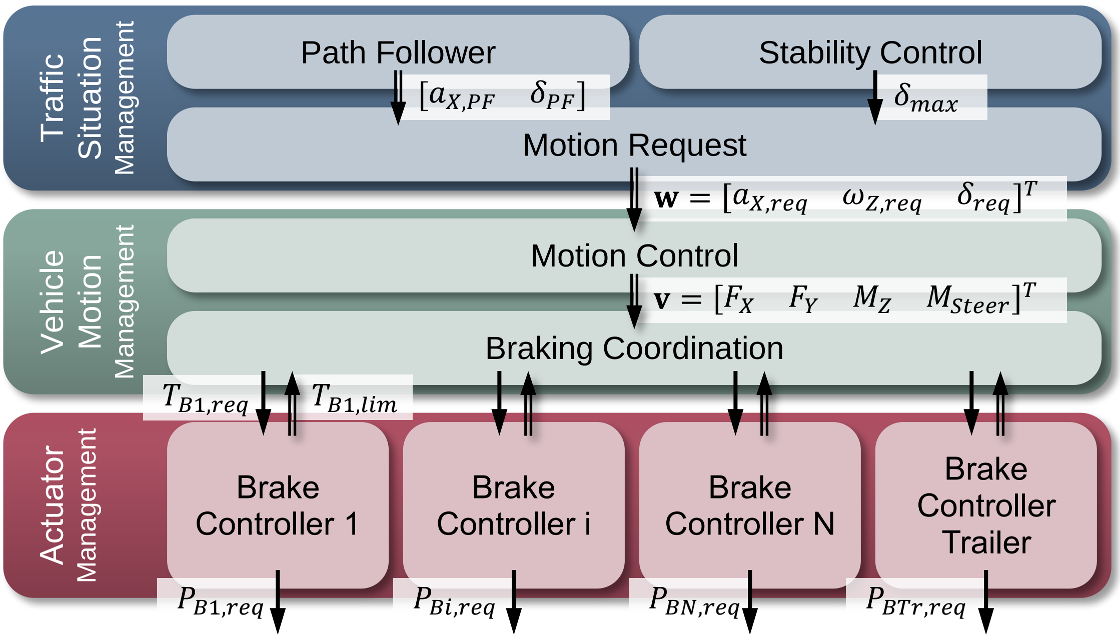

Figure 3.1: Architecture of the motion control design in hierarchy levels and modules. Furthermore, the directional signal flow between the modules is presented with arrows and the variables transferred.

As shown in Figure 3.1, the software architecture is divided into three hierarchy layers: traffic situation management, vehicle motion control and actuator control. The traffic situation management as top layer comprises functions for a stable vehicle motion along the desired trajectory representing a specific driving manoeuvre. Whereas the stability controller observes the physical limits to ensure a stable motion, the path following module guides the vehicle along the trajectory. In dependence of the vehicle position, the guidance functionality generates steering and acceleration commands. The motion request module merges the commands from the path follower with the stability information to calculate the variables of the global vehicle motion.

In the vehicle motion management layer, the motion control module converts the motion variables into virtual forces and moments, based on the vehicle configuration. Subsequently, the available braking actuators are coordinated in a way that their combined performance fulfils the requested forces and moments as effectively as possible. In the bottom layer, the individual brake control modules inform the coordinator about the brake and tyre limits. Simultaneously, the brake pressure is controlled based on the torque request from the coordinator. The pressure control variable is then sent to the EBS-ECU.

In general, the system boundary is defined by the bus interface: Via CAN bus, the sensor values are received and the actuator commands are sent in return. The signals which are transmitted within the controller between the modules and hierarchical levels are described in detail in the following subchapters with the associated function.

3.2 Traffic Situation Management

The functions of the traffic situation management layer stably guide the vehicle along the defined trajectory. Subsequently, the computed required vehicle motion is transmitted to the motion management module.

3.2.1 Path Follower

The path following function guides the vehicle along a given trajectory describing the driving manoeuvre. During the execution of the driving manoeuvre, the follower aims to minimize the vehicle's deviation from the path by calculating motion command variables.

The SBB function is an active safety system for automated driving vehicles. Therefore, it can be assumed that the trajectory planning function already exists. Furthermore, the planning problem is complex because the algorithm needs to consider multiple factors and criteria. For this reason, the path planning functionality is not part of this thesis project. Instead, the path planner is considered to be an upstream module which computes the driving path based on the required manoeuvre such as cornering or lane change. In the initialisation step, the trajectory of the respective driving manoeuvre is calculated once and transformed into the geographic coordinate system, as the vehicle is navigated using a global positioning system (GPS). Thereafter, the xy coordinates of the transformed trajectory are sent to the path following module, which is covered in this subchapter.

3.2.1.1 Vehicle Model

As described in the Vehicle Dynamics section, the motion of the vehicle is assumed to be planar. This allows the motion in longitudinal and lateral direction as well as the rotation about the yaw axis. However, the three motion capabilities are not independent: The non-holonomic driving characteristic prevents the vehicle from yawing or moving laterally without a forward movement. Firstly, the yaw and the lateral motion are coupled to a simultaneous longitudinal motion. And secondly, a lateral motion causes a yaw rotation and vice versa. These relations become apparent when parking sideways along the roadway: In addition to the steering, the manoeuvre requires the back and forth movement in longitudinal direction (Oubbati, 2009).

Similarly, the lateral offset of the vehicle from the defined trajectory is reduced by moving forward and steering in the direction of the trajectory. To account the motion constraints, the path follower uses a motion model of the vehicle. The implemented path follower calculates the steering command based on the geometric arrangement, which is why a bicycle model is sufficiently accurate.

While passenger cars are primarily utilized for the mobility of people, commercial vehicles and vehicle combinations transport loads of more than 40 tonnes. In order to evenly distribute the load on the tyres and axles and to limit the normal load per tyre, commercial vehicles are often equipped with multiple non-steered rear axles. Due to the additional axles, it is not possible to design a simplified, geometric model of the vehicle.

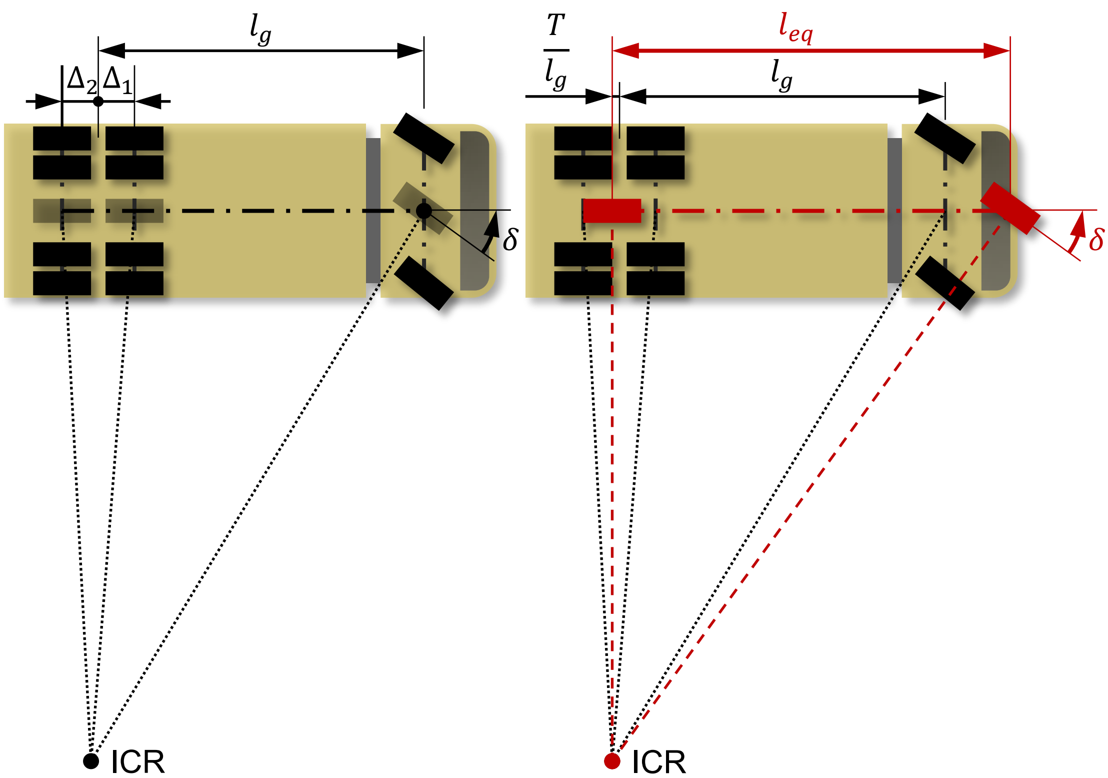

(a) three-axle vehicle with tyre slip (b) equiv. two-axle vehicle without slip

Figure 3.2: Cornering of a three-axle truck model in steady state at low speed; generation of the equivalent two axle bicycle model with the same turning characteristics. Note: The rear axle of the equivalent model deviates from the tandem centre (Stoerkle, 2013)

Figure 3.2 (a) illustrates the cornering of a three-axle truck model with the constant steering angle δ in steady state. As with a two-axle vehicle, all wheels move around the instantaneous centre of rotation (ICR) with a specific radius. However, the ICR is not on the centre lines of the rear axles. Because of this motion geometry, even in low speed turning and hence negligible centrifugal forces, the motion vector of the wheel suspension point is not in the related wheel rotation plane. Consequently, the non-steered rear wheels cause slip and thus lateral forces on all the tyres, which specifically affects the cornering characteristic of the vehicle (Stoerkle, 2013).

The same turning behaviour can be assigned to an equivalent two-axle vehicle with the related wheelbase l_{eq} and the steering angle δ, which is illustrated in Figure 3.2 (b). In contrast to the three-axle truck, the equivalent vehicle is free of construction-based lateral tyre forces, since the ICR is on the centre lines of both axles (ISO, 2011).

The equivalent vehicle model is based on the driving dynamics of a multi-axle vehicle during slow cornering in steady state. The low speed allows the neglect of the centrifugal forces as well as the normal load transfer. On the basis of the overall tyre force balance, the turning characteristic of the multi-axle truck is calculated, which is described in detail in (Stoerkle, 2013). The cornering characteristic mainly depends on the vehicle geometry and the tyre properties. In order to transfer the turning characteristics to a simplified single-track model with only two tyres, the cornering stiffnesses are summed up to a front and rear axle stiffness value, denoted as $C_{\alpha F}$ and $C_{\alpha R}$. For simplification, the stiffness values of the front and the rear tyres are assumed to be equal (Stoerkle, 2013).

$$C_{\alpha F} = \sum_{i=1}^{2} C_{\alpha i} \tag{3.1}$$

$$C_{\alpha R} = \sum_{i=3}^{6} C_{\alpha i} \tag{3.2}$$

Furthermore, the geometric influence of the non-steered rear axles is quantified in the tandem factor T, which is based on the number of non-steered rear axles N_R as well as the distances Δ_i from the centre of the rear axles to the respective axle:

$$T = \frac{\sum_{i=1}^{N_R} \Delta_i^2}{N_R} \tag{3.3}$$

Subsequently, the wheelbase l_{eq} of equivalent vehicle is calculated on the basis of the geometric wheelbase l_g (distance between front axle and rear axle centre), the tandem factor and the quotient of the combined tyre stiffnesses (Stoerkle, 2013).

$$l_{eq} = l_g + \frac{T}{l_g}\left(1 + \frac{C_{\alpha R}}{C_{\alpha F}}\right) \tag{3.4}$$

The model of the equivalent vehicle enables the use of the simplified geometric bicycle model with the same wheelbase. This model reduces the complex four-wheel model with an Ackermann steering to a linearized single-track model. In this simplified model, the tyre and suspension properties of each axle are combined in a centred representative tyre element, which is shown in Figure 3.3. Neglecting the tyre slip at low cornering speeds results in the illustrated motion geometry from which the steering angle can be derived (Wiedemann, 2016):

$$\tan(\delta) = l_{eq} \cdot R^{-1} \tag{3.5}$$

The equivalent bicycle model is used in the path following algorithm of this thesis project, which is described in the section hereafter.

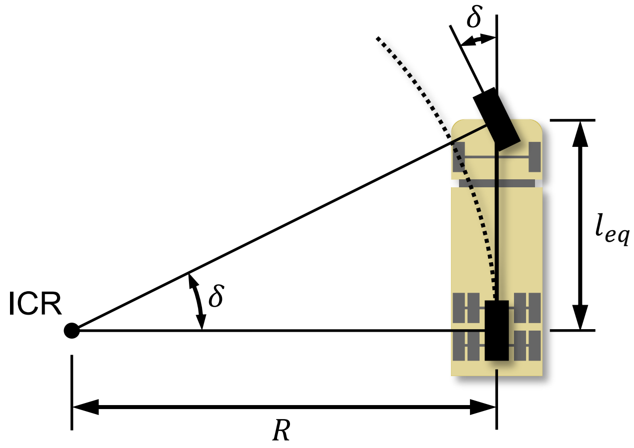

Figure 3.3: Motion of a single-track geometric model at low speed, showing the linearised Ackermann steering (Snider, 2009)

3.2.1.2 Path Tracking

The path tracking module has a central role in automated driving systems, since its algorithm generates the actual steering commands and is therefore directly responsible for the vehicle motion. In course of the increasing level of automation in vehicles, a lot of research has been done in the field of path following in recent years. The algorithms differ in terms of complexity, the implemented vehicle model and the applicable traffic situations such as highway travel, urban transport or parking. Due to the different requirements between the driving situations, there is no optimal tracking algorithm for all the situations.

The classification of path trackers is based on the applied vehicle model. Accordingly, there are geometric, kinematic and dynamic trackers. The level of detail and the modelling scope of the vehicle model determine the computational possibilities and complexity of the algorithm. An elaborate model enables precise vehicle control and prediction of movement. However, the computational effort increases. The direct comparison of simple geometric and complex dynamic path trackers reveals that the performance differences in standard driving manoeuvres are minor (Snider, 2009). For this reason, the geometric Pure Pursuit method is used in this thesis project.

The pure pursuit path tracker is based on the equivalent geometric vehicle model of the truck (Figure 3.3). Like all geometric trackers, the pure pursuit method is robust to disturbances, large deviations and discontinuities in the trajectory, since the algorithm considers the geometry between vehicle and path rather than the shape of the trajectory. Furthermore, the computing effort is low and the overshooting behaviour is moderate. Due to the velocity-dependent steady-state error, the operation speed of geometric methods is limited. This error is due to the open-loop control structure which has no feedback path. To achieve a superior robustness, the pure pursuit method tends to cut corners with increasing speed. Nevertheless, the tracking performance of the pure pursuit follower is comparable to the performance of more complex methods (Snider, 2009).

The tracking algorithm of the pure pursuit method calculates the steering command δ_{PF} based on the vehicle model as well as the positioning of the vehicle to the trajectory. Initially, the vehicle is localised in the global coordinate system via GPS data to determine the geometric arrangement of vehicle and trajectory shown in Figure 3.4. In order to use the Ackermann formulas, the algorithm references its calculations to the rear suspension of the single-track model. Instead of the lateral deviation from the path, the pure pursuit method targets a point at a defined distance ahead of the vehicle on the trajectory and determines the angular deviation φ. The distance between the vehicle reference in the rear wheel and the focus point is referred to as look-ahead distance l_{ah}, which is shown in Figure 3.4.

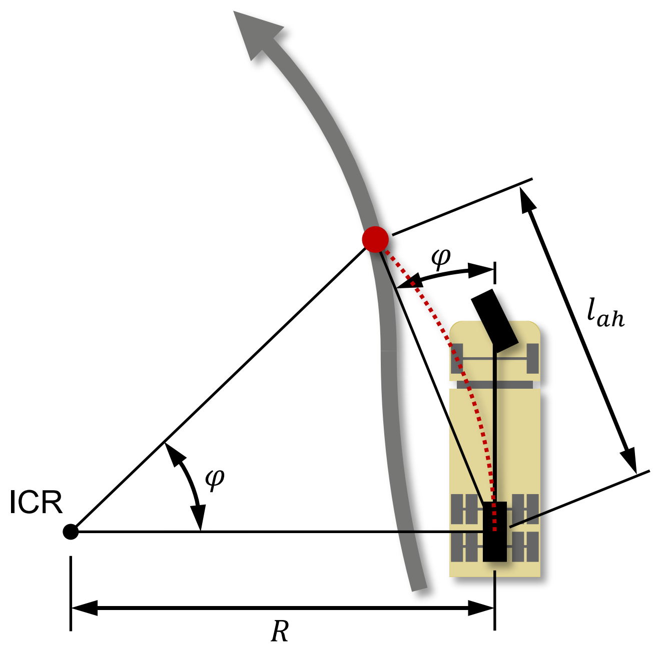

Figure 3.4: Calculation of the steering angle command with the pure pursuit method based on the geometric arrangement of vehicle model and trajectory of the driving manoeuvre (Snider, 2009)

By applying the law of sine, the circular motion arc of the rear wheel is calculated as function of the angular deviation φ and the look-ahead distance l_{ah}:

$$R = \frac{l_{ah}}{2\sin(\varphi)} \tag{3.6}$$

Rewriting equation (3.5) with the motion radius R yields function (3.8) for the steering angle command δ_{PF} according to the Ackermann steering formula:

$$\delta_{PF} = \tan^{-1}\left(\frac{2l_{eq}\sin(\varphi)}{l_{ah}}\right) \tag{3.7}$$

The steer angle command δ_{PF} is a function of the look-ahead distance as well as the angular deviation and the wheelbase of the model. While the wheelbase is assumed to be constant, the angular deviation results from the geometry in Figure 3.4, which is determined by the look-ahead distance. Consequently, this distance mainly influences the characteristic of the pure pursuit tracker: Longer distances enhance the driving stability, since the steering commands of the path follower are more anticipatory and smoother. However, due to the focussing on a more distant point, the tracker causes a cutting of corners and a higher lateral deviation from the path. This distance d_{CTE} is referred to as cross track error (CTE). In contrast, smaller values for l_{ah} result in a smaller CTE which improves the driving accuracy. Though, the driving stability is impaired, since the steering becomes more direct and abrupt. In order to avoid instability on the one hand and inadmissible lateral deviation on the other hand, the look-ahead distance is limited to a range of 3 to 25 metres. Within this range, the steering characteristic can be adapted by the look-ahead distance (Snider, 2009).

$$l_{ah} = f(v, \kappa, d_{CTE}) \tag{3.8}$$

In this thesis project, the value of l_{ah} is a function of vehicle speed, trajectory's curvature and cross track error. By defining a linear dependency between l_{ah} and vehicle speed, the tracking method prioritises driving safety as well as anticipation at higher velocities. Conversely, this dependency focuses on accuracy in terms of deviation from the desired path at lower speeds. In addition, the consideration of curvature and CTE helps to reduce the deviation in curvy path sections.

Furthermore, the kinematic and dynamic characteristic of the steering output are limited. Equation (3.9) restricts the maximum positive and negative steer angle, which is determined by the mechanical stops of the steering system. Furthermore, the dynamic limitation avoids sudden changes in the steering command to stabilize the motion controller.

$$-\delta_{PF,max} \leq \delta_{PF}(t) \leq +\delta_{PF,max} \tag{3.9}$$

$$-\dot{\delta}_{PF,max} \leq \dot{\delta}_{PF}(t) \leq +\dot{\delta}_{PF,max} \tag{3.10}$$

In addition to the steering angle, the path following module outputs the current CTE value and the acceleration command a_{PF}. The acceleration value is either defined for the individual sections of the driving manoeuvre by the upstream path planning module or specified by another high layer function. Consequently, the tracker only takes over the respective value during the driving manoeuvre. In this project, the acceleration command is always less than or equal to zero and defined in sections along the input trajectory.

3.2.2 Stability Control

The overriding goal of the stability control functions is to ensure the driving stability permanently. Stability in the vehicle motion context refers to the yaw and roll motion. While the yaw stability control prevents the vehicle from skidding and drifting, the roll stability control intervenes to avert a rollover.

In order to ensure the yaw stability during motion, the control function calculates and monitors the vehicle's sideslip angle β. This angle is defined by the ratio of lateral to longitudinal vehicle speed in the reference system. In a more general formulation, this angle describes the deviation of the direction of travel (direction of the velocity vector) from the vehicle's longitudinal axis in the COG. Consequently, the sideslip angle is calculated from the desired yaw motion expressed by the steering angle of the front wheels and the actual yawing of the vehicle. Accordingly, β characterises the under- or oversteering behaviour and is therefore a measure of yaw stability. As soon as the sideslip angle exceeds a certain threshold, the stability control detects an inconsistency in the vehicle motion and intervenes (Rajamani, 2012).

In order to stabilize the yaw motion by reducing the sideslip, the controller requests either a counteracting or assisting yaw moment. The required moment is dependent on the driving situation as well as the vehicle driving characteristic. In understeering vehicles, such as trucks, the stability control decelerates the inside rear wheels to generate an additional yaw moment. In case of an oversteering driving behaviour, the outside front wheel is braked to produce a counteracting moment (Neubeck, 2016). Due to the failure of the primary steering actuator, both the virtual yaw and the steering are controlled via the wheel brakes. For this reason, the yaw motion is continuously monitored and controlled. Consequently, the yaw stability function is included in the Motion Request and the Motion Control module.

For driving safety, the roll stability control is as important as the yaw stability functionality, since it prevents not only a rollover but also the one-sided lifting of the wheels. Compared to passenger vehicles, the z-position of the trucks' COG is higher due to the chassis structure and, moreover, varies depending on the current cargo. For these reasons, the roll stability controller has to adapt to the driving and loading situation. The roll stability is quantitatively phrased by the rollover index R which is based on the tyre normal forces on the left and right side of the vehicle (Odenthal, et al., 1999):

$$R = \frac{F_{ZTR} - F_{ZTL}}{F_{ZTR} + F_{ZTL}} \tag{3.11}$$

This index describes the lateral load change caused by the COG during cornering. An increasing lateral inclination does not only impair the driving stability, but also increases the asymmetry in the lateral load distribution on the wheels. The difference in tyre normal load between left and right wheels expresses this asymmetric distribution in mathematical way. By normalizing the difference with the total load force, the index becomes load-independent. The roll stability limit is reached when the total load is on solely one side of the truck wheels. As a result, the unloaded side is about to lose contact with the road and lift off. With respect to the rollover index in equation (3.11), the limits of driving stability are at $R = \pm 1$. Consequently, the vehicle motion is stable within the interval $R \in (-1,1)$.

However, it is not possible to measure the normal tyre forces to determine the index according to equation (3.11). Instead, the load change response is calculated by the means of the lateral and the roll dynamics, yielding the simplified equation (3.12). This equation describes the asymmetric normal load distribution using the two ratios of COG height to half track width w and lateral acceleration a_Y to gravity g.

$$R = \frac{2h_{COG}}{w} \cdot \frac{a_Y}{g} \tag{3.12}$$

As soon as the controller detects the risk of roll instability, it intervenes to limit the load change reaction (decrease of the rollover index). According to equation (3.12), the roll stability in a driving manoeuvre improves by reducing the lateral acceleration, since the COG height and wheelbase are constant. Rewriting formula (3.12) with the centripetal acceleration occurring during the circular motion yields formula (3.13):

$$R = \frac{2h_{COG}}{w \cdot g} \cdot \frac{v_x^2}{R_P} \tag{3.13}$$

The roll motion stabilizes when the vehicle speed is reduced or the driving radius is increased. According to (Odenthal, et al., 1999), rollover prevention measures have to be initiated when the index exceeds $|R| > 0.9$. However, the prevention actions only affect the roll acceleration and not the roll angle, which is why the lateral inclination and the rollover index might increase further. To account for this overshoot as well as the lower dynamics in the truck response, the actuation level is given additional safety and is therefore set to $|R| > 0.7$ in this project work. Instead of the initiation of a prevention measure, the roll stability function limits the maximum steering angle when the rollover index exceeds the stability range. By limiting the steering angle, the minimum turning radius and thus the maximum lateral acceleration is set. This enables the vehicle motion at the physical limits to exploit the maximum steering potential of the SBB system.

3.2.3 Motion Request

The motion request module is located in the traffic situation management layer of the control architecture (Figure 3.1) and generates the control variables for a stable vehicle motion along the manoeuvre's trajectory.

As shown in the detailed view of the control structure (Figure 3.5), the request function receives a steering and acceleration command from the path follower. These commands describe the desired vehicle motion based on a geometric bicycle model. However, the path tracker does not consider the physical limits which have to be adhered to ensure a stable vehicle motion. As described in the previous chapter, the driving stability refers to both rolling and yawing of the vehicle.

The Objective of this thesis is to maintain the steerability of the vehicle, which refers to the controllability of the steer and yaw motion. Consequently, the motion request functionality needs to permanently monitor and control the steering and yawing of the vehicle. As a result, the motion request module is responsible for the stabilization of the yaw motion. For this reason, the Stability Control only monitors the roll motion and informs the motion request function about the stability limit of the rolling by specifying the maximum steer angle. Subsequently, the motion request function processes these driving commands and limitations into the variables of the global vehicle motion, which are sent to the Motion Control layer.

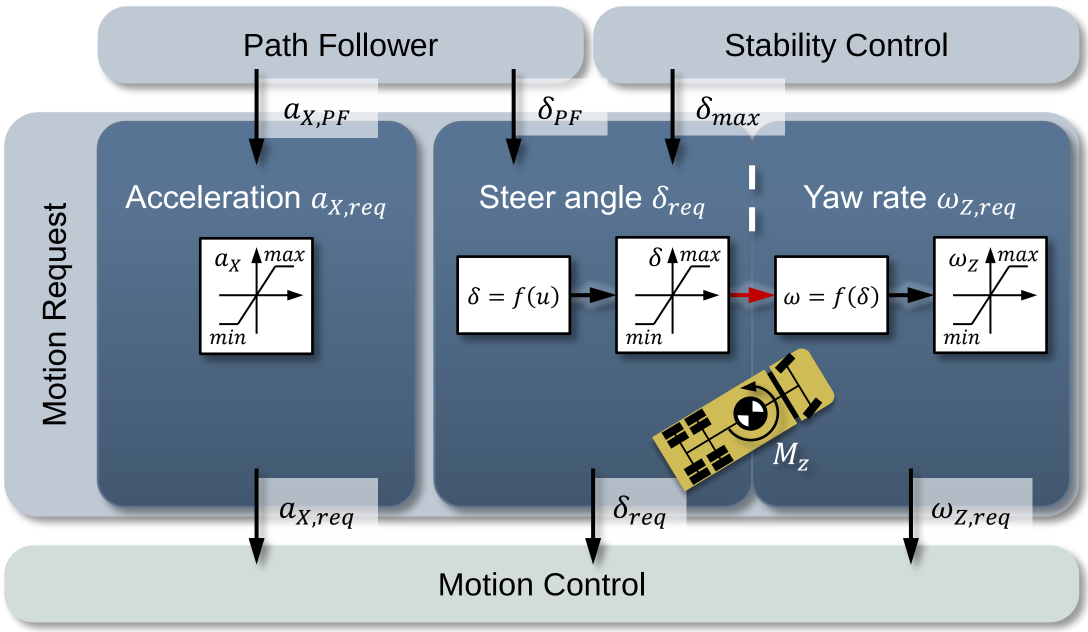

Figure 3.5: Structure and function blocks of the motion request module

According to the equations (2.55) and (2.60), the wheel brake actuators produce a defined torque resulting in a specific circumferential force. Therefore, the motion request module in Figure 3.5 is structured pursuant to the individual parameters which can be controlled with the longitudinal forces of the wheel brake actuators:

- Longitudinal acceleration a_X: Even at the steered wheels, the wheel plane is assumed parallel to the longitudinal axis of the chassis, which is why the acceleration mainly acts in the longitudinal direction.
- Yaw rate ω_Z: An asymmetric distribution of the applied longitudinal tyre forces generates a yaw motion of the chassis.
- Steer angle δ: The longitudinal forces produce a steering torque that causes a turning of these wheels (Steering Dynamics).

The longitudinal acceleration request $a_{X,req}$ is based on the path follower's command $a_{X,PF}$ and a vehicle-related limitation of the acceleration. Therefore, its computation is straightforward and independent from the other two control variables.

In contrast, the calculation of the yaw and the steering request is complex due to their interdependence which is illustrated as double unit in Figure 3.5: Assuming a stable vehicle motion, a defined steering input causes a specific yaw reaction. Conversely, the motion request functionality has to compute the yaw rate request $\omega_{Z,req}$, which ensures driving stability for a defined steering angle. As previously described, steering in the vehicle motion context primarily refers to yawing. For this reason, the manoeuvrability is enhanced by assisting the steering demand δ_{req} with a yaw request based on this demand. This guarantees driving stability as well as superior dynamics, which improves the overall driving safety.

Since the steer angle is controlled by the wheel brakes, the dynamics of the steering and thus the manoeuvrability of the vehicle are limited. In addition, the Stability Control sets the permissible steer angle to ensure the roll stability of the vehicle. However, the limitation of the steer angle by the request functionality prevents the execution of the path follower's command and results in a deviation from the desired path. In order to inhibit the vehicle from leaving the road, an extended stability controller has to be developed, which is able to reduce the velocity at an early stage, so that the limitation of the steer angle becomes redundant.

In order to control the steering angle of the front wheels, a differential brake force has to be generated with the brake actuators, which is expressed in equation (2.52). The asymmetric brake actuation on the steerable front wheels will not only affect the dynamics of the steering, but also creates a yawing torque on the vehicle. Due to the positive value for the kingpin offset at ground of heavy vehicles, the yaw moment from the differential braking boosts the yaw motion from the steered wheels. Since the computations of the path following commands are based on a bicycle model, the direct realization of the steering command would result in an incorrect vehicle motion. Accordingly, the amplification effect has to be considered in the steer angle request by the self-steering angle δ_{SS}.

The actual steer request δ_{req}, which takes the self-steering effect into account, is derived from the subsequent Newton-Euler equations for the planar vehicle motion (Wiedemann, 2016):

$$F_Y = m_V \cdot a_Y \tag{3.14}$$

$$M_Z = I_Z \cdot \dot{\omega}_Z \tag{3.15}$$

Due to the stable vehicle motion, the sideslip angle is small. Therefore, equation (3.16) applies to the lateral acceleration (Wiedemann, 2016).

$$a_Y = v \cdot \left(\omega_Z + \dot{\beta}\right) \tag{3.16}$$

Furthermore, the Newton-Euler formulations (3.14) and (3.15) are equated with the tyre-based definitions (2.19) and (2.20) to describe the lateral and the yaw motion of the planar dynamics:

$$m \cdot a_Y = \sum_{i=1}^{2} (F_{XTi}\delta + F_{YT1}) + \sum_{i=3}^{6} F_{YTi} \tag{3.17}$$

$$\begin{aligned} I_Z \cdot \dot{\omega}_Z = \sum_{i=1}^{2} \big(l_1 \cdot (F_{XTi} \cdot \delta + F_{YT1})\big) + (-1)^i \cdot \frac{w_1}{2} \\ \cdot (F_{XTi} - F_{YT1} \cdot \delta) \\ + \sum_{i=3}^{4} \left(-l_2 \cdot F_{YTi} + (-1)^i \cdot \frac{w_2}{2} \cdot F_{XTi}\right) \\ + \sum_{i=5}^{6} \left(-l_3 \cdot F_{YTi} + (-1)^i \cdot \frac{w_3}{2} \cdot F_{XTi}\right) \end{aligned} \tag{3.18}$$

For simplification, vehicle motion is examined in steady state ($\dot{\omega}_Z = 0$, $\dot{\beta} = 0$) in the section hereafter.

In order to ensure the driving stability, the SBB functionality envisages the operation of the tyres in the elastic range of their characteristic. This allows the application of the linear approximation of equation (2.34) for the representation of the lateral tyre forces. In addition, the cornering stiffness is a function of the tyre normal load, which is expressed by the designation $C_{\alpha i} = C_\alpha(F_{ZTi})$. For reasons of simplification, the cornering stiffness and the tyre normal force are assumed to be linear ($C_\alpha \sim F_{ZTi}$). To describe the formulas more visually, the values for the wheelbase are considered positive ($l_i \geq 0$). Therefore, the wheelbase's sign reverses in the slip angle formula (2.29) for the front axle, resulting in the following equations for the lateral tyre forces of the steered front wheels:

$$F_{YT1} = -C_{\alpha 1} \cdot \alpha_1 = -C_{\alpha 1} \cdot \left(\delta_1 - \beta - \frac{l_1}{v} \cdot \omega_Z\right) \tag{3.19}$$

$$F_{YT2} = -C_{\alpha 2} \cdot \alpha_2 = -C_{\alpha 2} \cdot \left(\delta_2 - \beta - \frac{l_1}{v} \cdot \omega_Z\right) \tag{3.20}$$

Rewriting the linear approximation (2.34) for the lateral dynamics of the non-steered rear axles ($\delta_i = 0$) with the definition of the tyre slip angle (2.29) yields the subsequent equations:

$$F_{YT3} = -C_{\alpha 3} \cdot \left(-\beta + \frac{l_2}{v} \cdot \omega_Z\right) \tag{3.21}$$

$$F_{YT4} = -C_{\alpha 4} \cdot \left(-\beta + \frac{l_2}{v} \cdot \omega_Z\right) \tag{3.22}$$

$$F_{YT5} = -C_{\alpha 5} \cdot \left(-\beta + \frac{l_3}{v} \cdot \omega_Z\right) \tag{3.23}$$

$$F_{YT6} = -C_{\alpha 6} \cdot \left(-\beta + \frac{l_3}{v} \cdot \omega_Z\right) \tag{3.24}$$

Neglecting the dynamic load transfer in longitudinal direction, the normal load that applies at each axle is constant. This allows the combination of the front tyre forces as well as the fusion of the rear tyre forces by the equations (3.25) and (3.26). Assuming the linear normal load dependency and similar tyre properties, the sum of the cornering stiffnesses at each axle is static. This results in a combined cornering stiffness of $C_{\alpha F}$ at the front axle and $C_{\alpha R}$ at the tandem axle.

$$\sum_{i=1}^{2} F_{YTi} = -2C_{\alpha F} \cdot \left(\delta - \beta - \frac{l_1}{v} \cdot \omega_Z\right) \tag{3.25}$$

$$\sum_{i=3}^{6} F_{YTi} = -2C_{\alpha R} \cdot \left(-2\beta + \frac{l_2 + l_3}{v} \cdot \omega_Z\right) \tag{3.26}$$

Since the circumferential tyre forces have a minor impact on the lateral dynamics in relation to the lateral tyre forces, the equation (3.17) is reduced to the formula (3.27):

$$m_V \cdot a_Y = \sum_{i=1}^{6} F_{YTi} \tag{3.27}$$

The application of the combined force formulations (3.25) and (3.26) as well as the definition of the lateral acceleration (3.16) yields function (3.28) for the sideslip angle β. The latter is linearly dependent on the steer angle as well as the yaw motion ω_Z and the velocity v, acting on the vehicle reference frame.

$$\begin{aligned}\beta = \frac{C_{\alpha F}}{C_{\alpha F} + 2C_{\alpha R}} \cdot \delta + \frac{-C_{\alpha F} l_1 + C_{\alpha R}(l_2 + l_3)}{C_{\alpha F} + 2C_{\alpha R}} \cdot \frac{\omega_Z}{v} \\ + \frac{m}{2C_{\alpha F} + 4C_{\alpha R}} \cdot v \cdot \omega_Z\end{aligned} \tag{3.28}$$

In the next step, the Steering Dynamics are consulted to formulate the tyre slip angle of the steerable front wheels as function of the differential brake force:

$$\alpha_1 = \alpha_2 = -\frac{\Delta F_{XT}}{2C_{\alpha F}} \cdot \frac{r_k}{t_m + t_p} \tag{3.29}$$

Finally, the definitions of the tyre forces (3.19) – (3.24), the sideslip angle (3.28) and the slip angle (3.29) are applied in the yaw motion equation (3.18). The resulting formula for the steer angle request (3.30) is the sum of the self-steering angle δ_{SS} and a term, which can be approximated by the Ackermann steer angle δ_A. The latter corresponds to the steer angle of single-track models with an Ackermann steering (Stoerkle, 2013).

$$\delta_{req} = \delta_A + \delta_{SS} \tag{3.30}$$

The self-steering angle is a function of the lateral tyre properties, the brake force distribution and the cornering behaviour in a specific driving status.

$$\delta_{SS} = \frac{1}{(F_{XT1} + F_{XT2}) \cdot l_1 + 2C_{\alpha F} \cdot (l_1 + l_{C\alpha})} \cdot \left(\frac{v^2}{R_P} \cdot m \cdot l_{C\alpha} + \frac{w_1}{2} \cdot (F_{XT1} - F_{XT2}) + \frac{w_2}{2} \cdot (F_{XT3} - F_{XT4}) + \frac{w_3}{2} \cdot (F_{XT5} - F_{XT6}) \right) \tag{3.31}$$

The mentioned cornering behaviour is mainly characterised by the longitudinal offset $l_{C\alpha}$. This displacement is derived from the weighting of the wheelbase with the cornering stiffness values. In dependence of the offset's sign and value the vehicle's characteristic is described as oversteering ($l_{C\alpha} < 0$), neutral ($l_{C\alpha} = 0$) or understeering ($l_{C\alpha} > 0$) (Wiedemann, 2016)

$$l_{C\alpha} = \frac{-C_{\alpha F} l_1 + C_{\alpha R}(l_2 + l_3)}{\sum_{i=1}^{N} C_{\alpha i}} \tag{3.32}$$

Since the path tracking is based on a geometric bicycle model, the Ackermann steer angle of equation (3.30) is equivalent to the steering command δ_{PF} in the motion request function:

$$\delta_{req} = \delta_{PF} + \delta_{SS} \tag{3.33}$$

The steering request δ_{req} represents the actual steer angle that is required to realize the desired vehicle motion which was calculated based on a single-track model. Hereby, the steering request takes the asymmetric brake actuation of the SBB function into account.

Like the steering request of equation (3.30), the yaw request is calculated based on the yaw motion definition (3.18) using the formulas for tyre forces (3.19) – (3.24), sideslip angle (3.28) and slip angle (3.29). Instead of applying Ackermann's steering angle definition, the equation is solved for the yaw rate. Furthermore, the differential brake forces of the axles are set to zero, since the yaw request only relates to the steering of the front wheels.

$$\omega_{Z,req} = \frac{\delta_{req} \cdot \left((F_{XT1} + F_{XT2}) l_1 + 2C_{\alpha F}(l_1 + l_{C\alpha})\right)}{\frac{1}{v}\left(-(\sum_{i=1}^{N} C_{\alpha i}) l_{C\alpha}^2 + C_{\alpha F} l_1^2 + C_{\alpha R}(l_2^2 + l_3^2)\right) + v m_V l_{C\alpha}} \tag{3.34}$$

The yaw request describes the yaw motion which matches the steering request to ensure driving stability and support the steering. This assistance enhances the vehicle's manoeuvrability.

Once per cycle, the command variable $\mathbf{w}$ is sent to the Motion Control module, describing the desired motion of the vehicle in order to follow the trajectory of the manoeuvre:

$$\mathbf{w} = [a_{X,req} \quad \omega_{Z,req} \quad \delta_{req}]^T \tag{3.35}$$

3.3 Vehicle Motion Management

In the vehicle motion management layer, the actual motion is controlled in order to realize the requested motion. Since the number of actuators for manipulating the vehicle motion exceeds the number of system variables to be controlled, the vehicle is an over-actuated system. Because of this system property, the motion management functions have to solve an allocation problem to put the motion request into effect.

Up to now, allocation problems are mostly known from flight control, as these systems have to control a large number of actuators. Apart from the actuator coordination, the flight control systems have to be designed fault tolerant and reconfigurable. In order to deal with these design requirements, several motion control techniques for flight applications have been developed. According to (Ducard, 2009), the following flight control techniques are commonly used:

- Control allocation
- Model reference adaptive control
- Sliding mode control

Among the listed control technologies, the control allocation has been successfully used for vehicle applications in previous projects at Volvo GTT. Due to its advantages in the motion control of over-actuated vehicles, the control allocation is also used in this project work. In the course of this, a comparison with the other control design techniques of the list is omitted.

In the control allocation design the superordinate motion management is separated into a preceding control activity and a subsequent distribution step, which are each assigned to a submodule (see modular architecture of Figure 3.1):

1. Control of the vehicle's motion with respect to the COG. Description of the control with forces and moments, which are assorted in the virtual control input $\mathbf{v}$.
2. Coordination of the actuators by mapping the virtual control input $\mathbf{v}$ to the real control input $\mathbf{u}$ taking into account the vehicle configuration as well as the arrangement of the actuators.

The main advantage of this subdivided control structure is the reconfigurability as well as the reusability of the SBB system for different and variable vehicle configurations. However, the system's over-actuation is the basic prerequisite for the separability of control and distribution and thus the application of the control allocation technique.

3.3.1 Motion Control

As the designation implies, this module controls the motion of the vehicle to meet the individual motion requests described in the command variable $\mathbf{w}$. The latter is sent by the Motion Request module as defined in the control architecture of Figure 3.1.

The request variables are fed as command variables into the control circuit of this module. In the controller, these variables are converted into virtual forces and moments using the vehicle-specific masses and inertia, which are controlled. Finally, the computed manipulated variables are combined in the so-called virtual control signal $\mathbf{v}$ (Eklöv, 2013). This virtual signal comprises the forces and the moment that must be applied to the COG to generate the required planar motion (acceleration and yawing), which is described by the equations (2.18), (2.19) and (2.20). To account for the additional motion capacity of the steering system, the virtual control signal is extended by the steering moment to control the steer angle. Subsequently, the virtual signals are handled by the Braking Coordination to coordinate the available wheel brake actuators such a way that their combined output power produces the calculated virtual forces and moments.

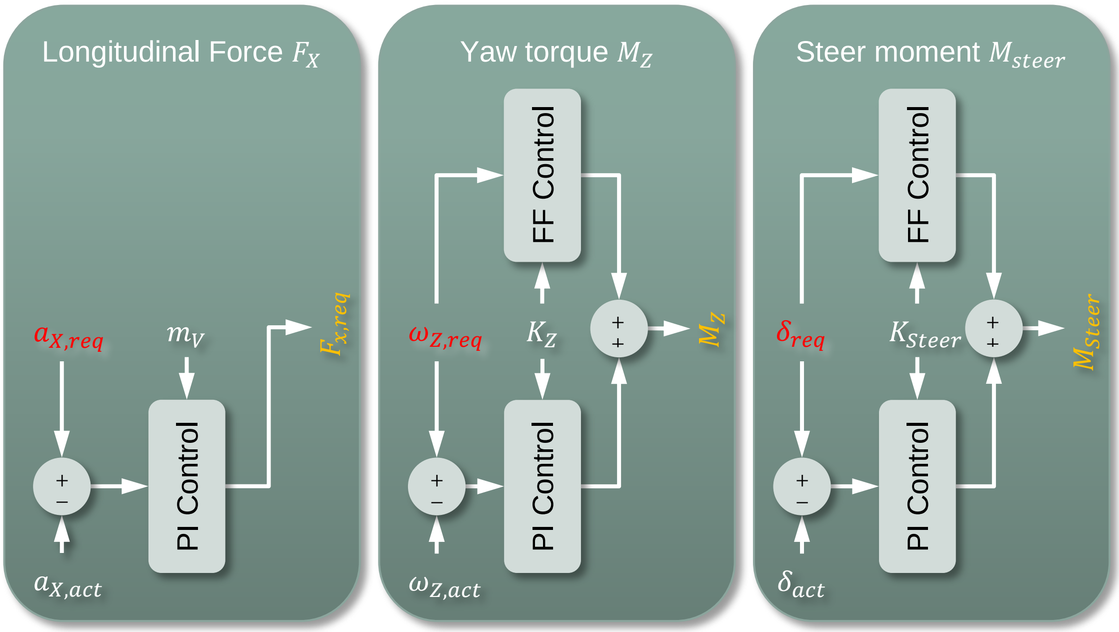

Figure 3.6: Modular structure of the motion controller; motion request signals are input as command variables (red), virtual control signals are output as manipulated variables (orange)

The motion control module in Figure 3.6 is structured pursuant to the command variables of definition (3.35), which is generated by the request module. Due to the fact that the motion request function handles the adaption and tuning of the command variables, the modules in the controller are set up independently of each other.

- Longitudinal force F_X: The forces that are produced by the actuators mainly apply in longitudinal direction and add up to a virtual force which accelerates or decelerates the vehicle.
- Lateral force F_Y: The motion request function determines the vehicle's motion without taking the lateral acceleration into account. Consequently, the virtual lateral force F_Y is not controlled in a separate module and therefore not shown in Figure 3.6. Nevertheless, the lateral force is introduced as virtual control signal to provide the ability of using it in advanced functions.

- Yaw torque M_Z: An asymmetric distribution of the applied longitudinal tyre forces generates a virtual yaw torque and thus a yaw motion
- Steering torque M_{Steer}: The differential longitudinal forces on the wheels of the steered axle produce a steering torque that causes these wheels to turn (Steering Dynamics).

The control modules for the individual virtual variables combine a feedback controller with a feed-forward (FF) controller (except in the longitudinal force module). In the feedback control loop, the requested variable is compared with the actual measured variable. A proportional-integral (PI) controller compensates for this deviation, which increases the system accuracy and reduces the influence of disturbances. In contrast, the feed-forward control inputs only the request signal, which is why it responds immediately to the input variable. As the control deviation is not considered, the FF controller is model-based to achieve sufficient accuracy (Ducard, 2009).

This thesis project focuses on the manoeuvrability of the vehicle. In order to ensure the required yawing and steering performance even at the friction limit, an overshoot of the longitudinal acceleration has to be avoided. Therefore, the virtual longitudinal force F_X is controlled by a PI controller with a moderate dynamic characteristic which is set by the proportional gain K_P and the integral gain K_I. The controlled force is a function of the acceleration error in longitudinal direction Δa_X (equation (3.36)), which is the difference between the acceleration request and the measured value. Consulting the Newton-Euler equations for the planar vehicle motion, the linear relation of force and acceleration is defined by the vehicle mass m_V (Eklöv, 2013).

$$F_X = m_V \cdot \underbrace{\left[K_P \cdot \Delta a_X + K_I \int \Delta a_X \, dt\right]}_{PI\ control} \tag{3.36}$$

The lateral force F_Y acting on the COG was introduced as virtual control signal. As explained in the preceding list, the motion in lateral direction is not controlled in this project, which is why the virtual lateral force is set to zero in the respective motion control module and therefore not shown in Figure 3.6. However, the introduction of lateral force as virtual variable enables the implementation of functional add-ons without changing the control structure.

$$F_Y = 0 \tag{3.37}$$

The yaw motion is controlled by the virtual yaw torque M_Z acting on vehicle's COG. To achieve an optimized manoeuvrability in terms of precision and response, the yaw torque controller is composed of a feed-forward and a feedback part. While the PI control reduces the yaw rate's control error $\Delta\omega_Z$, the FF branch directly amplifies the derivative of the $\omega_{Z,req}$ signal from the motion request function. The vehicle-specific K_Z-gain determines the relation between yaw rate and yaw torque.

$$M_Z = K_Z \cdot \left(\underbrace{\left[K_P \cdot \Delta\omega_Z + K_I \int \Delta\omega_Z \, dt\right]}_{PI\ control} + \underbrace{\left[K_F \cdot \dot{\omega}_{Z,req}\right]}_{FF\ control} \right) \tag{3.38}$$

The steering control module also takes advantage of a combined controller. For a reduction of the control deviation, the PI branch controls the steering error $\Delta\delta$. In contrast, the FF part as well as the control gain K_{Steer} are based on the Steering Dynamics and the definition of M_{Steer} in equation (2.50). This reference to the steering characteristics enables the control of the actual steering angle.

$$M_{Steer} = K_{Steer} \left(\underbrace{\left[K_P \Delta\delta + K_I \int \Delta\delta \, dt\right]}_{PI\ control} + \underbrace{\left[K_F \left(\delta_{req} - \beta - \frac{l_1}{R_P}\right)\right]}_{FF\ control} \right) \tag{3.39}$$

$$K_{Steer} = -(C_{\alpha 1} + C_{\alpha 2}) \cdot \left(t_m + t_p\right) \tag{3.40}$$

In conclusion, the virtual control signal $\mathbf{v}$ comprises the output forces and moments of the individual control modules in order to achieve the desired motion of the vehicle during the execution of a particular driving manoeuvre. This virtual signal vector is sent to Braking Coordination module.

$$\mathbf{v} = [F_X \quad F_Y \quad M_Z \quad M_{Steer}]^T \tag{3.41}$$

3.3.2 Braking Coordination

The braking coordination functionality transforms the virtual control signals from the Motion Control into real and individual actuator control demands which are sent to the Actuator Management layer, illustrated in the block diagram of Figure 3.7. In this transformation process, the overall goal is the calculation of an optimized actuator control, which induces the envisioned vehicle motion demanded by the virtual control signal.

The structure of Motion Control depends on the purpose of the overall control functionality and is tailored to the controlled variables. For these reasons, the motion control is independent from the vehicle configuration and includes specific vehicle parameters instead, such as vehicle mass or inertia. In contrast, the design of the braking coordination module requires adaptability to different vehicle configurations to ensure the reusability of the SBB system in various vehicles. The vehicle configuration mainly relates to the number and the arrangement of the actuators, depending on the amount of axles and the wheelbase.

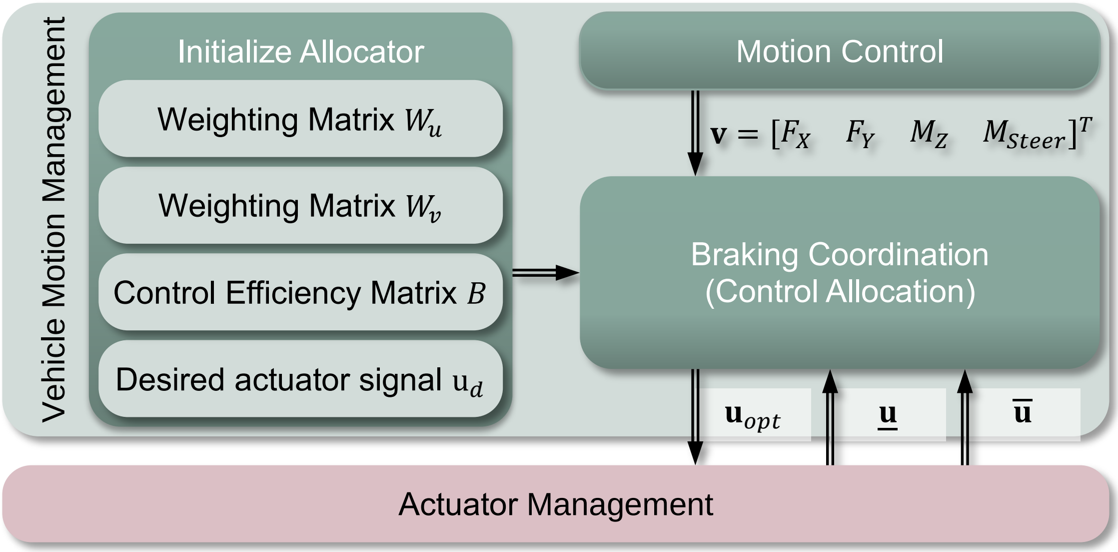

Figure 3.7: Structure of the control allocation functionality, which is a special braking coordination technique

From a mathematical point of view, the braking coordination functionality needs to solve the allocation problem of an over-actuated system. This means that the amount of controlled actuators exceeds the number of virtual control inputs. Conversely, each virtual control variable can be influenced by various combinations of one or more simultaneously driven actuators. Consequently, the actuators and thus the real control variables need to be coordinated in such a way that the combined output performance of the actuators produces the virtual control input representing the desired motion control. This corresponds to the redistribution and the mapping of the virtual control inputs to the real control signals ($\mathbf{v} \mapsto \mathbf{u}$). Along with the degree of over-actuation, the complexity of the allocation problem as well as the number of possible mapping solutions increase (Härkegård, 2003).

In the motion management layer, the control allocation technique itself is responsible for the coordination of the brake actuators. As with aerospace applications, the motion control systems of vehicles are over-actuated and subject to high safety requirements. Due to the listed characteristics, the control allocation used in flight systems is also suitable for vehicle motion control applications (Härkegård, 2003) (Laine, 2007):

- Compensation of an actuator failure without changing the control law. As the SBB system is a safety function, the compensation increases the system's availability and reliability.
- Limitation of the actuators' deflection and actuation speed based on their capabilities. In addition, the optimal operating range as well as the operational priority between different actuators can be defined. On the one hand, these measures enable an efficient operation of the actuators and, on the other hand, they avoid performance losses or failure due to overheating or wear.
- Synchronization of several actuators independent of their physical principles.

- Real-time capability of the allocation algorithm, which outputs the optimal solution within a finite number of optimization iterations. This allows the use of the control allocation technology in vehicle applications.
- Linear approximations are sufficiently accurate for most vehicle applications.
- High reusability of the system across vehicle platforms, due to separation layout and the simple adaptability of the allocator.

The control allocation technique reduces the various allocation solutions to the mathematical optimal control input $\mathbf{u_{opt}}$ for the current vehicle state and control situation, by extending the pure allocator with an optimization function. The latter is based on the actuator characteristics as well as the prioritization of the virtual control inputs. Furthermore, the solution space is constrained by the capability, availability and change rate of the actuators. This information is supplied by the actuator control function which cyclically recalculates the current individual constraints. In summary, the control allocator's task is the solution of an underdetermined and constrained system of equations (Härkegård, 2003).

In the following section the optimization function of the control allocator is elaborated in detail. The overall goal of the SBB system is the control of the vehicle motion with the wheel brakes. This control relation can be described by the subsequent nonlinear equation system (3.42), using the vehicle motion states $\mathbf{x}$ and the actuator control inputs $\mathbf{u}$:

$$\dot{\mathbf{x}} = f(\mathbf{x}) + g(\mathbf{x})\mathbf{u} \tag{3.42}$$

To simplify computing and control, the equation system is cyclically linearized around the current state of motion $\mathbf{x}(t)$. This linear approximation expressed by the control efficiency matrix $B_{k,m}$ whose dimensions are specified by the number of motion states k and the number of controlled actuators m. Due to the control system's over-actuation the relationship $m > k$ applies. For vehicle applications, this linear approximation is usually assumed to be state-independent, so that the efficiency matrix is invariable. In this project work, the linear approximation is supposed to be permissible for all motion states, which is why the efficiency matrix is constant after its initialization (Laine, 2007):

$$B\mathbf{u} \approx g(x)\mathbf{u} \tag{3.43}$$

Replacing the nonlinear term in (3.42) with the efficiency matrix of the approximation (3.43) results in the linear equation system (3.44). There, the efficiency matrix describes the effect of each control input on the respective motion state.

$$\dot{\mathbf{x}} = f(\mathbf{x}) + B\mathbf{u} \tag{3.44}$$

Due to the modular layout of the motion management layer, the Motion Control is separate from the allocation module. In the motion control, the control input for every motion variable is computed independently and combined in the virtual control input $\mathbf{v}$. Consequently, the control of the linear equation system (3.44) can be described equally using the virtual control input which directly affects the motion variables:

$$\dot{\mathbf{x}} = f(\mathbf{x}) + \mathbf{v} \tag{3.45}$$

Equation (3.46) is derived from the mathematical comparison of the equation systems (3.44) and (3.45), showing a linear dependency between virtual and actual control input. The dependency is determined by the control efficiency matrix, in which the effect of each actuator on every control input is defined.

$$\mathbf{v} = B\mathbf{u} \tag{3.46}$$

In order to satisfy the equation system (3.46), the allocator has to generate the requested virtual control input by optimizing the configuration of the actuator control input. Mathematically, this allocation problem is described by the minimization formulation Ω (3.47). According to Ω, the optimal actuator control is the minimum error between virtual and real control input. This is equivalent to the most accurate mapping of the actuator signal to the virtual control. In this optimization formulation, the weighting matrix W_v is used to define the priority of the virtual control signals or rather of the motion variables (Härkegård, 2003). Due to the focus on the manoeuvrability with the SBB functionality, the yawing and steering motion are prioritised over the acceleration. Moreover, the steering is weighted higher than the yawing to accomplish a natural stable driving behaviour.

$$\Omega = \underset{\underline{\mathbf{u}}<\mathbf{u}<\overline{\mathbf{u}}}{\arg\min} \|W_v(B\mathbf{u} - \mathbf{v})\|_2^2 \tag{3.47}$$

Furthermore, the solution space of the optimal control input is constrained by the actuator capabilities ($\underline{\mathbf{u}} < \mathbf{u} < \overline{\mathbf{u}}$). These constrains are computed by the Actuator Limitation function and describe the possible operation range of each actuator for the next cycle. While the limitation in normal operation is mostly based on maximum actuator dynamics, the operating range is severely restricted or set to zero when an error is detected. Accordingly, the design of the allocator is independent from the controlled actuators and reusable for various hardware configurations (Laine, 2007).

The second optimization term u (3.48) of the allocation formulation aims at the optimal operation of the actuators by minimizing the error between the actual control input and the desired control input $\mathbf{u_d}$. The latter quantifies the optimum operating condition, considering criteria such as performance, efficiency and service life. With respect to wheel brake actuators, the aim is to minimise their operation in order to increase the driving efficiency and avoid wear as well as overheating which impairs the performance. Therefore, the non-actuation is the optimal state of the wheel brakes, which is defined by setting the desired control inputs of $\mathbf{u_d}$ to zero (Härkegård, 2003).

$$u = \underset{\mathbf{u}\in\Omega}{\arg\min} \|W_u(\mathbf{u} - \mathbf{u}_d)\|_2^2 \tag{3.48}$$

Additionally, the weighting matrix W_u individually defines the strictness of compliance with the optimization criterion. In braking applications, the brake actuator facing a higher weighting is actuated less due to the amplification of the error in the optimization term. The determination of the weighting as function of the tyre normal load results in load-dependent brake torque distribution. This ensures a comparable operating point of all the tyres in their load-dependent characteristics.

Finally, the optimal actuator control input $\mathbf{u_{opt}}$ is a two-step optimization problem (3.49) based on the combination of the minimum terms (3.47) and (3.48). In order to design the allocator robust and less sensitive to actuator failure, the minimization formulation is a least squares problem in the L_2-norm. Based on this formulation, a solving algorithm generates the optimal control input within a finite number of optimization iterations.

$$\mathbf{u}_{opt} = \underset{\underline{\mathbf{u}}<\mathbf{u}<\overline{\mathbf{u}}}{\arg\min}[\|W_u(\mathbf{u}-\mathbf{u}_d)\|_2^2 + \gamma\|W_v(B\mathbf{u}-\mathbf{v})\|_2^2] \tag{3.49}$$

Since the problem formulation (3.49) combines the two separately analysed terms, the solution $\mathbf{u_{opt}}$ represents a compromise between the most accurate mapping of the real control inputs and the optimal brake torque distribution with respect to the tyre characteristics. The mathematical influence of the mapping term on the optimal solution is adjusted via the γ-factor.

In the SBB application of this thesis project, the control allocation is adapted to the configuration of a rigid 6x4 truck. Nevertheless, as mentioned in the bullet list, the allocator can be easily adapted to other configurations so that the system is reusable across the vehicle platforms. The following section details the specific setup of the 6x4 truck.

To begin with the virtual control input: The dimension and the control elements of $\mathbf{v}$ are determined by the functional scope of the system. With regard to the SBB system, the virtual control is fixed to the planar motion and the steering. Due to the modular layout of motion management, the computation of the virtual control is located in the upstream Motion Control module.

$$\mathbf{v} = [F_x \quad F_y \quad M_z \quad M_{steer}]^T \tag{3.50}$$

The dimension of the real actuator control input is set by the number of controlled actuators. As the description implies, the 6x4 truck is equipped with six wheel brake actuators whose brake torques are individually controlled by the SBB system:

$$\mathbf{u} = [T_{B1} \quad T_{B2} \quad T_{B3} \quad T_{B4} \quad T_{B5} \quad T_{B6}]^T \tag{3.51}$$

Finally, the control efficiency matrix $B_{4,6}$ is formulated and specified by the virtual and real control input. As the following calculations are based on tyre forces, the brake torque control input is converted into longitudinal tyre forces using the wheel dynamics formula (2.60). This relationship is taken into account by the linear factor. The line structure of the efficiency matrix bases on the virtual control input: The first and third row describe the effects of the individual longitudinal tyre forces on the virtual actuation of the vehicle's COG (longitudinal force and yaw moment), applying the vehicle dynamics formulas (2.18) and (2.20). Since the lateral motion is not controlled by the SBB functionality, the elements of the second row are set to zero. The last row quantifies the steering effect of differential longitudinal tyre forces acting on the steered wheels using the steering moment definition (2.41). Since the rear wheels are not steered, the associated matrix elements are set to zero.

$$B = \frac{1}{r_{dyn}} \cdot \begin{bmatrix} 1 & 1 & 1 & 1 & 1 & 1 \\ 0 & 0 & 0 & 0 & 0 & 0 \\ -\frac{w_1}{2} & +\frac{w_1}{2} & -\frac{w_2}{2} & +\frac{w_2}{2} & -\frac{w_3}{2} & +\frac{w_3}{2} \\ +r_k & -r_k & 0 & 0 & 0 & 0 \end{bmatrix} \tag{3.52}$$

In the simulation and the testing, the variables initialized with the vehicle specific data.

3.4 Actuator Management

The actuator control layer represents the interface between the motion management and the actuator hardware. As illustrated in the overview of Figure 3.8, the management task is divided into the computation of the present actuator capabilities as well as the realisation of the optimal control inputs. In order to exchange the commands and information, the actuator management is embedded in a bidirectional communication interface with both the motion management and the actuator hardware.

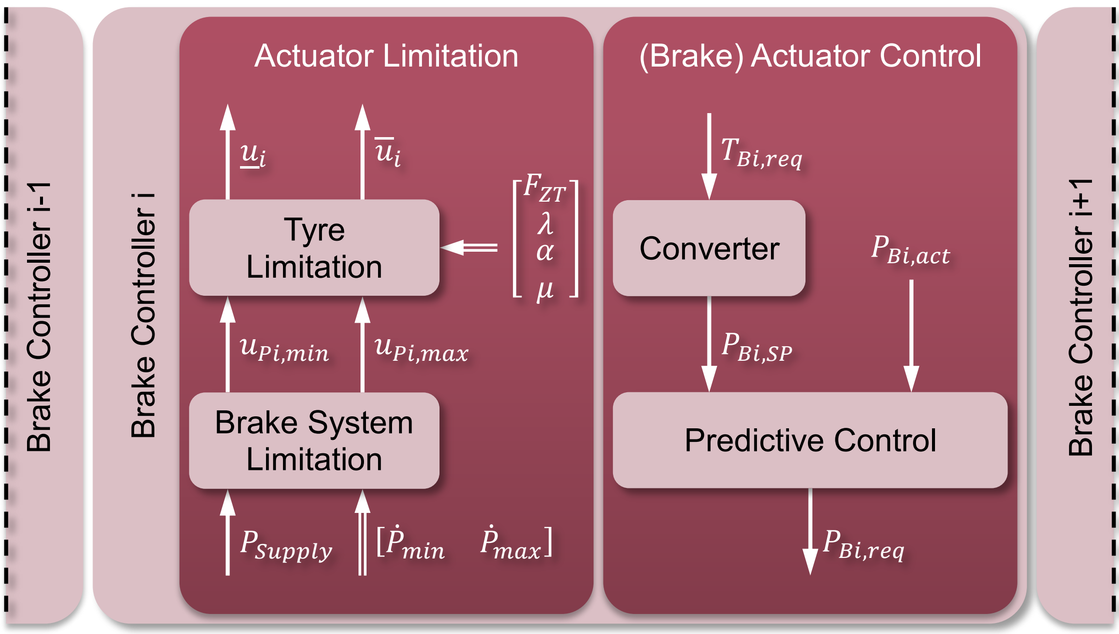

Figure 3.8: Brake control modules of the actuator management layer, including the limitation computation and the pressure controller

The actuator management layer is organised by individual and independent modules which are each assigned to a single actuator. In the communication with the motion management, the individual limitations $\underline{u}_i$ and $\overline{u}_i$ of all the modules are bundled into the vectors $\underline{\mathbf{u}}$ and $\overline{\mathbf{u}}$. Reversely, the optimized control input $\mathbf{u}_{opt}$ is split into its individual brake torque requests which are then assigned to the respective brake controller. This design enables the reusability of the system for various vehicle configurations by adding or removing control modules.

In the SBB application, this layer consists of equal modules, as the managed actuators are exclusively wheel brakes. For this reason, the following subchapters describe the functionality using the example of a single representative module illustrated in the block diagram of Figure 3.8.

3.4.1 Actuator Limitation

The actuator limitation continuously monitors the state as well as the capabilities of the actuator. This information is cyclically transmitted to the Braking Coordination module where it constrains the solution space of the allocator. Since the boundary conditions are based on the actuator capabilities, it is ensured that the calculated optimal control inputs can actually be realized by the actuators. This guarantees the optimum control of the requested motion.

The solution space of the allocator is constrained by the minimum and maximum values of formulation (3.53), which represent the capacities of all controlled actuators.

$$\underline{\mathbf{u}} < \mathbf{u}_{opt} < \overline{\mathbf{u}} \tag{3.53}$$

The actuator capabilities and thus the constraints are composed of position as well as rate limitations (Härkegård, 2003):

$$\underline{\mathbf{u}} = \max\{\mathbf{u}_{min}\,, \mathbf{u}_{opt,prev} + \Delta\mathbf{u}_{min}\} \tag{3.54}$$

$$\overline{\mathbf{u}} = \min\{\mathbf{u}_{max}\,, \mathbf{u}_{opt,prev} + \Delta\mathbf{u}_{max}\} \tag{3.55}$$

The position restrictions describe the individual operating range of the control input as function of the actuator’s physical limits such as travel, pressure, torque or temperature. In order to avoid an overload of the actuators, the operating points have to be kept within the physical limits represented by absolute minimum and maximum input values.

$$\mathbf{u}_{min} \leq \mathbf{u} \leq \mathbf{u}_{max} \tag{3.56}$$

In addition to the operating range, the actuator capabilities include the maximum change rate of the control variables. This rate limitation defines the permissible and feasible change of the control input within the next computing cycle, taking into account the related change of the actuator’s output:

$$\Delta\mathbf{u}_{min} = \dot{\mathbf{u}}_{min} \cdot T \tag{3.57}$$

$$\Delta\mathbf{u}_{max} = \dot{\mathbf{u}}_{max} \cdot T \tag{3.58}$$

Assuming a constant change rate within the calculation cycle, the offset is calculated by the means of the sampling time T and the allowable change rates of formulation (3.59):

$$\dot{\mathbf{u}}_{min} \leq \dot{\mathbf{u}} \leq \dot{\mathbf{u}}_{max} \tag{3.59}$$

To obtain absolute calculation values for the minimum and maximum problems in (3.54) and (3.55), this offset is added to the optimal control input of the previous cycle.

Besides the capabilities, this constraint implementation allows the communication of the actuator's failure by reducing the change rate to zero and setting the position to the appropriate error level. Furthermore, this design is independent from the type and number of actuators, so it is reusable for different hardware configurations (Härkegård, 2003).

The SBB system is actuated by the wheel brakes, whose brake torque is controlled by the individual actuator controllers. Applying the linear approximation (2.60) of the wheel dynamics, the torque is coupled to a certain longitudinal tyre force. Consequently, the limitation of the brake torque input is determined not only by the brake actuator, but also by the tyre capabilities. As shown in the block diagram of Figure 3.8, the brake and tyre limitation are processed successively and result in the individual limitations $\underline{u}_i$ and $\overline{u}_i$ for each wheel brake.

The brake system is primarily constrained by its pneumatic characteristics, which were analysed in detail in the Brake System Dynamics section. The working range of the connected pneumatic system components is determined by the ambient pressure and the supply pressure. In contrast, the pressure change rate is limited by the air flow between control element and brake actuator. For a reduction of the cylinder pressure, the air can directly escape at the pressure modulators into the environment. In comparison, the dynamics of a pressure build-up is lower, since the air has to be provided from the tanks via the supply lines. For simplification, the same dynamics are determined for the pressure increase and decrease, so that the transfer function of the pressure build-up (2.53) is applicable. Neglecting the system delay by assuming an optimized pressure control, the pressure dynamics are characterised by the second-order system. A step of $5\ \mathrm{bar}$ results in a system response with a peak pressure change rate of approximately $\pm 40\ \mathrm{bar/s}$. This change rate is considered to be the maximum rate of the pneumatic system. Since the constraints are described as brake torques, the pressure limitation of the brake system has to be transformed. Due to the comparatively high dynamics of the brake actuator, the brake torque is assumed to be a linear function of the cylinder or system pressure using the relational parameter K_B of definition (2.56).

In addition to limitation by the pneumatic components, the actuator control input is further constrained by the tyre-road connection. Overloading this connection by saturating the tyre contact patch not only reduces the driving stability but also causes the intervention of the ABS. Hereby, the ABS reduces the actuator's operating pressure and limits the maximum brake torque. In conclusion, the requested optimal brake torque distribution is not realisable, since the requested pressure exceeds the maximum pressure enabled by the tyre dynamics. In order to avoid an unfeasible brake torque request, on the one hand, and to achieve the desire vehicle motion, on the other hand, the limitation function needs to continuously monitor the tyre capabilities and adjust the brake torque distribution accordingly.

The combined tyre dynamics are illustrated in the friction cake chart of Figure 2.10 and the friction ellipse of Figure 2.5. Based on these models, the maximum permissible longitudinal tyre or brake force is defined by equation (2.37). Using the linear approximation of the lateral tyre force (2.34) and assuming a common friction coefficient (2.23) yields the following equation for the maximum longitudinal tyre force:

$$F_{XT,max} = \mu F_{ZT} \cdot \sqrt{1 - \left(\frac{-C_{\alpha}(F_{ZT})\alpha}{\mu F_{ZT}}\right)^2} \tag{3.60}$$

Applying the linearized wheel dynamics definition of equation (2.60), the permissible longitudinal force is converted into a maximum brake torque for the respective wheel brake actuator:

$$T_{B,max} = r_{dyn} \cdot \mu F_{ZT} \cdot \sqrt{1 - \left(\frac{-C_{\alpha}(F_{ZT})\alpha}{\mu F_{ZT}}\right)^2} \tag{3.61}$$

The brake torque limitation from the tyre capabilities is dependent on several quantities, which are not measurable with sensors. For this reason, the torque constraint is subject to uncertainties, which have to be balanced with a safety factor. While the slip angle is derived from the vehicle motion and steering, the normal force distribution and the tyre-road friction coefficient need to be estimated.

3.4.2 Actuator Control

As illustrated in the block diagram of Figure 3.8, the actuator control module receives the individual optimal actuator control input from the coordinator. This input variable is converted into the set point value for the actuator output representing the control process. To establish a closed-loop control, the control variable is computed based on the set point and the measured process variable. Subsequently, the control variable is sent to the actuator ECU. In the case of the SBB application, the actuator controllers are adapted to the wheel brake actuators which are equal in terms of their characteristic and functionality. For this reason, the following sections describe the processing of the brake torque request from the coordinator into a controlled pressure request by the means of one representative actuator. The computed request variables are transmitted to the EBS-ECU to control the pneumatic components.

According to the equations (2.55) and (2.56), the brake actuator is a first-order system in which the brake torque output is a function of the effective pressure. While the motion control is defined by forces and moments, the brake actuators are part of the pneumatic brake system. In order to design a controller for the pneumatic actuator, the brake torque request is converted into the corresponding pressure value. As with the limitation functionality, the brake torque is assumed to be proportional to the effective system pressure due to the high actuator dynamics. Therefore, the conversion function uses the brake gain K_B of definition (2.56) to describe this linear relation. Furthermore, a constant pressure offset is added to the pressure set point to compensate for the threshold value of equation (2.54) caused by the pretension.

Subsequently, the actual control function controls the pneumatic brake system by computing the manipulated pressure variable for the EBS-ECU. The system boundaries of the EBS as control process are defined by the actuated pressure modulators and valves as well as the sensors for monitoring the cylinder pressures. Inside these boundaries, the brake system dynamics are represented by a delayed second-order transfer function (2.53). In order to generate the desired set pressure and thus the brake torque, the brake system is controlled by a closed-loop system in which the actual pressure distribution is fed back and processed. Due to the delay and low dynamics of the system in comparison with the more responsive brake actuators, a predictive control is required. According to (MathWorks, 2017), the Smith Predictor is beneficial for this type of control processes as it increases the dynamics and compensates for the delay.

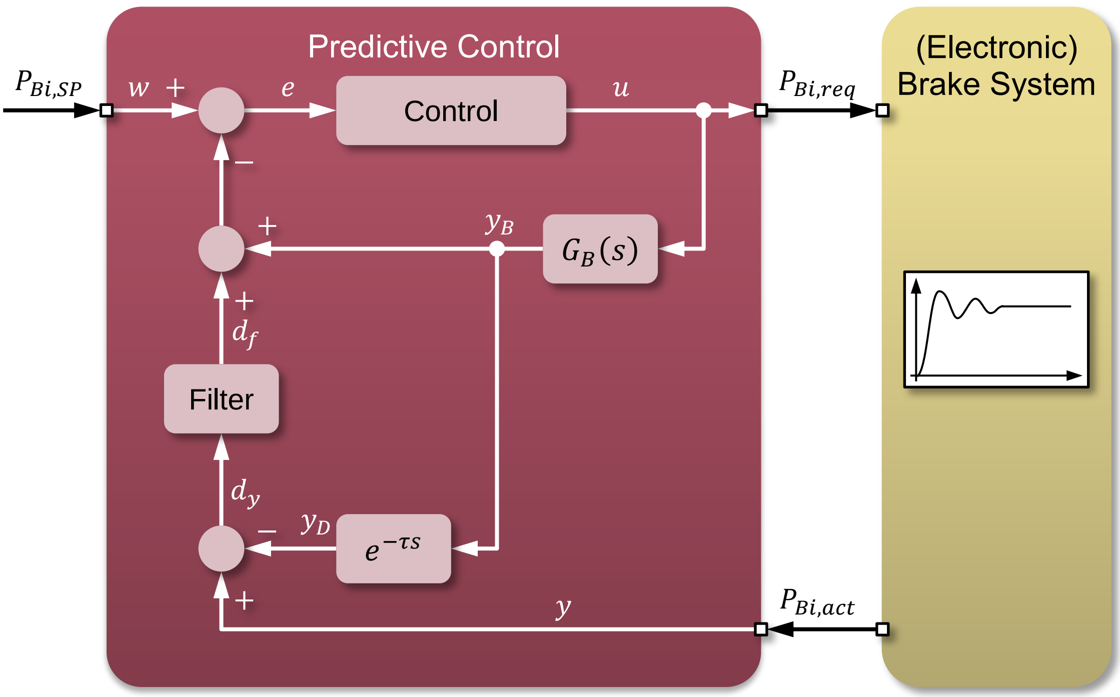

Figure 3.9: Structure of the control loop, showing Smith Predictor and the EBS control process

As shown in the control structure of Figure 3.9, the Smith Predictor is built up with control, filter and model-based elements. To reduce the control error e between the set point w and the multilevel feedback value, a straightforward PI controller is implemented, which sets the manipulated variable u accordingly. The computed control variable is sent to the actual control process as well as the internal two-part model representing the dynamic characteristics of the controlled plant. Consequently, the feedback value is composed of the returned values of the outer and inner loops. While the outer loop returns the measured value of the real process variable y, the inner two loops feedback the response signals of the process model based on transfer functions. This two-part model outputs both the delay-free response y_B and the delayed response y_D. Subsequently, the undelayed predicted response is compared with the set point value to express the required adjustment of the control variable by the controller. In order to increase the control accuracy and reduce the susceptibility, the delayed model response is compared with the actual process variable. The filtered signal d_f of their difference d_y then contributes to the common control error (MathWorks, 2017).

In the Smith Predictor of the SBB application, the process model of the brake system (2.53) is used: The system dynamics are mainly determined by the pneumatic characteristics and represented in a second-order transfer function. In contrast, the delay is constant and can be traced back to the data transmission via CAN bus. The latter establishes the bidirectional data transfer between brake controller and EBS-ECU to exchange the pressure request signals and the measured pressure distribution. The following simulation results illustrate the improved system response due to the implementation of the Smith Predictor in the actuator control module.

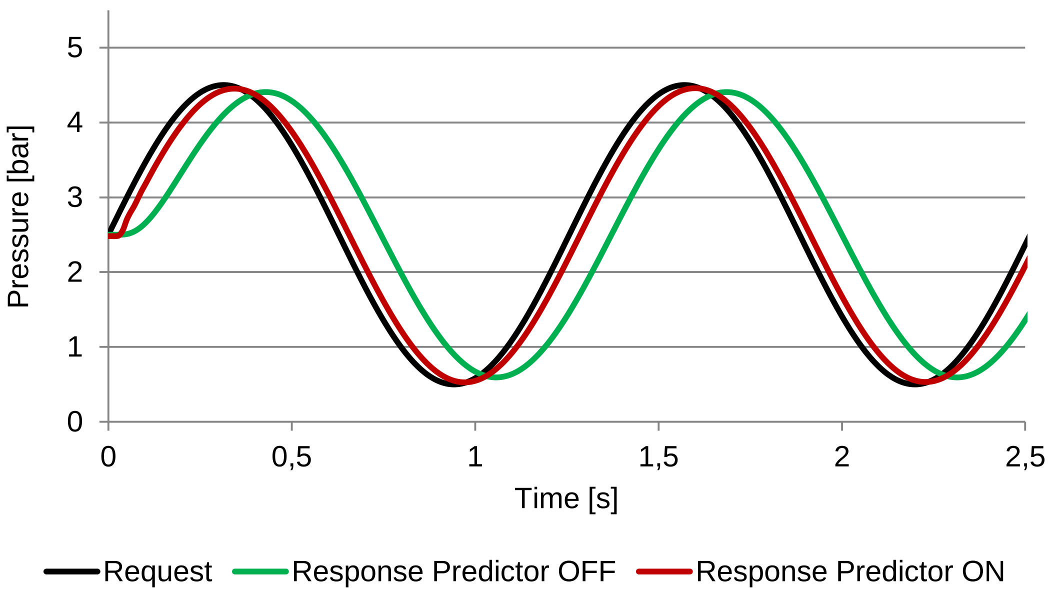

Figure 3.10: Dynamic response of the brake system with and without predictive pressure control for a sinusoidal request

As shown in the simulation results diagram of Figure 3.10, the uncontrolled brake system shows a noticeable delay as well as a lower response amplitude for a sinusoidal pressure request. The application of the Smith Predictor significantly reduces the delay of the system response and keeps the pressure amplitude nearly identical.

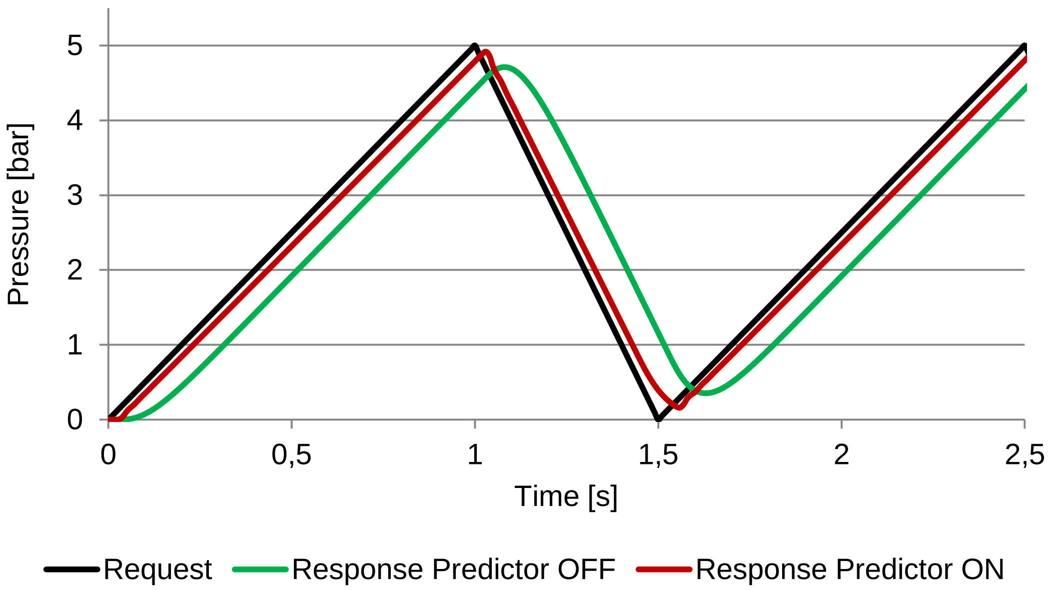

Figure 3.11: Dynamic response of the brake system with and without predictive pressure control for a sawtooth request

The simulation results of the sawtooth pressure request in Figure 3.11 clarify the outcome of the first simulation. Besides the delay and the reduction of the amplitude, the uncontrolled system smoothes the form of the request signal in the discontinuous sections. In contrast, the Smith Predictor is able to reduce the delay and reproduce complex signal forms in the system response. In summary, the predictor increases the dynamic and minimizes the delay. Furthermore, it reduces the overshoot characteristic (MathWorks, 2017).

However, the simulation results are not directly transferable to the real application because the predictor uses exactly the model of the simulated brake system. In reality, the predictor's model does not exactly match the control process which is subject to variations in its dynamics and delay. To compensate for the deviations in the model, the predictor has to be designed sufficiently robust. The robustness as well as the disturbance rejection are mainly defined by the filter layout and setting. Though, the robustness is in contradiction to the control dynamics, which is why each application requires an individual compromise (MathWorks, 2017).

3.5 Tractor-Trailer Combination Control

During the service life of a vehicle, neither the chassis structure nor the number and type of installed components usually change. This allows the unique design of the controller for a specific vehicle configuration. In contrast, the composition of tractor-trailer combinations varies during normal operation: Since a tractor is not set to a particular trailer, the combination's composition changes by attaching and removing different trailers. The trailers differ not only in their type and manufacturer, but also in their configuration and equipment. Consequently, it is neither possible nor practical to develop a motion control for the entire semitrailer.

Instead, the motion control of the combination is designed independently of the trailer by reducing the trailer to the forces it causes in the coupling point of the tractor reference frame (see Figure 2.24). Furthermore, it is not possible to control the trailer motion by requesting an asymmetric brake torque distribution, as not every trailer is equipped with an EBS to control the brake actuators independently. For this reason, only the longitudinal motion of the trailer is controllable by requesting an evenly distributed brake torque which is expressed by the single trailer brake force $F_{XTr,req}$. In addition, the control of this braking force requires the measurement of the effective coupling forces and the yaw articulation angle. By summarizing these limitations, there are two ways to integrate the trailer braking in the motion control of the SBB function:

1. Reduction of the trailer's impact on the tractor's motion by minimizing the coupling forces with an independent brake force controller for the trailer. The minimized coupling forces are treated as separate disturbance forces in the braking coordinator, which need to be compensated by the allocator and motion controller.
2. Utilization of the trailer as an additional actuator to actively manipulate the motion of the tractor. Consequently, the brake coordinator considers the trailer as an actuator which is controllable in longitudinal direction with respect to the trailer reference frame (Tagesson, 2017) (Volvo Trucks, 2012)

4 Results

In this chapter, the developed SBB system is put to the function tests, which are carried out in the simulation environment with detailed vehicle models as well as in a truck on the test track. In the first step, the control design is implemented and configured in both the simulation and testing environment. The SBB function is then tested using predefined driving manoeuvres. Subsequently, the individual results are evaluated and compared, which allows the validation of the simulation results with data from the real vehicle.

4.1 Simulation & Vehicle Testing Setup

The following subchapters will elaborate the setup for simulating and testing the SBB system.

4.1.1 Simulation Environment

The development and simulation of the SBB controller is done in Simulink by MathWorks, which allows the model-based design of dynamic systems and controllers. The integrability of coded MATLAB modules as well as multibody mechanical systems enables the use of the Volvo Transport Models (VTM) library. This library provides advanced models of the current Volvo trucks and tractors which can be coupled with trailer units.

In the VTM library, the vehicles and trailers are represented as mechanical multibody systems, in which the chassis, cab, payload, axles, wheels and tyres are modelled and linked via joints or suspensions. The models are limited to the mechanical vehicle parts and their dynamic characteristics. Consequently, the models are stimulated by applying forces and moments on the mechanical parts, since the actuators are inoperable rigid bodies. Use cases of the VTM library are the simulation and analysis of the vehicle dynamics of trucks and vehicle combinations as well as the development of model-based control systems. Furthermore, the vehicle models are used in the driving simulators for real-time simulations and HIL-applications (Fröjd, 2017).

For the simulation of the SBB functionality, the VTM of the desired vehicle configuration is integrated in the control loop, as illustrated in Figure 4.1. In the simulation process, the truck model inputs the control commands from the SBB controller and generates the associated dynamic response. Reversely, the VTM allows the control unit full access to all vehicle parameters.

In contrast to the real vehicle, the function of the actuators is not included in the truck models of the VTM library. In order to ensure the comparability of simulation and vehicle testing results, the VTM needs to be extended by a model of the brake system and the related actuators, which was elaborated in the chapter about the Brake System Dynamics. At the same time, the brake pressure interface between control unit and brake system is established, which is similar to the EBS input module of the real vehicle. The brake model processes the applied pressure request and outputs the related brake torque distribution to the vehicle model.

Furthermore, the path following module is separated from the SBB control unit. This design enables the simulation of different path following methods independent of the SBB function as well as the straightforward integration of the existing path following module, which has already been tested and adapted to the test truck.

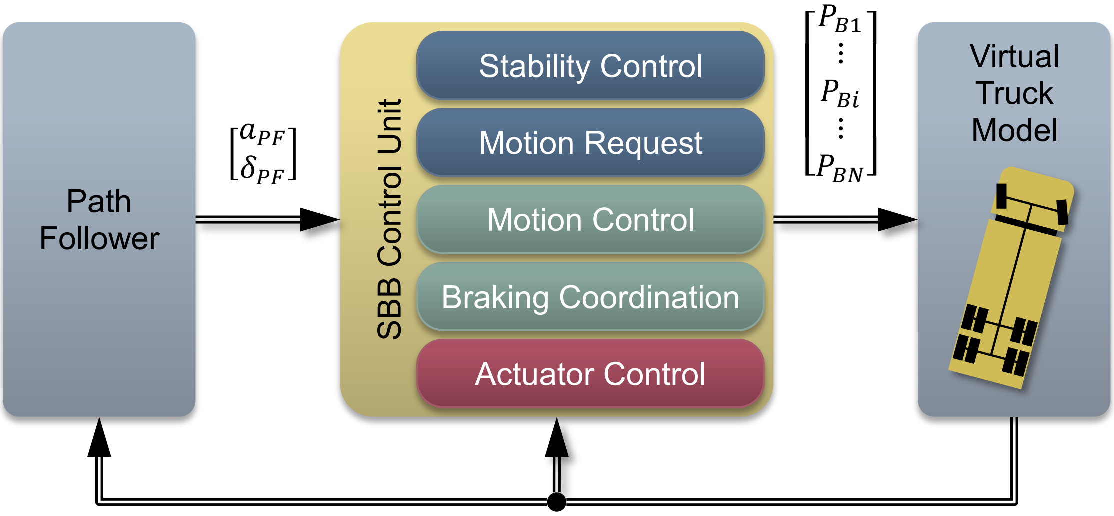

Figure 4.1: Setup of the SBB system for model, software and hardware in the loop simulations

4.1.2 Vehicle Testing Environment & Procedure

In comparison between the simulation setup in Figure 4.1 and the test setup in Figure 4.2, the SBB system controls a real test truck instead of the virtual truck model. In addition, sensors and estimators provide the control unit with the required vehicle process variables and replace the direct feedback path in the simulation control structure of Figure 4.1.

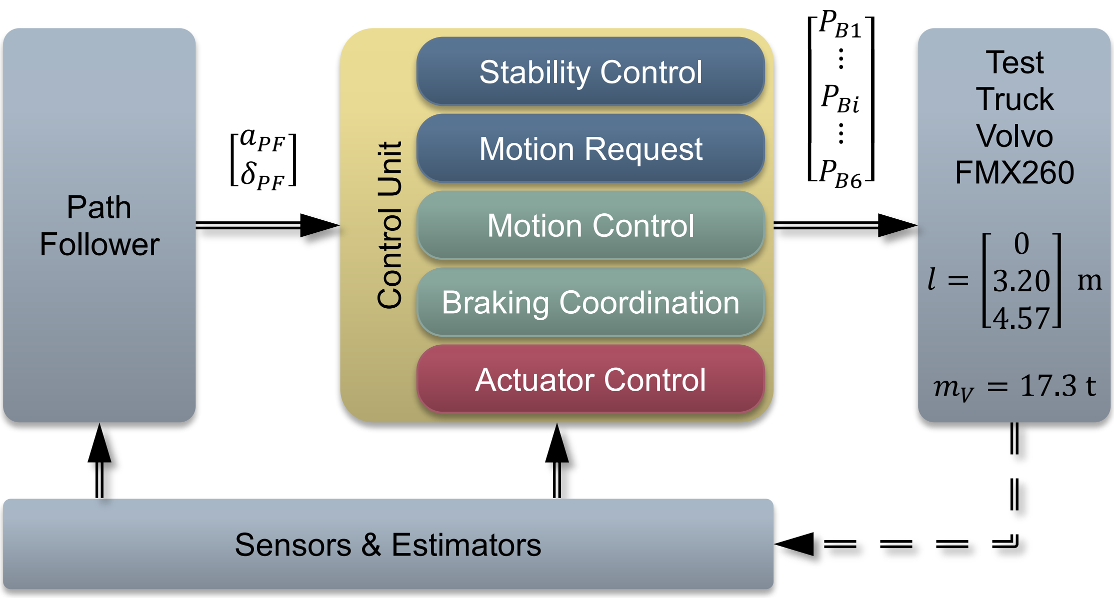

Figure 4.2: Setup of the SBB system for real vehicle testing

The functional tests are performed with a Volvo FMX 8x4 (see Figure 4.3) which is primarily designed for the use on construction sites. Besides the dump body, the test truck is equipped with a tridem bogie. Furthermore, the truck provides an EBS which is required to control wheel brakes independently. To improve the test truck's manoeuvrability, the vehicle configuration is changed from 8x4 into 6x4 by lifting the tag axle. In this tandem configuration, the wheelbase is $l = [0 \quad 3.20 \quad 4.57]$ metres with respect to the front axle. The total mass of the unladen truck is $m_V = 17.3$ tonnes. Due to the combination of dry asphalt on the test track and off-road tyres with coarse tread mounted on the truck, the friction level is assumed to be a constant value of $\mu_{Test} = 0.7$.

Figure 4.3: Test truck Volvo FMX260 8x4 tridem (AB Volvo, 2017)

Sensors continuously provide the controller with vehicle measurement data required for the control functions. In order to keep expenses and effort low, the SBB control unit accesses the existing sensor data of the following sensors:

- Gyroscope: Yaw rate ω_Z
- Accelerometer: Acceleration in longitudinal direction a_X and lateral direction a_Y with respect to the vehicle reference frame
- Wheel speed sensors: Wheel-spin velocity ω_{Wi}
- Steer angle sensor: Steer angle δ
- Brake pressure sensors: Brake pressure distribution P_{Bi}
- Global positioning system (GPS) module: Position in global coordinates plus vehicle speed longitudinal direction v_X and lateral direction v_Y with respect to the reference frame. Note: This sophisticated sensor module is currently not installed in the production vehicle. Nevertheless, it is going to be a standard component in automated driving vehicles.

The sensors, their signals and their measuring positions are illustrated in Figure 4.4. Since the vehicle models and motion controllers refer to the load center of gravity, the sensor values of the gyroscope, accelerometer and GPS sensor have to be corrected according to their measurement position in the reference frame.

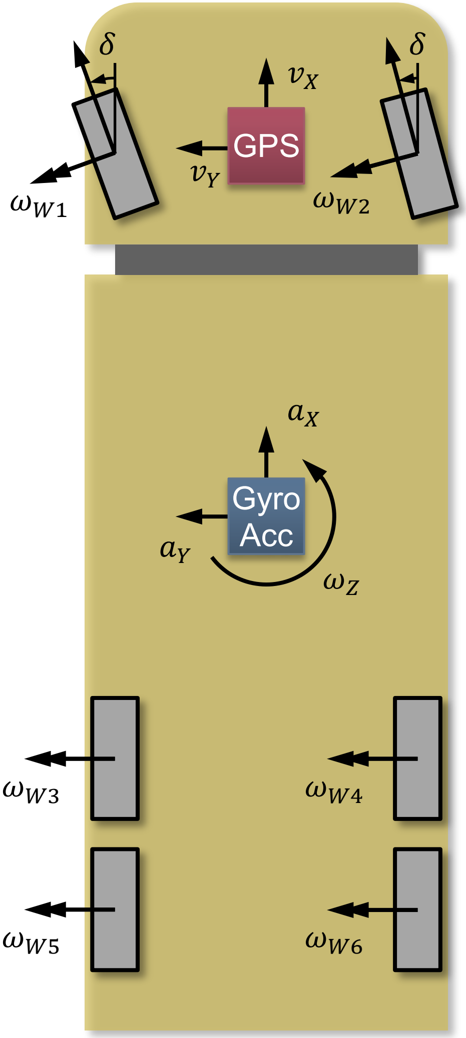

Figure 4.4: Kinematic sensors and sensor signals in the test vehicle

Moreover, the control functions of the SBB system require further vehicle data such as normal load distribution or tyre-road friction level, which can not be measured with the (installed) sensors. Instead, estimation functions or external measurements are used to acquire the required information. Assuming constant road and test conditions on the testing ground, the friction value is determined in a preceding measurement. In contrast, the normal load distribution changes while driving due to the dynamic load transfer. For this reason, the individual tyre normal forces have to be recalculated online with an estimator using a vehicle model.

In the test truck, the code of the SBB functionality and the estimators are running on a dSPACE AutoBox, which is a real-time capable computing unit. Due to its compact and robust design, the AutoBox is mainly used for rapid prototyping of in-vehicle applications. In conjunction with the instrumentation software ControlDesk by dSPACE, the AutoBox allows the reconfiguration of system parameters online (dSPACE, 2017). Besides the function code, the AutoBox is initiated with the global coordinates of the trajectory. The latter is defined by the GPS recording of the manually performed driving manoeuvre in advance. Afterwards, the external path follower is initialised with the GPS data of the smoothed path.

For the function test of the SBB system, the test vehicle is autonomously driven to the starting point of the manoeuvre and accelerated to the desired initial speed. Once the SBB function is activated, the steering actuator is turned off to simulate the faulty steering. Simultaneously, the gearbox shifts into neutral to avoid any braking or propelling effect by the engine on the wheels of the driven axles.

4.2 Test Manoeuvres

In order to investigate the SBB function, several test manoeuvres are defined, representing different real driving situations. The defined manoeuvres are inspired by the several standardized driving tests for motion control systems. An important test for the evaluation of stability control systems is the sine-with-dwell manoeuvre of the National Highway Traffic Safety Administration (NHTSA), in which the vehicles have to perform a double lane change (Neubeck, 2016). In contrast to the specific and exactly defined NHTSA test, (Reif, 2010) assesses motion control systems on the basis of four generally formulated driving situations (Table 4.1). The driving manoeuvres of (Reif, 2010) are used for the functional tests of the SBB system in this project.

Table 4.1: Driving manoeuvres for the functional tests (Reif, 2010)

Straight	Transition	Curve	S-Curve

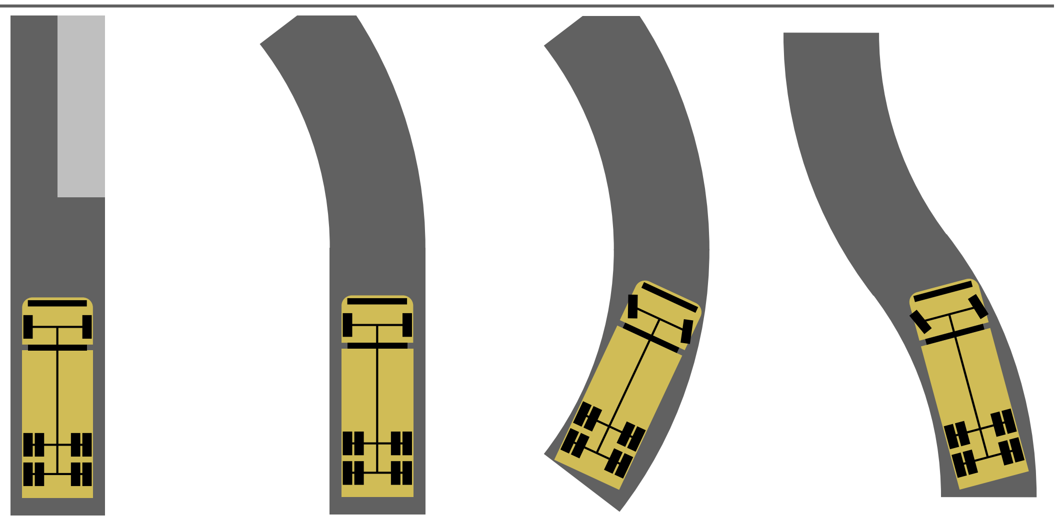

The minimum or critical curve radii in these manoeuvres mainly depend on the vehicle speed and the friction level. Conversely, the vehicle speed has to be adapted to the driving situation in order to guarantee driving safety. The vehicle guidance along the motion trajectory including the adaption of the speed is the task of the path following module by computing appropriate steering and braking commands. The deceleration of trucks during normal braking is up to $-0.5\ \mathrm{m/s^2}$ and may increase up to $-6.5\ \mathrm{m/s^2}$ during safety braking (Cheng, 2013) (ADAC, 2015). As a fallback level for the steering system, the functionality of SBB system has to be ensured in a vehicle speed range of 0 to $85\ \mathrm{km/h}$.

In the functional tests, the driving behaviour of the vehicle is examined with regard to manoeuvrability and driving safety. To assess the manoeuvrability, the system behaviour is investigated in terms of steering accuracy, compensation of disturbances and dynamic response to steering commands. Conversely, driving safety is evaluated on the basis of the yaw and roll stability. The mentioned criteria are examined by means of the different driving manoeuvres of Table 4.1:

- Straight: Analysis of the directional stability in the event of lateral disturbances due to (split friction) braking, side wind or steering offset.
- Transition: Investigation of the cornering behaviour with load transfer, the adaptability to steering command changes and the driving stability
- Curve: Examination of the steering accuracy (lateral deviation) and the cornering stability in the event of lateral disturbances due to (split friction) braking.
- S-curve: Composite of two curves and a transition. Analysis of the vehicle stability in situations with high load transfer and the adaptability to changes in direction.

4.3 Simulation & Vehicle Testing Results

In this subchapter, the simulation and vehicle testing results are presented and analysed. As mentioned in the previous section, the testing manoeuvres are recorded manually and based on the manoeuvres of Table 4.1. This ensures both the compliance of the physical driving limits in terms of vehicle stability, as well as the optimal utilization of the available test area. Due to the effort and complexity, only the first two manoeuvres are performed on the test track.

In the following sections, two manoeuvres defined and performed on the test track are analysed and compared with the simulation results of the same input trajectory. Since the development of position and velocity differ between vehicle testing and simulation, the results to be compared can not be displayed in the same diagram. Instead, the vehicle testing and simulation results are evaluated separately and successively. For the analysis of the results, the parameters are displayed in the following charts:

- Position: XY-position progression of path and truck
- Steer angle: Requested and actual steer angle plus the command from the path following function
- Yaw rate: Requested and actual yaw rate
- Acceleration: Requested and actual acceleration in x-direction plus lateral acceleration
- Velocity: Vehicle speed in the COG
- Brake torque: Requested brake torque distribution from the brake coordinator

Due to technical issues with the brake system on the test truck, the wheel brakes of the second drive axle can not be actuated, which is why the brake torque request of these two actuators is limited to a small value in the allocator. During the test preparation, the inner loops of the predictor caused a high level of noise in the system which impaired the control of the actuators. In order to focus on the main function of the SBB system, the actuator controllers are bypassed with a linear gain which converts the torque into a pressure request signal.

4.3.1 Manoeuvre 1 – S-Curve

The first test manoeuvre is an S-curve path, which represents a country road with a combination of a right and a left turn. Due to the initial speed of $v_0 = 60\ \mathrm{km/h}$, this manoeuvre provokes a critical load transfer, which requires stabilization measures by the SBB system. Furthermore, the narrow curve radii result in high centrifugal forces, so that the tyres operate at their adhesion limit.

4.3.1.1 Vehicle Testing Results

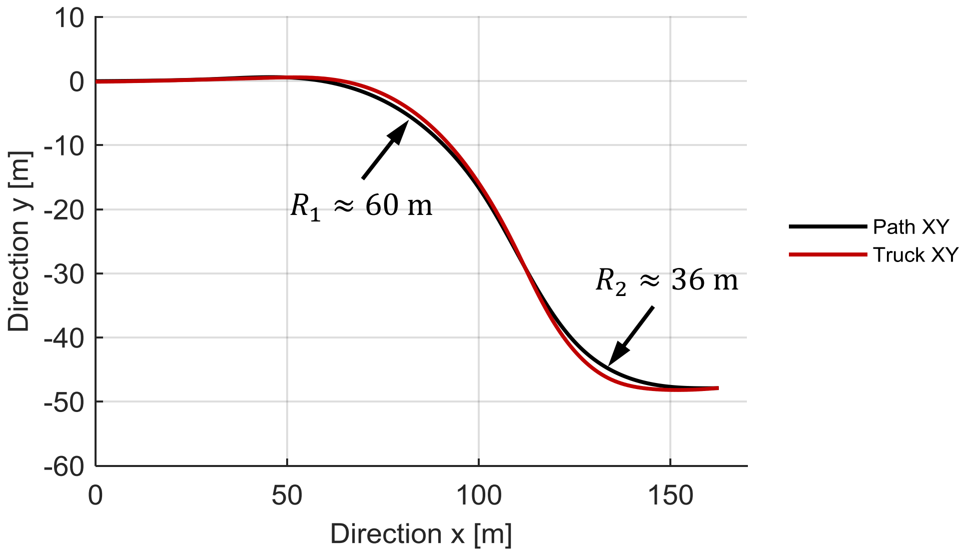

Figure 4.5: Manoeuvre 1 / vehicle testing – Position of path and vehicle

As shown in position course of Figure 4.5, the maximum deviation of the vehicle position from the desired path is $d_{max,R1} \approx 0.5$ m in the first bend and $d_{max,R2} \approx 1$ m in the second curve. It is noticeable that the vehicle position is always on the outside of the corner which indicates a delayed steering motion. In order to compensate for this offset, the SBB function increases the steer angle which results in a smaller cornering radius.

The suspected delay in the steering is confirmed in the steer angle chart of Figure 4.6: The actual steer angle δ_{act} follows the steering request δ_{req} delayed. Due to this time delay, the change in motion direction is retarded, which results in the position offset shown in Figure 4.5. Furthermore, the delay is accompanied by an increased steer amplitude to compensate for the deviation. Consequently, the steering delay is a critical value as it determines both the deviation from the trajectory and the steering angle amplitude.

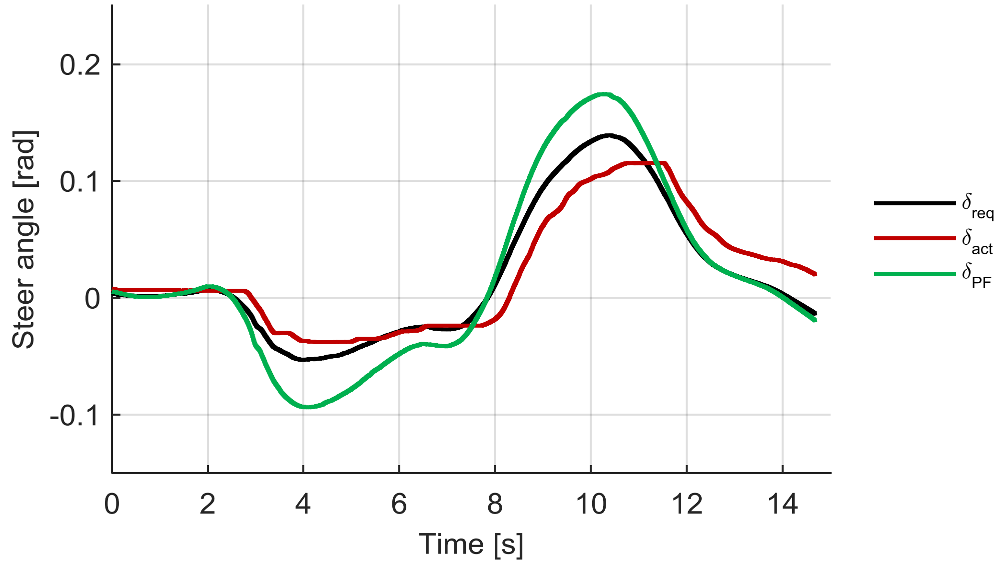

Figure 4.6: Manoeuvre 1 / vehicle testing – Steer angle

Regardless of the delay of the actual steering, the shapes of the steer angle signals are similar to each other. However, the amplitude of the actual steer angle does not accomplish the level of the request signal. Due to the self-steering effect based on the asymmetric brake force distribution, the motion request function reduces the amplitude of path follower's steering command δ_{PF} . Consequently, the asymmetric braking of the wheels reduces the required steer angle to generate the desired vehicle motion.

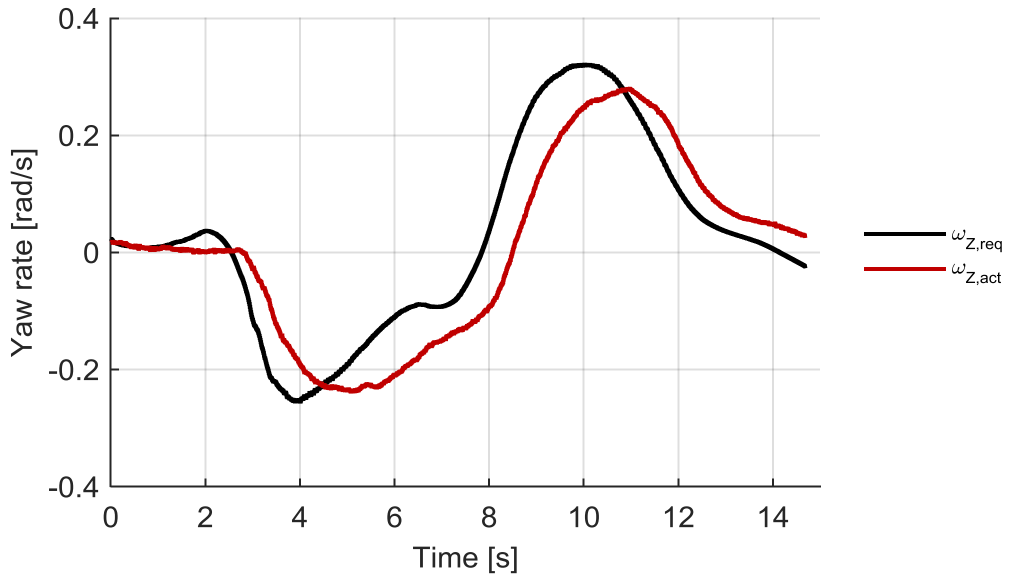

Figure 4.7: Manoeuvre 1 / vehicle testing – Yaw rate

As shown in Figure 4.7, the shape of the actual yaw motion is similar to the yaw request. However, the yaw motion of the vehicle is delayed as well, indicating a delay in the operation of the wheel brakes.

Another reason for the deviation of the vehicle to the outside of the corners is the high lateral acceleration of approximately $0.35\,g$, which applies on the COG. Simultaneously, the brake actuation causes a longitudinal acceleration in the range of normal braking between 0 and $-1\ \mathrm{m/s^2}$.

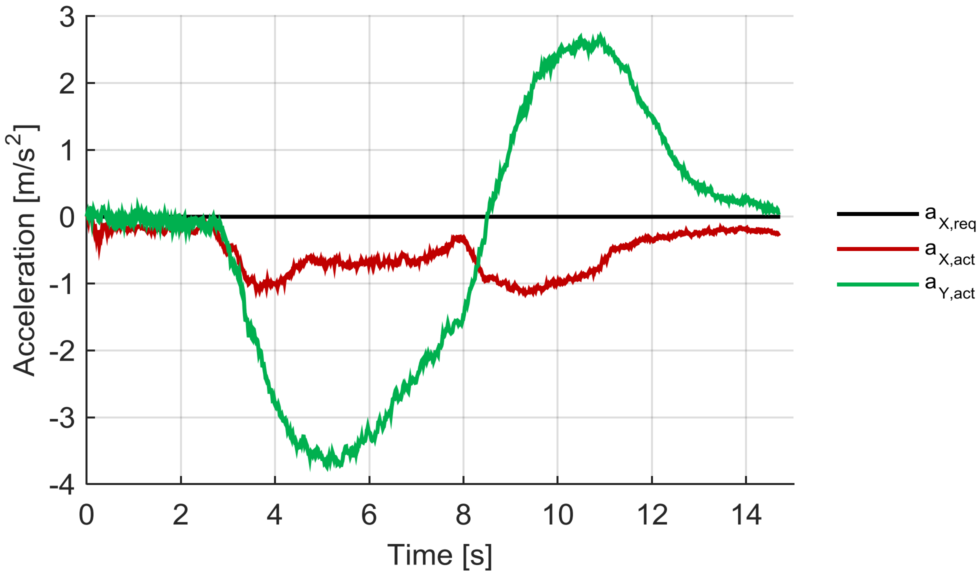

Figure 4.8: Manoeuvre 1 / vehicle testing – Acceleration

Assuming a constant sideslip angle in equation (3.15), the lateral acceleration is linear function of the yaw motion. For this reason, the two signals are comparable in terms of signal delay and shape. In contrast, the longitudinal acceleration determines the progression of velocity in Figure 4.9: The decrease in speed is mainly set by the integral of the longitudinal acceleration. Furthermore, the velocity is an indicator of the (energy) expenditure required for the manoeuvring. Since the brakes are used intensely for the steering in this manoeuvre, the velocity decreases by $10\ \mathrm{m/s}$.

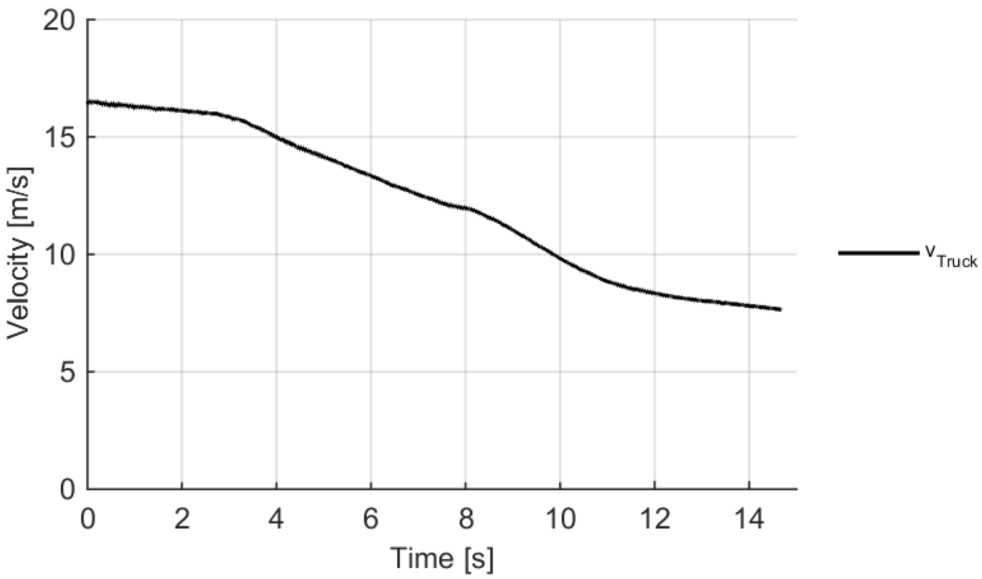

Figure 4.9: Manoeuvre 1 / vehicle testing – Velocity

Figure 4.10 illustrates the brake torque distribution from the allocator. In accordance to the Steering Dynamics, the SBB controller generates the differential brake force to steer the front wheels by applying brake torque on the inside wheel. Conversely, the rear wheel brakes are actuated to support the steering and to stabilize the vehicle motion: At the beginning of the (right) turn, the braking of the inner (right) rear wheel supports the yaw motion. The subsequent transition zone from the right to the left turn causes a destabilizing load transfer. To ensure driving stability, the controller reduces the yaw motion along with the steering by braking the opposite rear wheel. As mentioned above, the brakes of the second drive axle are deactivated due to technical problems with the valves of the EBS.

In general, the brake torque application to the wheels immediately follows the request signal in steering and yawing. This fact becomes clear in the direct comparison of the steering request to the actuation of the front brake. Consequently, the reason for the delay in the steering and yawing has to be in realization of the actual brake forces.

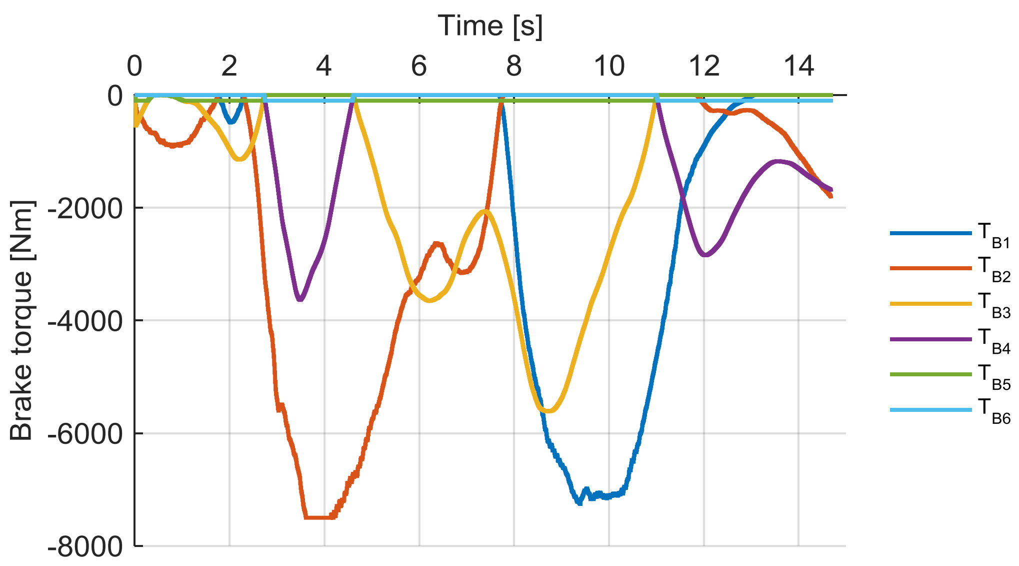

Figure 4.10: Manoeuvre 1 / vehicle testing – Brake torque

In this demanding manoeuvre, the vehicle is operated at the physical limits. Nevertheless, the SBB system stabilized the motion throughout the testing and compensated the deviation in position by adapting the steering. Although the braking torque request follows the steering and yawing control signals immediately, the actual steering and yawing motion is delayed. These delays can be traced back to the linear bypass function instead of the actuator controller: Firstly, there is no reduction for the delays in the brake system and secondly the pressure offset is not compensated. Consequently, the brake has to overcome the threshold before the actual brake torque is generated. For these two reasons, the actual torque is not only delayed but also lower than the requested torque. Furthermore, the coarse tyre profile dampens the brake torque and reduces the dynamics. In addition, the coarse tyre profile dampens the brake force generation in the contact patch. All in all, this results in a delay of the steering and thus the yawing motion.

4.3.1.2 Simulation Results

In contrast to the vehicle testing, the actuator control is activated in the simulation.

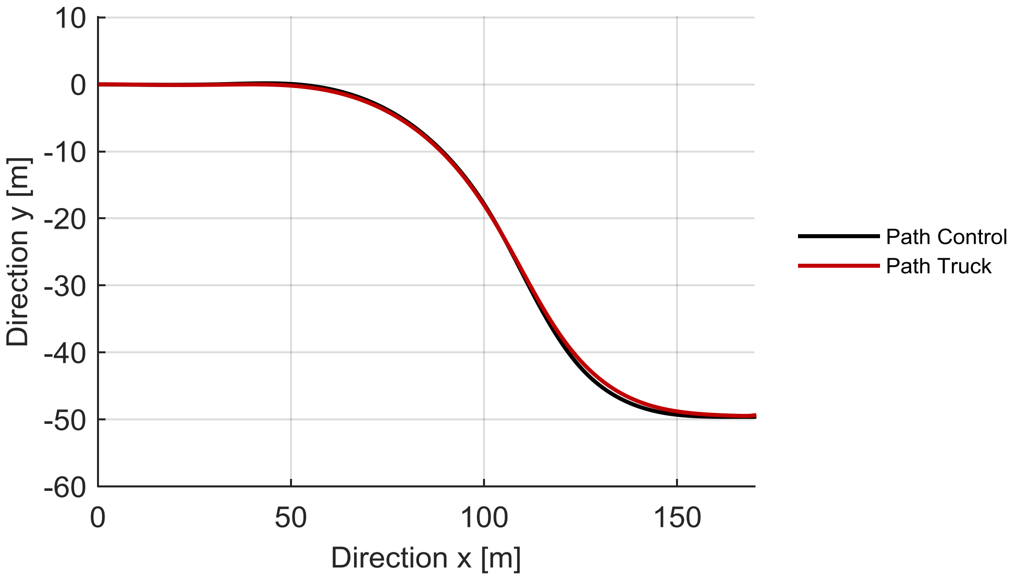

Figure 4.11: Manoeuvre 1 / simulation – Position of path and vehicle

In the simulation, the deviation of the vehicle's position from the path reduces to less than $0.3\ \mathrm{m}$, which is shown by the motion trajectory in Figure 4.11. Moreover, this time the vehicle tends to cut the corners, resulting in larger turning radii and indicating a significant reduction of the steering delay.

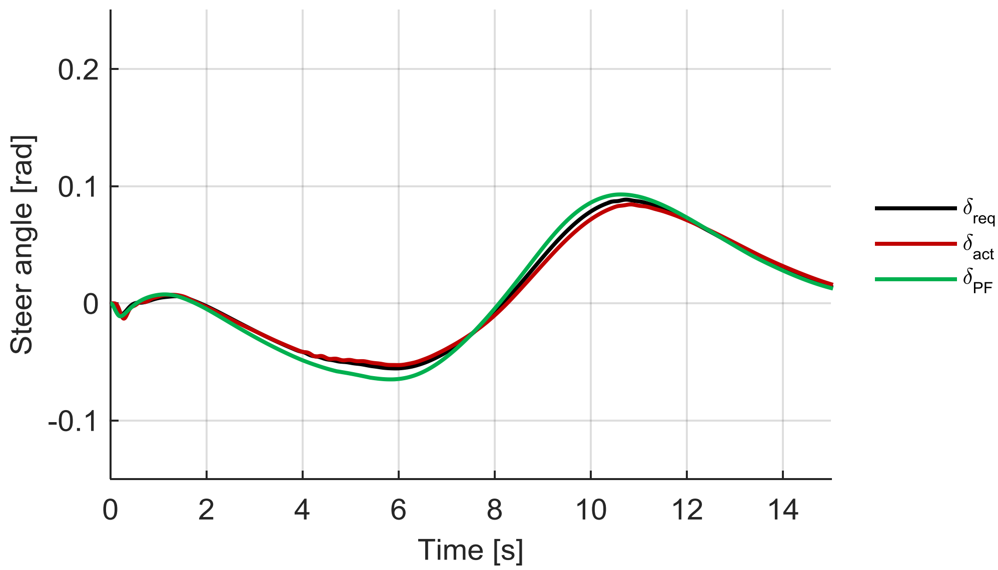

Figure 4.12: Manoeuvre 1 / simulation – Steer angle

The impression of the position chart is confirmed in the steering diagram of Figure 4.12, as the measured signal's delay is minimized. In addition, the signal level and shape of the actual and the requested steer angle are almost equal. Due to the larger radii, the required steer angle for the same manoeuvre is significantly smaller, which also reduces the differential braking on the front wheels. For this reason, the difference between the path follower's command and the requested steering is smaller, since the self-steering effect based on the braking reduces.

In the simulation results of Figure 4.13, the measured yaw motion follows the requested motion with a short delay. Furthermore, shape and amplitude of the signals are equal. In comparison to the vehicle testing results in Figure 4.7, the peak yaw value has decreased due to the larger cornering radii.

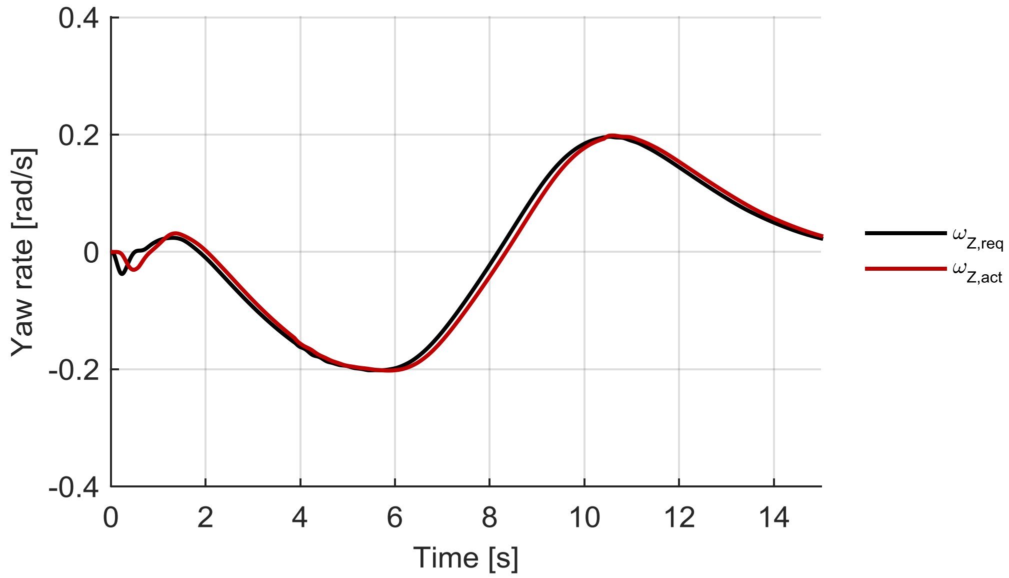

Figure 4.13: Manoeuvre 1 / simulation – Yaw rate

Due to the reduction of the yawing amplitude, the lateral acceleration also decreases (see Figure 4.14).

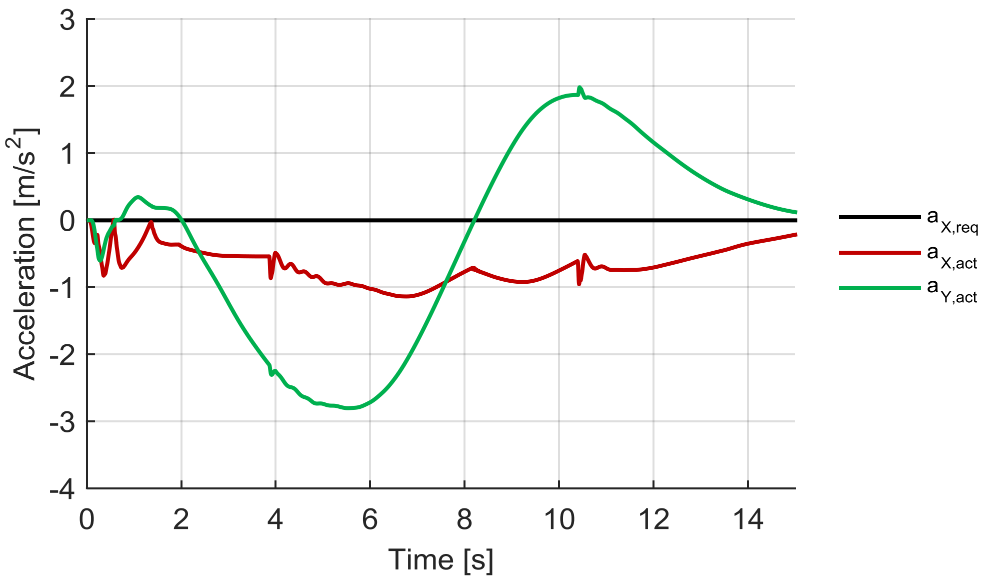

Figure 4.14: Manoeuvre 1 / simulation – Acceleration

According to the Steering Dynamics, a reduction in the steering results in a decrease of the differential brake forces on the front wheels. In comparison with the testing, the rear brakes are actuated slightly earlier, which simplifies the turning by an initial yaw momentum. In order to ensure comparability between vehicle testing and simulation results, the brakes of the second drive axle are also deactivated in the simulation.

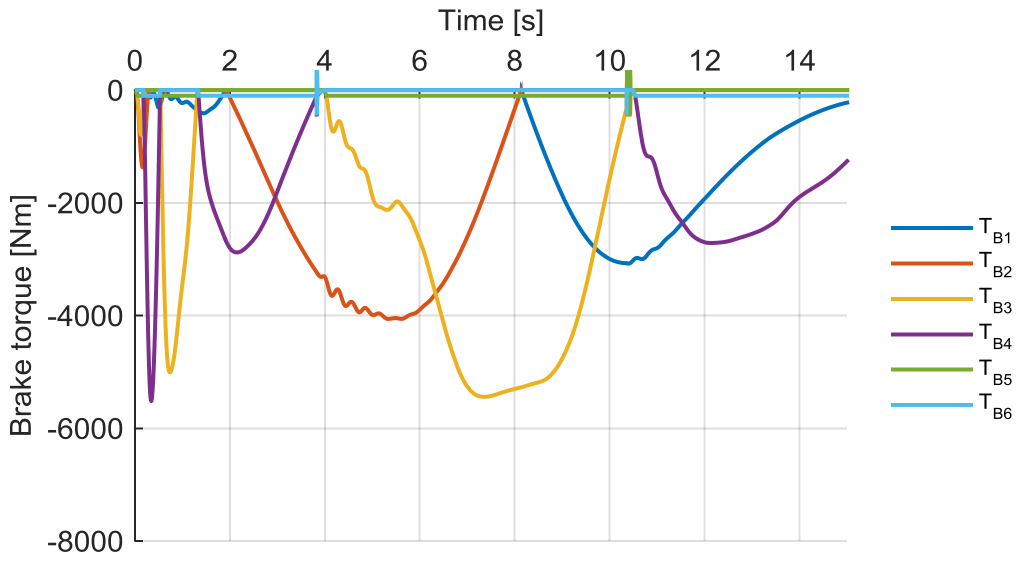

Figure 4.15: Manoeuvre 1 / simulation – Brake torque

In the simulation, the SBB system manages this manoeuvre with a high accuracy even in the narrow corner. Furthermore, the system ensures driving stability and minimizes the delays in the actual motion.

4.3.2 Manoeuvre 2 – Double Lane Change

In the second test, a double lane change is performed at a speed of $v_0 = 60\ \mathrm{km/h}$. Since this test represents an avoidance manoeuvre, the investigation of the system dynamics is of importance. Moreover, the dynamic motion in combination with the transitions causes load transfers which require the stabilization of the vehicle. At the same time, driving precision is important in order not to leave the prescribed traffic lane.

4.3.2.1 Vehicle Testing Results

As with the vehicle testing of the first manoeuvre, the steering response is delayed, resulting in the vehicle's depicted deviation in Figure 4.16. The maximum lateral deviation occurs at the vertices of the four curves, due to the smallest radii. Nevertheless, the critical lateral deviation from the imaginary traffic lane centres ($y_1 = 0\ \mathrm{m}$ and $y_2 = -4\ \mathrm{m}$) is less than $0.3\ \mathrm{m}$, so the truck does not leave the prescribed lane. Furthermore, the dynamic directional changes in the trajectory cause an overshooting driving behaviour.

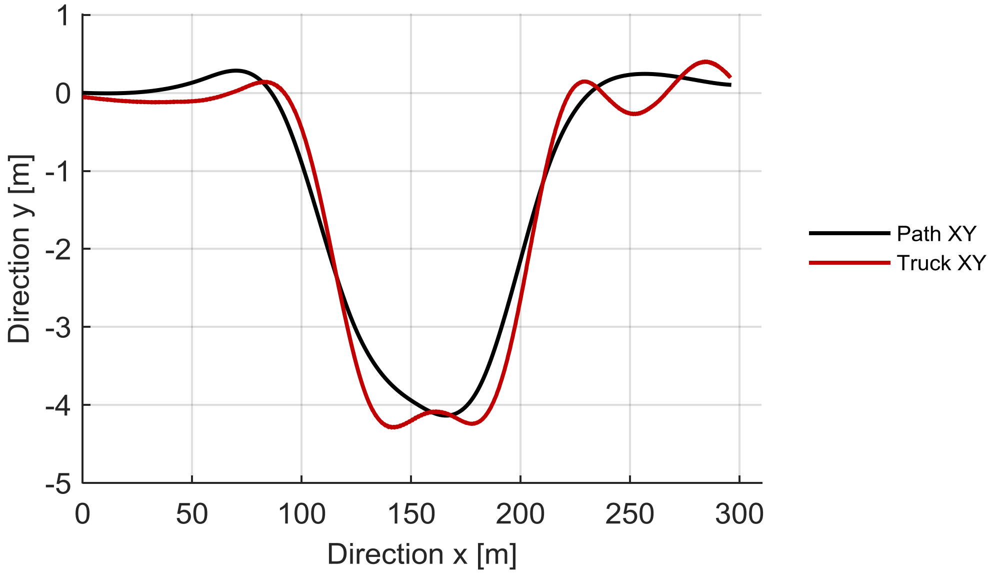

Figure 4.16: Manoeuvre 2 / vehicle testing – Position of path and vehicle

In order to compensate for the deviation from the desired trajectory, the SBB function has to increase the steering amplitude. In combination with the dynamically changing steering motion, however, the time delay causes a reduction in the amplitude of the actual steer angle. As shown in the steer angle diagram of Figure 4.17, the measured steer angle deviates in time and amplitude from the requested signal. Moreover, the delay in the reversing of the steer angle results in the mentioned overshooting characteristic.

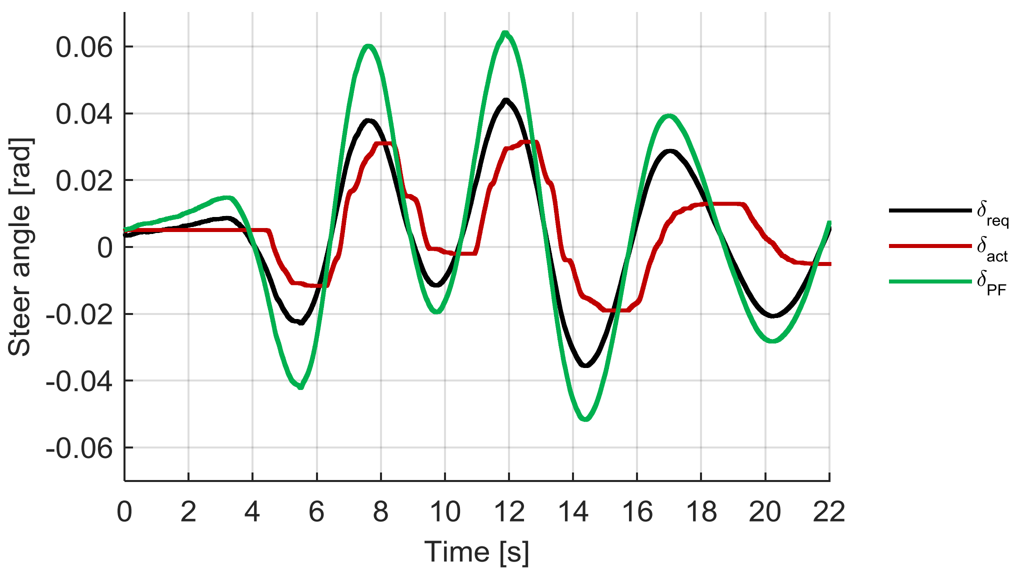

Figure 4.17: Manoeuvre 2 / vehicle testing – Steer angle

The steering's deviation in time and signal strength affects the yaw motion similarly, which is derived from the comparison of the requested and measured yaw rate in Figure 4.18.

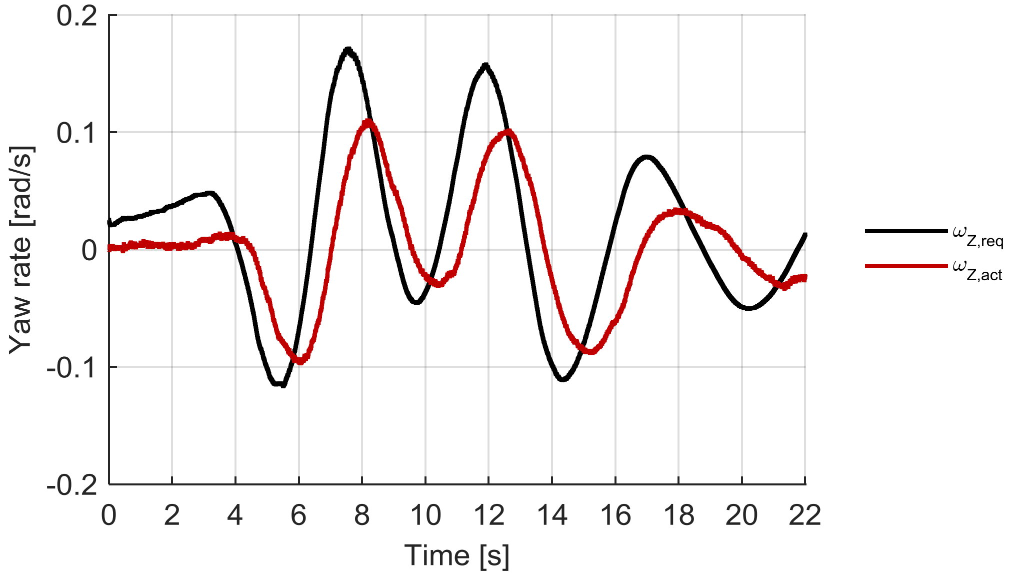

Figure 4.18: Manoeuvre 2 / vehicle testing – Yaw rate

As illustrated in Figure 4.19, the SBB controller actuates both the front and rear brake of one vehicle side together to steer in the related direction. Since only minor stabilization measures are required, the rear brake operation slightly overlaps the front brake actuation.

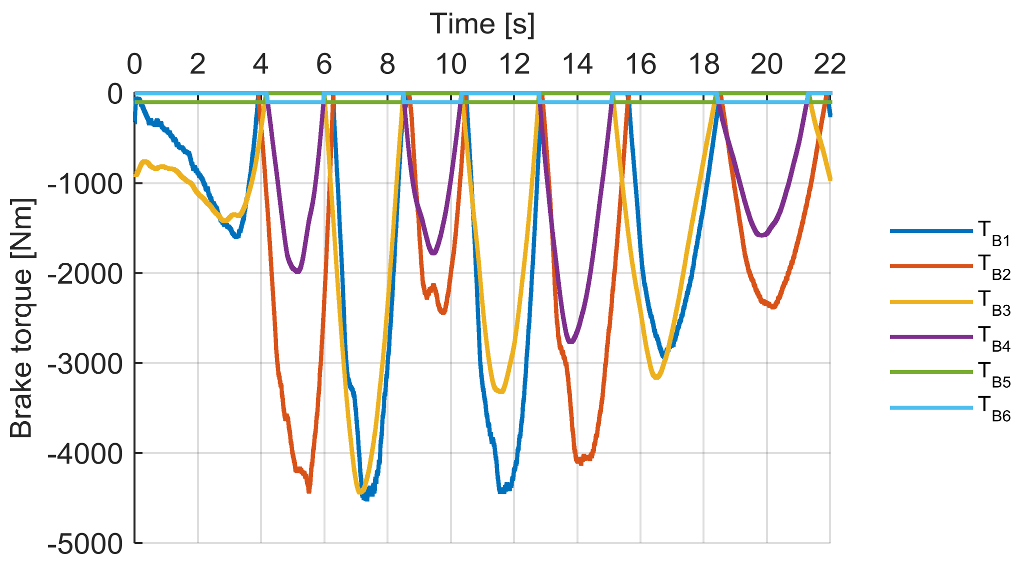

Figure 4.19: Manoeuvre 2 / vehicle testing – Brake torque

4.3.2.2 Simulation Results

In the simulation of this lane change manoeuvre, the deviation between vehicle position and specified path reduces to less than $0.3\,\mathrm{m}$, which is illustrated by the recorded positions in Figure 4.20. As with the simulation of the first manoeuvre, the cornering radii are wider and the overshooting behaviour is reduced, suggesting a reduced steering delay.

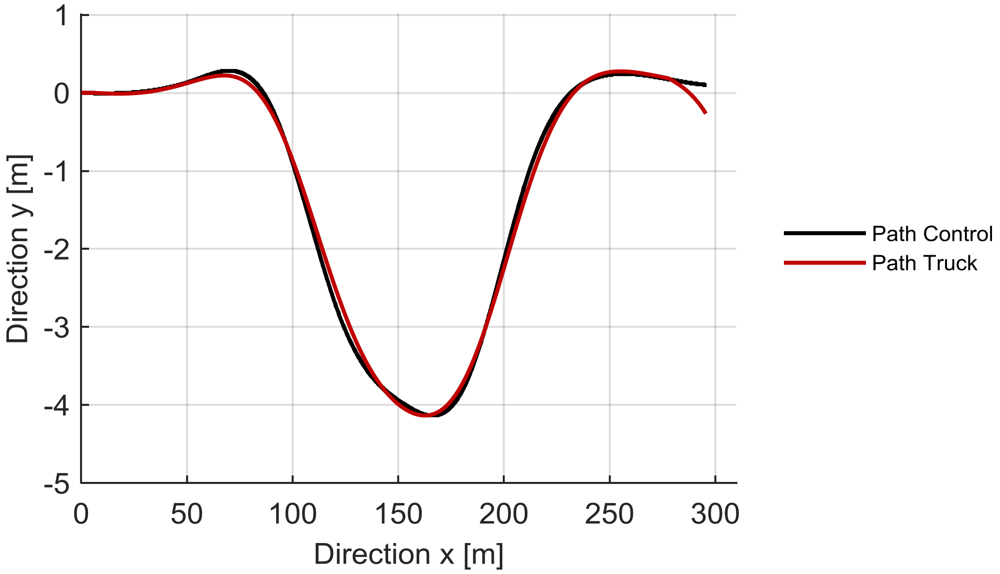

Figure 4.20: Manoeuvre 2 / simulation – Position of path and vehicle

As already assumed, the delay of the measured angle is minor (see Figure 4.21). Furthermore, the actual and the requested steer angle are equivalent regarding the signal level and shape. At the same time, the larger radii result in smaller steering angles compared to the vehicle testing. Due to a smaller self-steering angle, the signal levels of path follower and motion request are similar, indicating an even brake torque distribution.

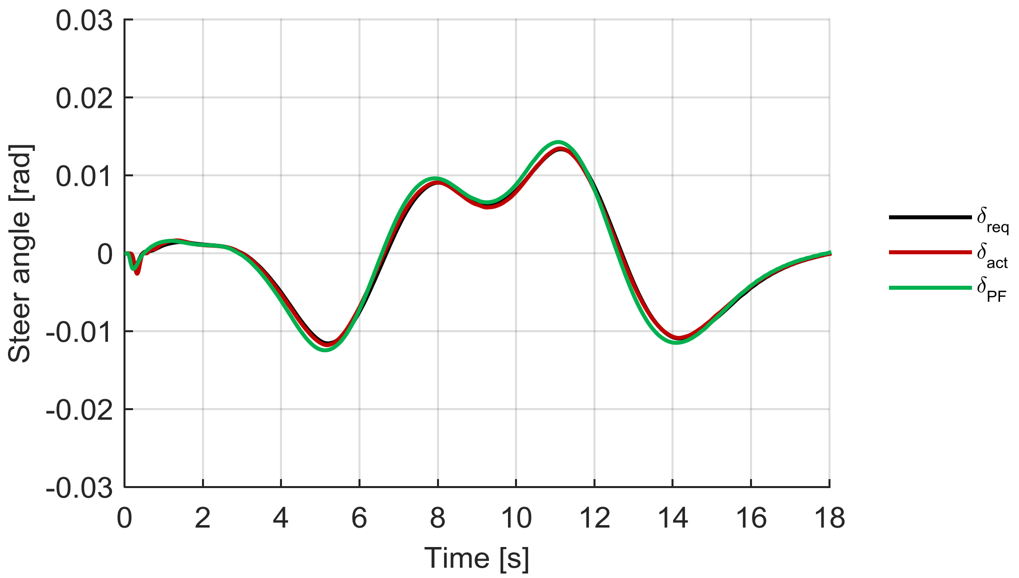

Figure 4.21: Manoeuvre 2 / simulation – Steer angle

Due to the lager cornering radii, the peak yaw value decreases in the simulation, as shown in Figure 4.22. Furthermore, the measured yaw motion follows the requested motion with a short delay, resulting in a stable vehicle motion.

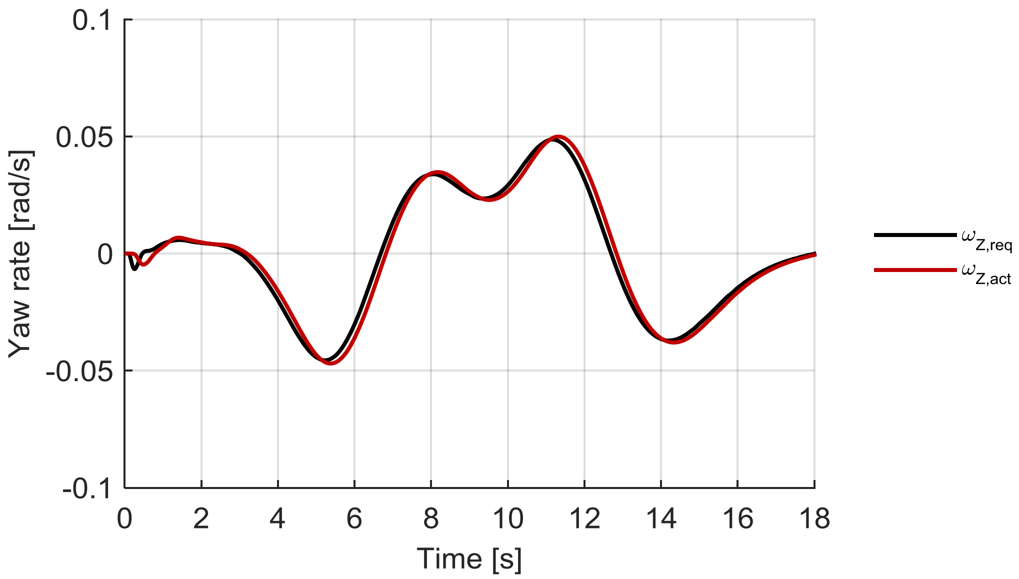

Figure 4.22: Manoeuvre 2 / simulation – Yaw rate

The decrease in the steering angle request results in a significant reduction of the required differential brake forces on the front wheels to a maximum value of 1000 Nm, which is illustrated in the resulting brake torque distribution of Figure 4.23. Furthermore, the reduced overshooting characteristic requires less steering actuations and corrections in comparison to the vehicle testing. As shown in the testing results of Figure 4.19, the SBB system alternates the wheel brake actuation between the left and right vehicle side. In the simulation, the SBB system alternates the brake actuation axle-related. For this reason, the actuation of the front and rear axle overlap, resulting in a more homogenous, stable and precise vehicle motion.

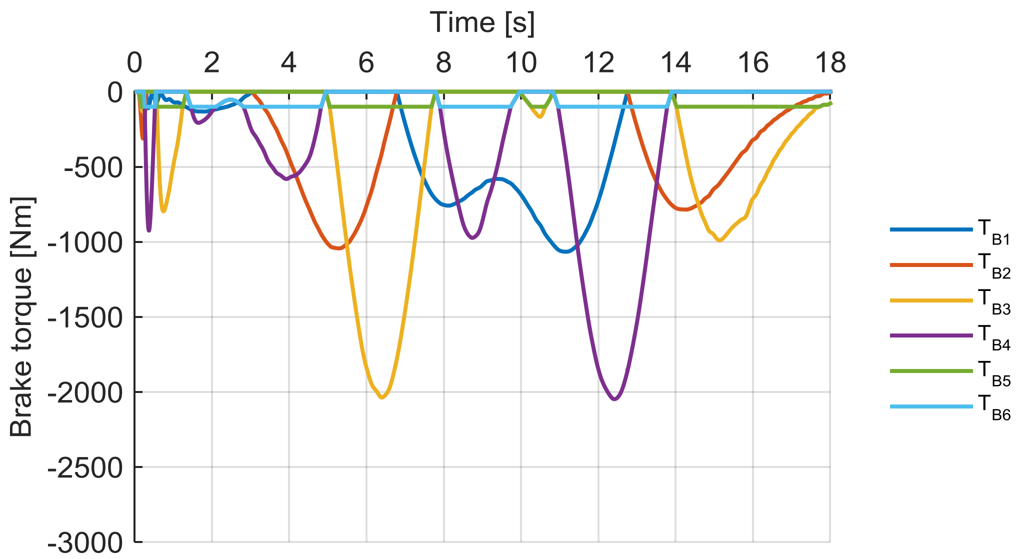

Figure 4.23: Manoeuvre 2 / simulation – Brake torque

The consistency of driving accuracy and stability by execution of the requested steer angle and yaw rate with the corresponding brake torque distribution proves the functionality of the control design and the developed motion request module.

4.4 Comparison VDS and SBB Performance

The SBB system is considered a fall-back level for the primary steering actuator. For this reason, the performance of the VDS is the benchmark for assessing the manoeuvrability of a vehicle. Although the SBB system was able to handle the different driving manoeuvres, a direct comparison to the driving characteristics with a functional VDS is necessary in order to ultimately evaluate the system performance.

For this comparison, a double lane change is performed with both systems on the test track, since this manoeuvre demands ambitious steering response and accuracy. Furthermore, the yaw control of the SBB function is deactivated to compare the pure steering behaviour. The testing results are presented separately as the development of position and the velocity varies.

4.4.1 VDS Performance

In the first test, the VDS-steered truck carries out the lane change at a constant speed of $v_0 = 17\ \mathrm{m}/s$. As shown in the position development of Figure 4.24, the vehicle drifts to the outside of the corner. Nerveless, the deviation from the driving path is always less than $0.3\ \mathrm{m}$.

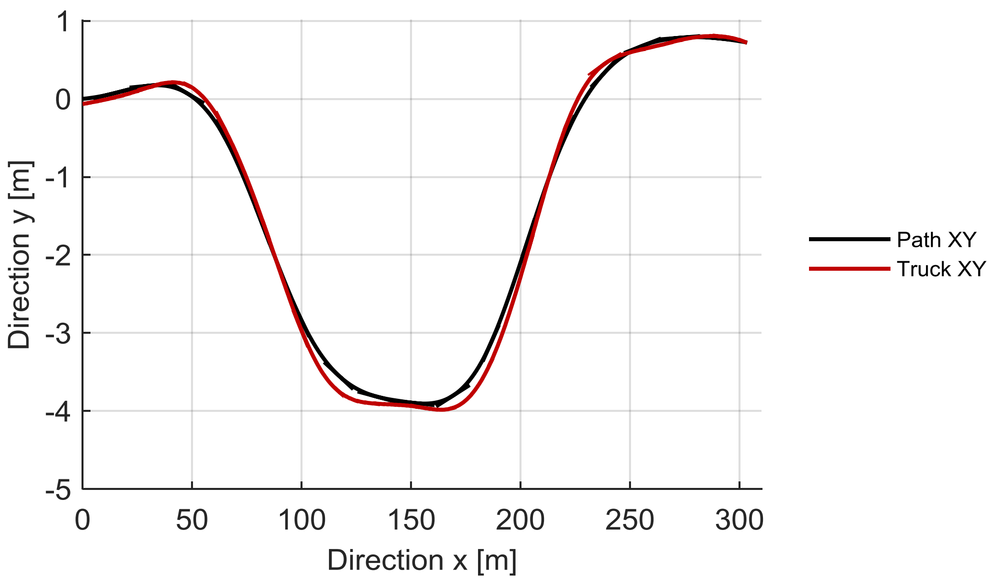

Figure 4.24: Double lane chang e with VDS operation – Position

The VDS is directly connected to the path follower and receives the steer angle request δ_{PF}. In the time direction, the actual steer angle follows the command almost undelayed and the electric actuator reacts dynamically to changes in the request (see Figure 4.25). Due to a correcting offset $\Delta\delta_{VDS}$ in the software, the actual steer angle is constantly shifted by about $+0.15°$.

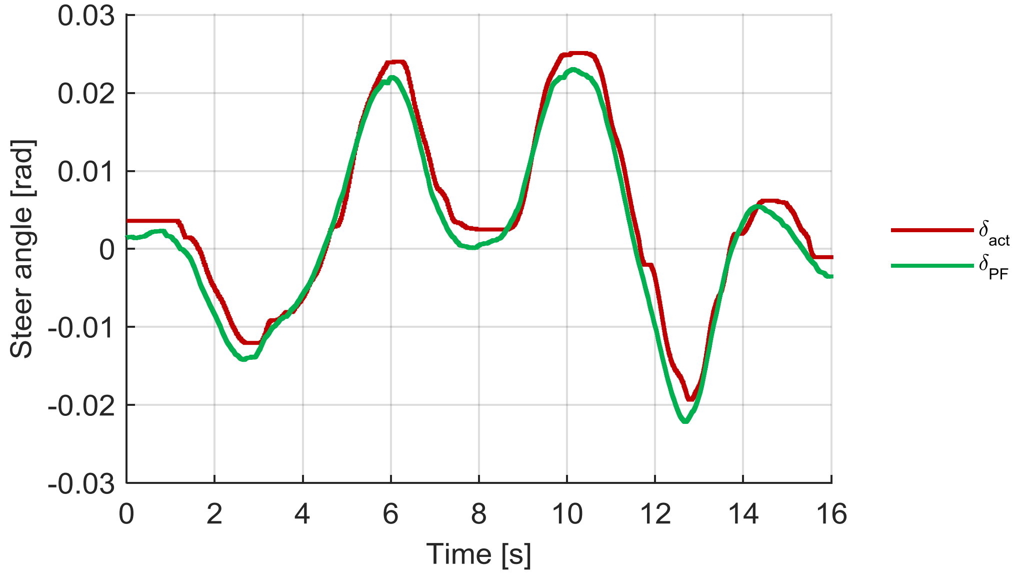

Figure 4.25: Double lane chang e with VDS operation –Steer angle

4.4.2 SBB Performance

Subsequently, the VDS system is deactivated in order to perform the same manoeuvre by steering with the SBB function. The initial vehicle speed is increased to $v_0 = 18.5\ \mathrm{m/s}$ to compensate for the loss of speed because of the brake actuation.

The steering performance in terms of position deviation between the VDS-steered vehicle and the requested trajectory in Figure 4.26 is comparable to the results with the VDS operation in Figure 4.24. However, the SBB system has to make minor counter steering interventions to reduce the offset.

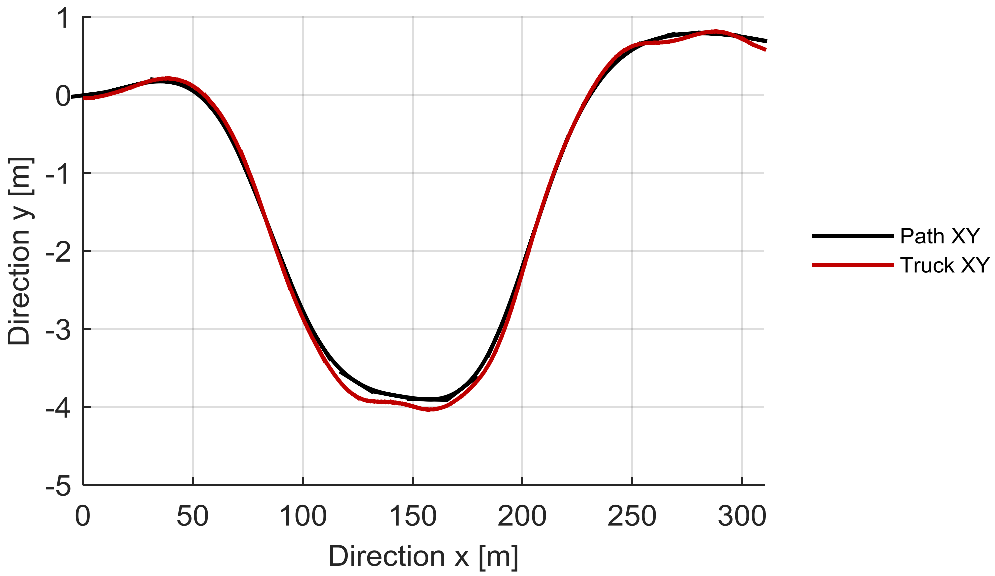

Figure 4.26: Double lane chang e with SBB operation –Position

In contrast to the equivalent positioning with both systems, the actual steering characteristic differs. As ascertained in the previous chapter, the steering reaction to the request signal is delayed (see Figure 4.27). Furthermore, the shape and amplitude of the angular signal differs from the steering request by a maximum of $\pm 0.25°$. In comparison to the VDS testing, the required steering amplitude for the manoeuvre is lower due to the yaw amplification from the asymmetric bake force distribution.

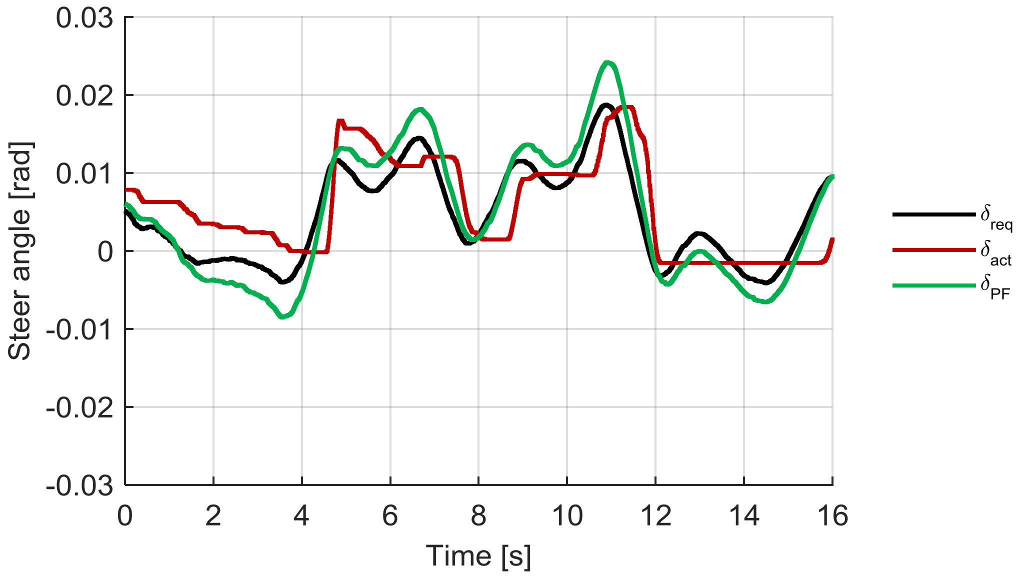

Figure 4.27: Double lane chang e with SBB operation –Steer angle

As shown in Figure 4.28, the operating range of the front brakes is moderate (maximum torque values of 2 to $3.5\,\mathrm{kNm}$) while the rear brakes are not actuated ($T_{B3} = T_{B4} = T_{B5} = T_{B6} = 0\,\mathrm{Nm}$). This brake actuation causes a reduction in velocity of approximately $4\ \mathrm{m/s}$ throughout the manoeuvre.

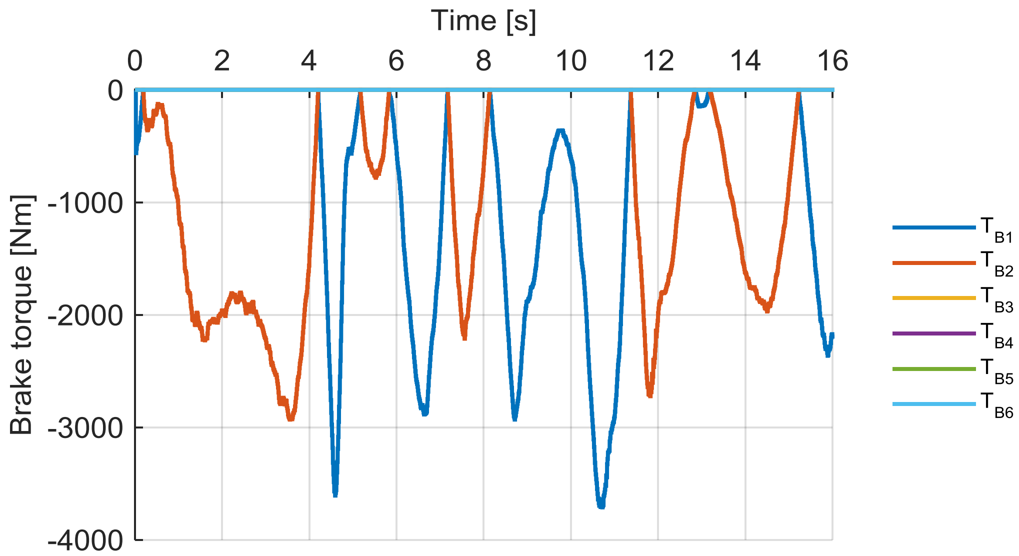

Figure 4.28: Double lane chang e with VDS operation –Brake torque

In summary, the SBB system is able to provide a comparable steering performance for the vehicle in terms of positioning. However, the VDS actuator is more precise in realizing the steering request from any high layer function such as the path follower. Due to its dynamic characteristics, the VDS steering is capable of following quick changes in the request signal. In contrast, the dynamics of the SBB system are limited by the maximum change rate of the tyre forces, which are characterised by the braking system and the tyre contact patch (chapter Actuator Limitation). The limitation determines the change rate capabilities of the steering angle, which can be improved by activating and modifying the actuator control modules in future vehicle tests.

5 Concluding Remarks

This chapter summarizes and concludes the previous sections about modelling, designing and testing. Furthermore, it presents an outlook for future improvements and functional expansions.

5.1 Conclusions

The investigation on the manoeuvrability of over-actuated commercial vehicles by asymmetric braking shows promising results for the future automated driving. This analysis has been an important step towards the highly reliable execution of steering commands in autonomous applications to ensure maximum manoeuvrability and driving safety in any situation.

One of the major objectives of this thesis project was the development of a reconfigurable motion control system which generates the desired vehicle motion using the wheel brakes. The designed control unit was intensely tested in the simulation environment and on the test track. Both testing results prove the manoeuvrability of the vehicle by controlling the wheel brake actuators independently. Moreover, the steering performance of the asymmetric braking is equivalent to that of the intended steering actuator, creating an independent level of redundancy. Compared to an additional steering actuator as fall-back solution, the usage of the mounted brake actuators of the respective vehicle configuration keeps the system costs and box volume as well as the development effort low.

The motion control system is based on a vehicle model with planar dynamics allowing longitudinal, lateral and yaw motion. Nevertheless, the vehicle's roll motion is considered by the control system to ensure driving stability. The modelling comprises all the components which affect the manoeuvrability of the vehicle: chassis, steering, brake system, wheels and tyres. For most components and characteristics, it is applicable to use linear approximations to minimize the complexity in modelling and computing. Furthermore, simple models reduce the amount of failures as well as the computational effort and enhance the controllability. This facilitates the establishment of a working system which can be simulated and tested. Nevertheless, it is possible to replace the simplified components by more complex models in the future.

The control architecture has been divided into three hierarchical layers, in which the individual function modules are implemented (see Figure 3.1). While the hierarchy determines the processing relevance and rate of the associated functions, the modular structure allows the function-oriented development and simulation of the motion control system. Furthermore, this architecture enables the replacement of single modules and the reusability of the whole system across the vehicle platforms. With the exception of the brake coordinator, the individual modules are adapted to the respective vehicle configuration via a parameter file containing the vehicle specific data. Furthermore, the actuator management layer has to be proportioned to the configuration by adding or removing actuator control modules. In the following sections, the individual modules of the system are conclusively discussed.

The traffic situation management modules in the top layer determine the kinematics of the vehicle, including the steering, to perform a predefined driving manoeuvre. To begin with, the path follower computes the required steering and acceleration commands to optimally guide the vehicle along the trajectory representing a specific driving manoeuvre. The implemented pure pursuit method calculates the steering commands geometrically on the basis of a simple single-track model of the vehicle. Because of its open-loop structure, this tracking technique is straightforward, yet robust and sufficiently accurate for the application in this project.

On par with the path follower is the stability controller, which monitors the physical limits of the actual roll motion using the lateral acceleration since the tyre normal load distribution is not measured. Taking a safety margin to the absolute roll limit, this approach is reliable and simple. The subsequent motion request functionality is one of the system’s core modules since it computes the required vehicle motion variables based on the merging of the driving commands from the path follower with the stability information. While the acceleration variable is specified by the path follower, the request function has to calculate the required steer angle which is equivalent to the steering command input, taking into account the actual vehicle motion state and the brake torque distribution. To enhance the overall manoeuvrability and driving safety, the module computes a yaw request as additional motion control input which exactly matches the calculated steering request signal.

The motion management layer is designed to control the requested vehicle motion and to coordinate the available actuators. Due to the subdivided structure in control and coordination, the entire system can be reconfigured and reused in a simple way. The motion controller is model-based, combining a feed-forward and a feedback branch. This design results in a control characteristic which is robust, sufficiently accurate and has a moderate dynamic response. Based on the vehicle parameters, the control module computes forces and moments as virtual control inputs for the allocation module.

The brake coordinating module maps the virtual control inputs to real control inputs sent to the individual actuator controllers, taking into account the vehicle configuration as well as arrangement of actuators. At Volvo GTT, the control allocation technique has been successfully used in previous projects to solve similar allocation problems in over-actuated systems. The allocation algorithm coordinates and optimizes the control inputs of the available braking actuators in such a way that their combined output performance optimally fulfils the requested virtual variables. In this optimization process, the allocator considers the current status and capability of each actuator to actually perform the motion request and to avoid overloading or saturation of the actuators. As the algorithm finds the optimal solution within finite number of iterations the control allocator is real-time capable, which is important for vehicle applications. Furthermore, the adaption of the coordinator to any vehicle configuration and number of actuators is straightforward.

In the bottom layer of the architecture, the individual brake control modules establish the interface between the motion control unit and the wheel brake actuators. Each actuator is assigned to a single control module that controls the output performance and monitors the actual capabilities. In this application, the capabilities are limited on the one hand by the characteristics of the pneumatic brake system and on the other hand by the transferable tyre forces. While the brake characteristics are described by a delayed transfer function, the maximum tyre forces are calculated on the basis of the friction ellipse. Simultaneously, each module controls the brake pressure of the respective actuator based on the optimal control input from the coordinator. In order to increase the dynamics and compensate for the delays in the brake system, a model-based predictive controller has been implemented.

Finally, the driving behaviour of the vehicle with regard to manoeuvrability and driving safety has been examined in the functional tests. In order to operate the system at the physical limits, it had to complete several demanding driving manoeuvres. In these manoeuvres, the SBB system was able to compete with the primary steering actuator in terms of vehicle positioning. The realization of the steering motion was accurate but delayed. Nevertheless, the yaw control kept the vehicle motion stable throughout the testing and enhanced the overall manoeuvrability.

5.2 Future Challenges

In order make the SBB system an essential function for the future automated driving of trucks, it is necessary to optimize the system performance and to extend the functionality. An important part is to perform further driving manoeuvres in the simulation environment and on the test track in order to tune the configurable control parameters.

5.2.1 Performance

As examined in the testing and simulation, the delay in the brake force generation is the primary driver influencing the motion characteristics in terms of steering accuracy, system dynamics as well as required brake torque. As a first measure, the predictive actuator control module has to be developed for the implementation on the test vehicle, since this function proved a significant reduction of the brake delay in the simulation (see Actuator Control). Furthermore, this control module compensates the pressure offset which causes an additional delay in the brake response and a reduced effective brake torque.

Moreover, the driving precision and dynamics as well as the braking efficiency can be improved by a more detailed modelling of the single system components. This includes the consideration of nonlinearities and the reduction of simplifications. For a more precise computation of the lateral tyre forces and the associated aligning moment of the front wheels (equation (2.42)), the combined simplified steering angle has to be replaced by an individual angle for each front wheel in the model of the steering system. In addition, the steering dynamics have to be extended by the moments from the tyre normal forces and the system friction. However, these values have to be calculated, since they can not be measured. While the tyre normal forces changes as a function of the dynamic load transfer during the manoeuvring, the value of the friction moment is unpredictable, as the moment of the VDS is undefined in the event of failure. This uncertainty can be resolved by a system identification function which determines the friction and adapts the steering parameters online.

Since the tyre characteristics and capabilities have a strong impact on the manoeuvrability, the changeable tyre parameters need to be monitored at a detailed level. Therefore, estimators are required to recalculate the initial tyre values of the stiffnesses and the normal load distribution, which affect the tyre forces of the individual contact patches and the vehicle motion equations. Furthermore, the present friction coefficient has to be provided by an estimation function, on the one hand to ensure driving stability by avoiding saturation and, on the other hand, to maximize the operation range of the tyres as well as the allocator's solution space.

Finally, each brake control module has to be extended by an observer model which is capable of detecting the actuator's failure. For higher control accuracy, it is desirable to increase the brake models' level of detail by considering the variable disc temperature and the supply pipe length which depends on the actuator's mounting position. A coupled system identification function could update the parameter set of the actuator model online, since the brake characteristics are subject to further influencing parameters such as pad-disc friction or brake wear. This results in a more accurate brake application and avoids failure due to overheating.

5.2.2 Functionality

(Odenthal, et al., 1999) introduce a roll damping functionality based on the steering input to reduce the oscillations of the tyre normal forces. Since the applicable tyre force is a non-linear function of the normal load, the reduced oscillations allow a greater utilisation of the tyre friction level (Wiedemann, 2016). This results in the enhancement of the manoeuvrability and the driving safety.

In the course of electrification of vehicles, electric wheel actuators are installed. These actuators individually generate positive as well as negative wheel torques in order to propel or (regeneratively) brake the vehicle. The extended actuator capabilities result in a wider solution space of the optimal actuator control input. This offers new possibilities in the wheel torque distribution as well as an enhanced controllability of the vehicle motion. Furthermore, the steering actuator can be permanently supported with a differential wheel torque applied on the steered wheels. This solution would allow the implementation of a smaller primary steering actuator consuming less electric energy. In summary, the asymmetric torque distribution could increase the steerability and the driving efficiency.

References

AB Volvo, 2017. *Volvo Trucks Image and Film Gallery.* [Online]
Available at: Volvo Intranet
[Använd 20 10 2017].

ADAC, 2015. *Bremswege im Vergleich.* u.o.:ADAC e.V..

Băjenescu, T. I. & Bâzu, M. I., 1999. *Reliability of Electronic Components.* Heidelberg: Springer-Verlag Berlin Heidelberg GmbH.

Breuer, B. & Bill, K. H., 2012. *Bremsenhandbuch.* 4th red. u.o.:Springer Vieweg.

Brilon, W. & Krammes, R., 1997. Die neuen Entwurfsstandards für Außerortsstraßen im internationalen Vergleich. *Straßenverkehrstechnik,* p. 529 – 536.

Cheng, Q., 2013. *A Study of Truck Driver Deceleration Initiation Behavior.* Gothenburg: Chalmers University of Technology.

Dannenberg, J. & Burgard, J., 2015. *A comprehensive study on innovation in the automotive industry,* Munich: Oliver Wyman Automotive.

Day, A., 2014. *Braking of Road Vehicles.* s.l.:Butterworth-Heinemann.

dSPACE, 2017. *MicroAutoBox.* [Online]
Available at: https://www.dspace.com/en/pub/home/products/hw/micautob.cfm
[Använd 20 10 2017].

Ducard, G. J., 2009. *Fault-tolerant flight control and guidance systems: Practical methods for small unmanned aerial vehicles..* London: Springer Science & Business Media.

Eklöv, J., 2013. *Real-time implementation of a vehicle motion coordinator for a single unit truck.* Gothenburg: Chalmers University of Technology.

Fröjd, N., 2017. *VTM Plant Model Description.* Gothenburg: Volvo Group Trucks Technology.

Gillespie, T. D., 1992. *Fundamentals of Vehicle Dynamics.* Pittsburgh: Society of Automotive Engineers.

Hettich, G., 2016. *Einführung in die Kraftfahrzeug Systemtechnik.* Stuttgart: University of Stuttgart.

Härkegård, O., 2003. *Backstepping and control allocation with applications to flight control.* Linköping: Linköping University.

ISO, 2011. *International Standard 26262: Road Vehicles – Functional Safety.* Geneva: International Organization for Standardization (ISO).

ISO, 2011. *International Standard 8855; Road vehicles – Vehicle dynamics and road-holding ability – Vocabulary.* Geneva: International Organization for Standardization (ISO).

Jazar, R. N., 2017. *Vehicle Dynamics – Theory and Application.* 3rd red. Melbourne: Springer International.

Kkandiyil, S. T., 2016. *Influence of Steering Axis Inclination and Scrub Radius on Steering Effort of Passenger Car.* u.o.:SAE International.

Källstrand, B., 2016. *Control Allocation for Vehicle Motion Control.* Gothenburg: Chalmers University of Technology.

Laine, L., 2007. *Reconfigurable Motion Control Systems for Over-Actuated Road Vehicles.* Gothenburg: Chalmers University of Technology.

Magnusson, A., Laine, L. & Lindberg, J., 2018. *Rethink EE Architecture in Automotive to facilitate Automation, Connectivity, and Electro Mobility.* Gothenburg, ICSE-SEIP.

MAN Truck & Bus AG, 2016. *Grundlagen der Nutzfahrzeugtechnik.* 4th red. Munich: MAN Truck & Bus AG.

MathWorks, 2017. *Control of Processes with Long Dead Time: The Smith Predictor.* [Online]
Available at: https://www.mathworks.com/help/control/examples/control-of-processes-with-long-dead-time-the-smith-predictor.html
[Använd 2 10 2017].

Mercedes-Benz, 2014. *Mercedes-Benz Truck front axle systems.* [Online]
Available at: https://www.mercedes-benz.com/en/mercedes-benz/vehicles/aggregates/powertrain-trucks-front-axle-systems/
[Använd 06 09 2017].

Neubeck, J., 2016. *Fahreigenschaften des Kraftfahrzeugs 2.* Stuttgart: University of Stuttgart.

Nyman, P. & Uhlén, K., 2014. *Coordination of actuators for long heavy vehicle combinations using control allocation.* Gothenburg: Chalmers University of Technology.

Odenthal, D., Bünte, T. & Ackermann, J., 1999. *Nonlinear Steering and Breaking Control for Vehicle Rollover Avoidance.* Karlsruhe, European Control Conference (ECC).

Oubbati, M., 2009. *Einführung in die Robotik.* Ulm: University of Ulm.

Pacejka, H. B., 2012. *Tire and Vehicle Dynamics.* 3rd red. Amsterdam: Butterworth-Heinemann.

Pfeffer, P. E., Harrer, M. & Johnston, D. N., 2008. Interaction of vehicle and steering system regarding on-centre handling. *Vehicle System Dynamics,* pp. 413-428.

Pfeffer, P. & Harrer, M., 2013. *Lenkungshandbuch.* 2nd red. Wiesbaden: Springer Vieweg.

Pischinger, S. & Seiffert, U., 2016. *Handbuch Kraftfahrzeugtechnik.* Wiesbaden: Springer Vieweg.

Prokop, G. & Stoller, A., 2012. *Der Güterverkehr von morgen - LKWs zwischen Transporteffizienz und Sicherheit.* Berlin: Heinrich-Böll-Stiftung.

Rajamani, R., 2012. *Vehicle Dynamics and Control.* 2nd red. Minneapolis, Minnesota: Springer.

Reif, K., 2010. *Bremsen und Bremsregelsysteme.* 1st red. Wiesbaden: Vieweg+Teubner Verlag.

Reuss, H.-C., 2015. *Kraftfahrzeug-Mechatronik 1.* Stuttgart: University of Stuttgart.

Reuss, H.-C., 2016. *Automobiltechnisches Fachpraktikum Elektromobilität.* Stuttgart: University of Stuttgart.

Reuss, H.-C., 2016. *Kraftfahrzeug-Mechatronik 2.* Stuttgart: University of Stuttgart.

Rocco, M., 2014. *Fox Business.* [Online]
Available at: http://www.foxbusiness.com/features/2014/07/10/attorney-sees-5000-deaths-from-gm-ignition-switch-issue.html
[Använd 19 May 2017].

SAE, 2014. *Standard J3016: Levels of Automation for On-road Vehiles,* s.l.: SAE International.

Snider, J. M., 2009. *Automatic Steering Methods for Autonomous Automobile Path Tracking.* Pittsburgh, Pennsylvania: Carnegie Mellon University.

Statistisches Bundesamt, 2015. *Verkehr - Verkehrsunfälle.* Fachserie 8, Reihe 7 red. Wiesbaden: Statistisches Bundesamt.

Stoerkle, J., 2013. *Lateral Dynamics of Multiaxle Vehicles.* Zurich: Swiss Federal Institute of Technology (ETH) Zurich.

Svensson, J., 2010. *Autosar at AB Volvo.* Stuttgart, Volvo Group.

Tagesson, K., 2013. *Brake Pressure Request Interface Evaluation.* Gothenburg: Chalmers University of Technology.

Tagesson, K., 2017. *Driver-centred Motion Control of Heavy Trucks.* Gothenburg: Chalmers University of Technology.

Temple, C. & Vilela, A., 2014. Fehlertolerante Systeme im Fahrzeug – von "fail-safe" zu "fail-operational". *Elektronik automotive,* Issue Safety Automotive.

Thorvald, B., Wennerstroem, E. & Nordmark, S., 2011. *Vehicle Dynamics.* Stockholm: KTH Royal Institute of Technology.

United Nations Economic Commission for Europe, 2011. *Addendum 12: Regulation No.13, Revision 7.* u.o.:United Nations Economic Commission for Europe.

Waldron, S., 2014. *Introduction to AUTOSAR,* s.l.: Vector Informatik GmbH.

VDA, 2016. *Annual Report 2016: The automotive industry in facts and figures,* Berlin: Association of the German Automotive Industry (VDA).

Weber, R., 1981. *Reifenführungskräfte bei schnellen Änderungen von Schräglauf und Schlupf.* Karlsruhe: University of Karlsruhe.

Wiedemann, J., 2016. *Fahreigenschaften des Kraftfahrzeugs 1.* Stuttgart: University of Stuttgart.

Volvo Group Trucks Technology, 2016. *Volvo Dynamic Steering.* [Online] Available at: http://www.volvotrucks.de/de-de/trucks/innovationen/volvo-dynamic-steering.html
[Använd 05 09 2017].

Volvo Trucks, 2012. *Stretch Brake makes downhill driving safer.* [Online] Available at: https://www.youtube.com/watch?v=6k1WdzSHBfc
[Använd 20 10 2017].

Volvo, 2013. *Volvo Dynamic Steering – a breakthrough for effortless steering without strain or pain,* Gothenburg: Volvo Trucks.